UNIVERSITA’ DEGLI STUDI DI PARMA

PhD in Science and Technology of Innovative Materials

Cycle XXVI

Organic electronics at the interface with bio-medicine

Supervisor:
Dr. Salvatore Iannotta

Co-supervisors:
Prof. Pier Giorgio Petronini
Università degli Studi di Parma

Prof. Róisín M. Owens
Ecole Nationale Supérieure des Mines de Saint-Étienne

PhD candidate: Agostino Romeo

Abstract

The work carried out in this PhD thesis falls into the domain of the Organic Bioelectronics. This field, outstandingly emerged in the last few years, combines several disciplines, mainly Organic Electronics, that relies on carbon-based semiconductors, and biomedicine, in its connotations related to biosensors and diagnostics.

In particular, this work concerns the development and study applications of electrochemical devices based on organic conductors for bio-sensing and bio-electronics, applied in particular to the detection of molecules and biologically-relevant systems, cellular stress induced by drugs and control of bacterial adhesion.

The relevant results obtained qualify electrochemical devices as very promising for biomedical applications in a perspective of cheap, easy to handle systems that could contribute to the development of point-of-care diagnostics and theranostics.

Chapter 1 provides the basic theoretical background for the themes and questions that motivate this work. First, the basic concepts of Organic Electronics are illustrated in detail, providing a description of the physical properties that make organic semiconductors an extremely interesting class of materials. The applications of organic-based devices are described, focusing in particular on Organic Electrochemical Transistors (OECTs), a type of Organic Thin film Transistor (OTFT) that represents the device of choice in the present work. An overview on Organic Bioelectronics is also given, with a special focus on recent applications of OECTs to bio-sensing and cellular biology. Finally, a discussion of questions concerning sensing of bio-molecules and biologically-relevant systems (melanins and nano-particles, respectively) is given, together with an introduction to biofouling and cellular stress.

Chapter 2 deals with the demonstration that OECTs can efficiently sense biologically relevant pigment molecules, such as eumelanin. Its electrical properties were also studied by exploring redox reactions that occur at the gate electrode providing appropriate experimental conditions. Of particular interest is that the study of the electrical measurements gives information on stability and evolution of these

bio-molecules in response to electrochemical stress. Such changes shall be deemed to be the basis of the peculiar properties and the role of melanin within biological organisms.

Chapter 3 discusses another field of application of OECTs, addressing the detection and monitoring of magnetic nanoparticles functionalized with polymeric shell, widely studied as drug delivery systems and for hyperthermia in cancer treatments. Monitoring of the electrical response of OECTs allowed to sense such nano-systems as a function of their concentration. Here it is demonstrated that OECTs represent a valuable tool for low-cost and real-time monitoring the dynamics of such systems in an aqueous solutions.

Control of bacterial adhesion and biofilm formation by means of conducting polymers is the central topic of **Chapter 4**. The role of surface properties is studied on the ability of *E. coli* bacteria to adhere and form the systems known as biofilms. Devices based on two of the most used organic conductors, PEDOT:PSS and PEDOT:Tos, were designed and manufactured, with the aim of modulating the surface adhesion properties by simply electrically controlling the polarization of the conducting polymers. The outcome of this project shows that the redox state of the surface plays a key role in promoting (or inhibiting) the formation of bacterial biofilms. We hence obtained new information on the technologies and methods used to control biofilms, which are often detrimental impact but in some cases beneficial in processes with high social impact.

In a contest of increasing complexity, **Chapter 5** deals with interfacing of OECTs with biological systems, such as mammalian cells, to develop a system for sensing the cellular stress induced by drugs. To this end, a measurement protocol, based on the integration of micro-porous supports with OECTs, was developed, that allows to monitor the viability of cells in response to drugs. Cellular stress was monitored by analyzing the electrical response of OECTs, once placed in contact with cells forming a barrier tissue. This application is aimed to develop a point-of-care diagnostic system for *in situ* and real-time sensing of the viability of cancer or normal cell in response to specific drugs.

Finally, **Chapter 6** gives an outlook and conclusive remarks on the results achieved in this work. Perspectives and speculation on the future developments and achievements of Organic Bioelectronics are provided.

“Si piensas que estás vencido, lo estás.
Si piensas que no te atreves, no lo harás.
Si piensas que te gustaría ganar pero no puedes, no lo lograrás.
Si piensas que perderás, ya has perdido.
Porque en el mundo encontrarás
que el éxito comienza con la VOLUNTAD del hombre.
...
Piensa en grande y tus hechos crecerán.
Piensa en pequeño y quedarás atrás.
Piensa que puedes y podrás.
...”

(based on Christiaan Barnard’s *Poema del Exito*)

Table of contents

List of figures

Chapter 1

1. Introduction

1.1. Organic electronics and bio-medicine

1.1.1. Conducting organic molecules and polymers

Since the discovery of the conductive properties of polyacetylene in 1977 by A. J. Heeger, A. G. MacDiarmid and H. Shirakawa,[1] awarded of the Nobel Prize in Chemistry in 2000, organic electronics has increasingly gained interest. Organic electronics refers to a wide range of organic species (molecules and, more abundantly, conjugated polymers), that show exciting conducting properties (**Figure 1**). In particular, conducting polymers were initially attractive because of the fundamental interest in the doping and the doping-induced metal/insulator transition. However, the chemistry and physics of these polymers were also of great interest because they enabled a new technology, known as “plastic electronics”. Indeed, in conjugated polymers the electronic configuration is fundamentally different from that of saturated polymers (in which all of the four valence electrons of carbon are involved in covalent bonds, which makes them insulators).[2] Their structure provides the “highway” for charge mobility along the backbone of the polymer chain.

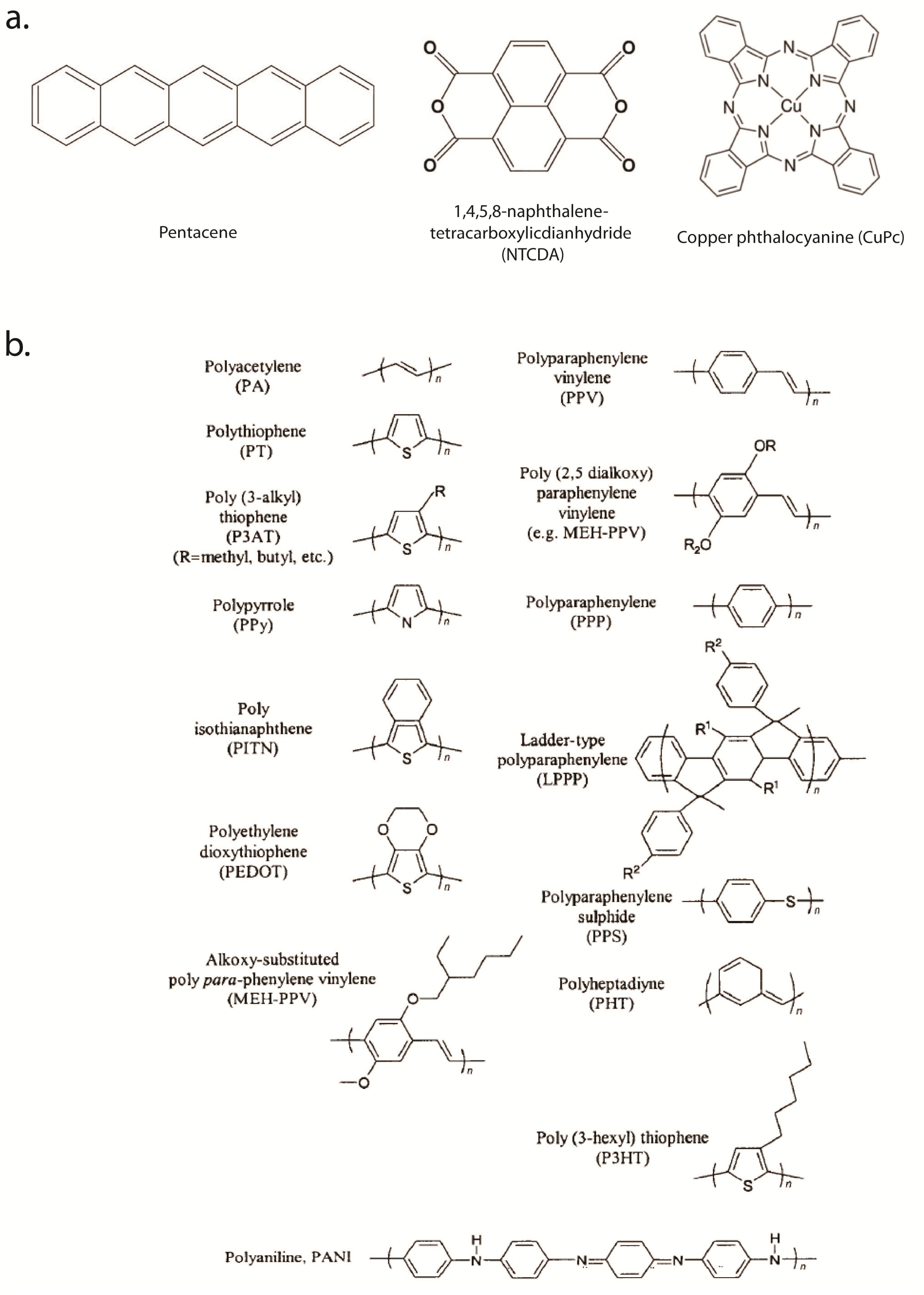

Figure 1 *Chemical structure of some important organic conducting molecules (a.) and polymers (b.). (Adapted with permission from A.J. Heeger[3], © (2001) Wiley)*

Several and strong motivations led to the rise of an electronics based on organic conductors: the ease of processing of organic materials, their unique combination of electronic and ionic transport, and the possibility to chemically tune properties such as solubility in organic solvents and the color of light emission. The discovery of light-emitting diodes (LEDs) in 1990[4] provided the stimulus for a major push in this direction. The emerging class of "plastic" opto-electronic devices, including lasers, high sensitivity plastic photodiodes (and photodiode arrays) and photovoltaic cells, ultrafast image processors, thin-film transistors, and all-polymer integrated circuits, include components fabricated from semiconducting and metallic polymers.

Since the 1980s, when the opportunity to synthesize new conducting polymers with improved/desired properties began to attract the attention of synthetic chemists, a long way has been made toward the goal of controlling the energy gap of semiconducting polymers through molecular design.

1.1.2. Structure and charge transport in organic semiconductors

Organic electronics is based on π-conjugated organic small molecules and polymers, characterized by the alternation of double- and single-bonded sp^2 hybridized carbon atoms along the polymer backbone. In conjugated polymers, the chemical bonding leads to one unpaired electron (the π electron) per carbon atom and to the delocalization of these electrons along the backbone of the polymer. The electronic result is an energy gap between a completely filled π band (HOMO level) and an empty π* band (LUMO level). As a consequence of this electronic structure, conjugated polymers exhibit semiconducting or even metallic properties (**Figure 2**). Similar to inorganic semiconductors, such as silicon, conjugated polymers show very low conductivities in their pristine state. In order to enhance their conductivity, these materials can be doped p-type or (less frequently) n-type to a highly conducting state, for instance, by adding a chemical that either oxidizes or reduces the π-conjugated structure. Other than by chemical doping, control of the electrical conductivity of conducting polymers over the full range from insulator to metal, is also accomplished by electrochemical doping, acid-base chemistry (as in the case of Polyaniline), photo-doping and charge injection at a metal-semiconducting polymer interface.[3] Un-doped conjugated polymers only have a low electrical conductivity of around 10^{-10} to 10^{-6} S/cm. Even at a very low level of doping (< 1%), electrical conductivity increases several orders of magnitude up to values of around 0.1 S/cm. Subsequent doping of the conducting polymers will result in conductivities as high as ~10 kS/cm.[5]

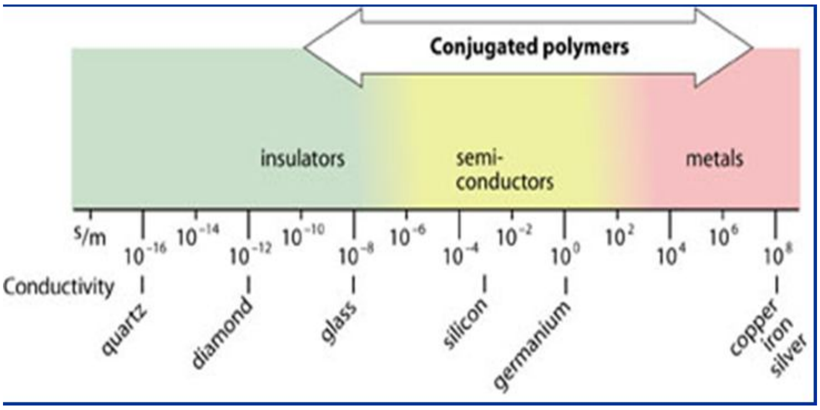

Figure 2 *Conductivity of conducting polymers compared to that of other materials, from quartz (insulator) to copper (conductor). Reproduced from http://www.nano.org.uk/news/may2008/latest1402.htm.*

Charges that are introduced in polymers and oligomers are stored in novel excited states, called excitons (polarons, bipolarons, or solitons).[6] These states, which correspond to localized charge defects, include a charge and a lattice distortion. In most conjugated polymers, the lattice distortion due to charge addition/removal favors the formation of a polaron. A polaron is formed when an electron is added to or removed from the conjugated chain. This change results in a chain deformation and a change in the energy level structure.[6] One electronic level is moved from the valence band into the gap with its two electrons and an addition level is moved from the conducting band into the gap. In the case of an electron polaron, the added electron is stored in the newly created level drawn from the conduction band. In the case of a hole polaron, an electron is removed from the newly created level moved up from the valence band. In both cases a half-filled level is created with spin ½.

Figure 3 *Schematics of the structure of a conducting polymer. Polymer chains are represented by black lines. The dashed squares indicate the regions where polymer chains show crystalline order. (Adapted with permission from V.N. Prigodin et al.*[7]*, © (2003) Elsevier).*

The structure of a conjugated polymer is by far less regular than solid semiconductors, such as silicon. Polymers contain individual molecules with different chain lengths, varying amounts of defects, and chain ends. Disorder in the organics is not usually associated with broken chemical bonds, because covalent bonds within molecules or polymer chains remain intact. This inhomogeneity cause these materials to be amorphous, with ‘‘crystalline’’ regions within which polymer chains are well ordered (**Figure 3**).[7] As a consequence, the disorder in conjugated polymers has a strong effect on the conducting properties of organic semiconductors, as it can localize charges and excitons on lattice sites. Indeed, electronic wavefunctions would tend to delocalize over the entire macromolecular chain as far as the conjugation is preserved. However, order itself is not a sufficient condition for charge transport, since even in a highly ordered system, macroscopic charge transport is not possible unless the charges can hop or diffuse from one chain to another. Experimental studies have established that in conducting polymers, the electrical properties improve as the degree of chain extension and chain alignment are improved (**Figure 4**).[8]

In general, charge transport in conjugated polymers involves several processes such as: conduction along the polymer backbone, hopping across chains due to inter-chain interactions, and tunneling between conducting segments that are separated by less conducting regions.[9] The first two processes are the most relevant for un-doped semiconducting polymers.

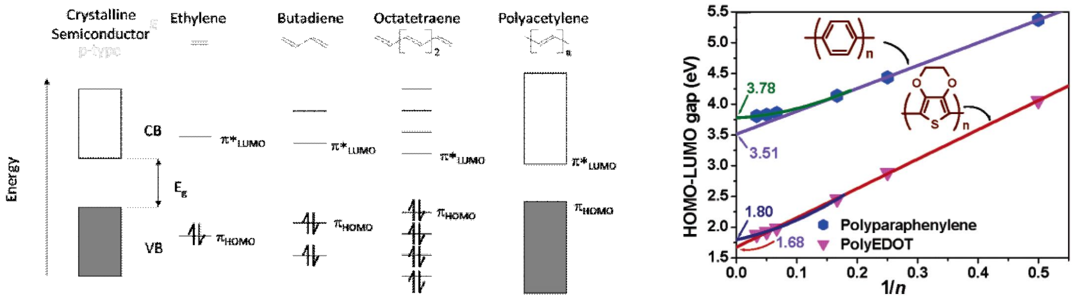

Figure 4 *Left panel: dependence of HOMO-LUMO levels on the conjugation length. Right panel: HOMO-LUMO gap versus the reciprocal of the number of oligomer units for oligoparaphenylene and -EDOT. (Adapted with permission from S.S. Zade et al.*[8] *© (2006) American Chemical Society).*

1.1.3. Poly(3,4-ethylene dioxythiophene) (PEDOT)

PEDOT, a polythiophene derivative,[10–12] is one of the best known π-conjugated polymers, mainly because of its good electrical conductivity and electro-optic properties, as well as processability. Prepared using standard oxidative chemical or electrochemical polymerization methods. PEDOT was initially found to be an insoluble polymer, especially in water, yet it exhibited some very interesting properties. In addition to a metallic behavior,[13–15] PEDOT was found to be almost transparent and highly stable in thin oxidized films.[16,17] Its highly electron-rich nature plays a profound role in the optical, electrochemical, and electrical properties of the resultant polymers. PEDOT films are highly electro-active and have a low oxidation potential and a relatively low bandgap, which provides facile, long-term electrochemical switching. Neutral PEDOT exhibits an electronic bandgap located at the transition between the visible and near-IR regions of the spectrum, making it deep blue in color.[18]

As previously mentioned, one method for enhancing the properties of conducting polymers, while simultaneously preparing useful materials, is through polymer blending. The number of counterions used in the electrochemical polymerization of PEDOT is quite large (typically PSS, ClO_4^-, BF_4^-, PF_4^-, NO_3^-, SO_4^-, $CF_3SO_3^-$,etc.), while counterions for chemically polymerized PEDOT are relatively few, the oxidation agent being typically Iron(III) salts, such as Iron(III)-Tosylate. The highest conductivities are obtained in the presence of perchlorate, using acetonitrile as solvent, while, using water as a solvent leads to lower conductivities than organic solvents for the same counterions. Using water as solvent, the highest conductivity was found in the presence of nitrate.[19]

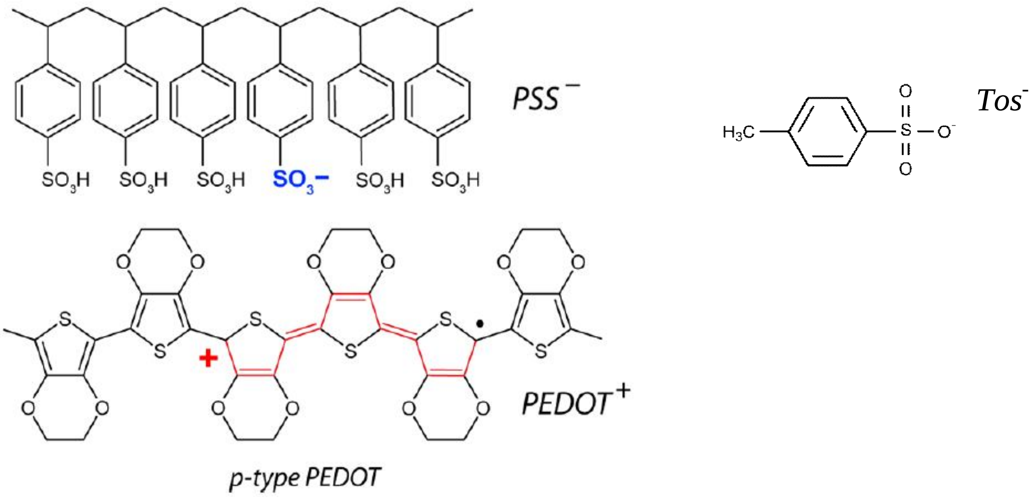

Figure 5 *Chemical structures of the organic semiconductor PEDOT and of two common counterions, PSS and Tosylate anions. Note the polaron created along the backbone of PEDOT by doping with the counterion. (Adapted with permission from J. Rivnay et al.*[20]*, © (2013) American Chemical Society).*

The most common charge balancing counterion used to prepare PEDOT blends is poly(styrene sulfonate) (PSS) (**Figure 5**); this yields PEDOT:PSS, that is a degenerately doped organic semiconductor, in which the semiconductor chain (PEDOT) is p- type doped due to the presence of uncompensated sulfonate anions on the PSS chain. PEDOT:PSS combines high conductivity, ranging between 10^{-3} and 1 S/cm, and good transparency in the visible region with excellent stability under ambient conditions. It can be easily processed from aqueous dispersions by spin coating. In fact, the water-soluble PSS counterion allows circumventing the solubility problem of PEDOT, providing a water-dispersible blend. In PEDOT:PSS dispersions, PEDOT and PSS form a poly-ion complex, where the PSS, in excess, forms a PSS-rich shell around a PEDOT rich core, yielding colloidal gel particles in suspension.[21] After proper shearing and sonication, such colloidal particles are known to be in the range of 5–30 nm.[19] The film microstructure is generally described as the physical interconnection and flattening of these colloidal gel particles upon film casting. In spin-coated thin films, PEDOT:PSS is a phase segregated material[22,23] consisting of PEDOT-rich clusters with a thickness of ~5 nm and a diameter of ~20 nm surrounded and separated by PSS lamellas 30-40 nm thick[24,25] (**Figure 6**). In the normal direction, the separating barriers, that is, the PSS lamellas are quasi-continuous, whereas the separations in the lateral direction appear to be not fully closed. As a consequence of this morphological anisotropy, the temperature dependent conductivity in doped organic materials like PEDOT:PSS has been described in the framework of variable range hopping (VRH) as:

$$\boldsymbol{\sigma = \sigma_0 exp\left[-\left(\frac{T_0}{T}\right)^{\alpha}\right]} \qquad \text{Eq. 1}$$

where σ_0 is the conductivity at a temperature much higher than T_0, the characteristic temperature, and α the exponent that in standard VRH theory is equal to 1/(1+D), where D is the dimensionality of the system. Differences in electrical transport properties exist in the ∥ and ⊥ directions. In the ∥ direction, that is, within the PEDOT-rich lamella, conduction can take place by 3D VRH because in this direction the PEDOT-rich domains are only separated by the not-completely closed constrictions. These are likely to either form a thin barrier, or no barrier at all, thereby allowing carriers to hop to nonnearest- neighbor sites, resulting in relatively high σ values (~10^{-3} S/cm at room temperature). In the ⊥ direction, the PEDOT-rich domains are separated by thick barriers, formed by the PSS lamella, which enforce nearest-neighbor hopping and cause a reduction of σ (~2×10^{-6} S/cm at room temperature).

Another common counterion for PEDOT is the Tosylate anion, mainly used for chemically polymerized PEDOT.[26–28] PEDOT:tosylate films prepared by chemical polymerization show conductivities as high as 1000 S/cm.[29] The dopant ions form distinct planes, which alternate with stacks of polymer chains.[30] Films are in a paracrystalline state, with small size of the individual paracrystalline regions. The high structural anisotropy implies the strong optical anisotropy observed.

Conductivity enhancement by several orders of magnitude can be achieved also upon addition of secondary dopants such as organic solvents (ethylene glycol, sorbitol, DMSO, THF, DMF, etc.).[31–35] This enhancement is associated to an increased interchain interaction, deriving from a conformational change of PEDOT chains.

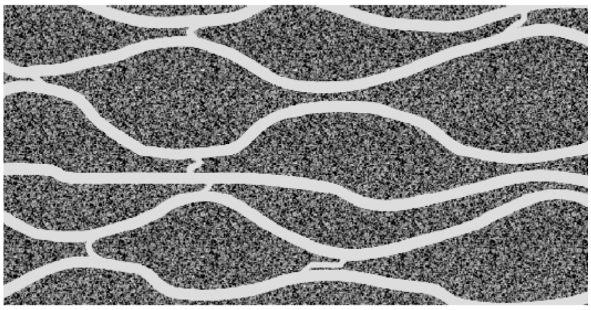

Figure 6 *Cross-sectional view of the schematic morphological model for PEDOT:PSS thin films. (Adapted with permission from A.M. Nardes et al.*[23]*, © (2007) Wiley).*

1.1.4. Organic Thin Film Transistors

Conducting polymers combine the advantageous characteristics of conventional polymers, such as low weight, easy processability, flexibility, and high conformability with the functional physical properties of conventional semiconductors, such as absorption and emission of light and a tunable conductivity.

Conducting polymers have been exploited in several fields, ranging from organic light-emitting diode (OLED),[36] organic photovoltaics (OPV)[37] and organic thin film transistors (OTFT).[38] Even though organic devices will probably never compete with inorganic devices in terms of performance and stability, their use is conceivable in applications which can withstand lower charge carrier mobility. Their low processing temperature is compatible with plastic flexible substrates and their low elastic modulus is consistent with bending. Deposition processes are simple and therefore potentially inexpensive. Many organics are deposited from solution and therefore suitable for printing systems. Another decisive advantage of organic-based devices is the possibility of tailoring the organic material to adjust its properties. This is of primary importance for sensors for which particular chemical and physical properties are required to covalently attach the recognition elements.

Among the previously mentioned organic devices, OTFT are attracting a great deal of interest for sensor applications due to their simple electrical readout, high sensitivity, inherent signal amplification, miniaturization, and facile incorporation into arrays and circuits. To date, OTFT have been intensively investigated for applications in flexible active matrix displays,[39–42] radio-frequency identification (RFID) tags,[43,44] and sensors of mechanical deformation and pressure, humidity and organic vapors, pH and ion concentrations, and a variety of biologically relevant analytes.[45,46]

In general, OTFTs utilize a thin film of organic semiconducting material as the active layer of the transistor. The organic semiconductor can be made of oligomers or polymers that are deposited as films (a few tens of nanometers thick) by solution casting, spin coating, sublimation and printing techniques. Two electrodes (‘‘source’’ and ‘‘drain’’) in contact with the organic semiconductor are used to apply a source–drain voltage (V_{ds}) and measure the source–drain current (I_{ds}) that flows through the organic semiconductor, while a third electrode (‘‘gate’’) is used to modulate the magnitude of I_{ds}. A transistor-based sensor usually achieves high sensitivity because the device is the combination of a sensor and an amplifier, in which, for example, a small change of the effective gate voltage induced by an analyte may lead to a pronounced variation of channel current.

OTFTs can be classified into two primary categories: organic field effect transistors (OFET), based on organic semiconductors, and organic electrochemical transistors (OECT), based on electrically conducting polymers (**Figure 7**). In the next sections, OFET and some OFET-derived architectures will be presented, followed by a detailed description of OECT, which is the main device used in this work.

1.1.4.1. OFETs

In OFETs, I_{ds} is modulated by field-effect doping, where the charge carrier density in the organic semiconductor is controlled by the gate electrode via an electric field applied across an insulating layer (e.g. vacuum, oxides, polymers, self-assembled monolayers). When the gate is negatively (positively) polarized in a p-channel (n-channel) device, free holes (electrons) in the semiconductor are drawn toward the semiconductor–insulator interface to compensate an equivalent negative (positive) charge at the gate–insulator interface. This leads to the formation of a conducting channel at the semiconductor–insulator interface (**Figure 8a**).[47] The field generated by the negative V_{gs} bias applied across the dielectric layer leads to a band-bending in the organic semiconductor as depicted in **Figure 8c.**

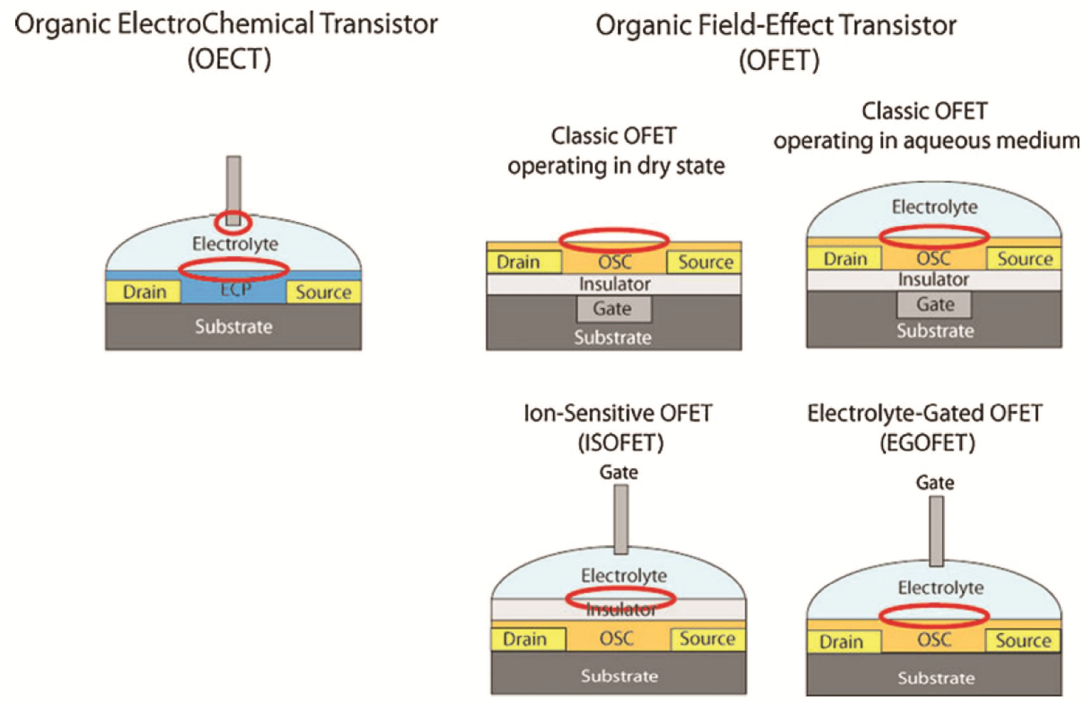

Figure 7 *Schematic illustration of OECT and OFETs architecture. The red circles indicate the different interfaces involved in the detection of analytes. (Adapted with permission from L. Kergoat et al.,*[47] *© (2012) Springer).*

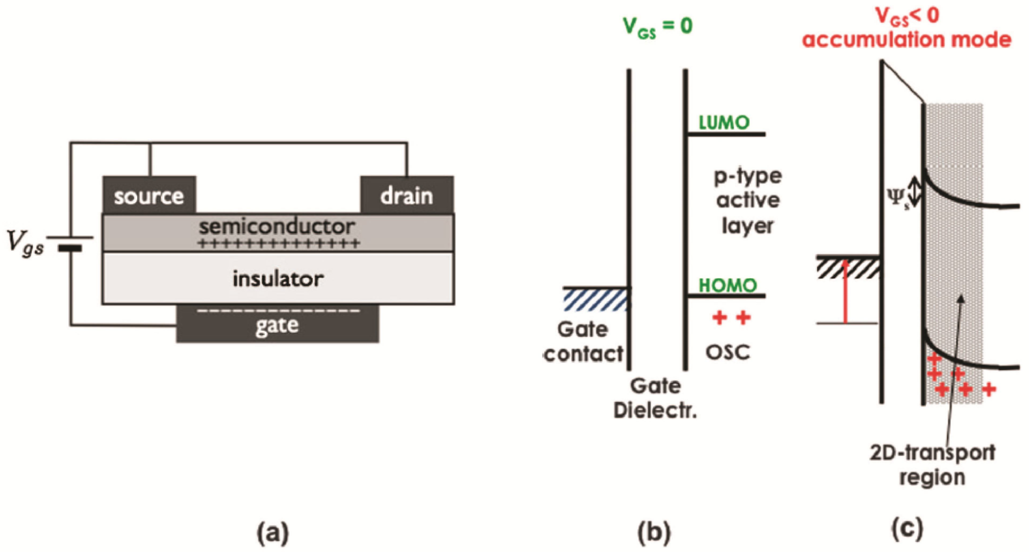

Figure 8 *(a) Formation of the conducting channel in an organic field-effect transistor. (Adapted with permission from L. Kergoat et al.,*[47] *© (2012) Springer). (b) Band diagram of metal–insulator–(p-type) semiconductor (MIS) structure at zero gate ($V_{gs} = 0$) and (c) accumulation ($V_{qs} < 0$) mode. (Adapted with permission from L. Torsi et al.,*[48] *© (2013) The Royal society of Chemistry).*

When a negative (positive) voltage is applied between source and drain, holes (electrons) are injected from the source and current flows inside the channel. OFETs mostly operate in the so-called *accumulation mode*, and a highly resistive organic semiconductor, resulting in a low I_{ds} current in the off state ($V_{gs} = 0$), is necessary. The I_{ds} current flowing in the on-state ($V_{gs} < 0$) must be, instead, as high as possible. For *p-type* organic semiconductors, the device is commonly operated by independently negatively biasing the drain and the gate contacts applying the V_{ds} and V_{gs} potentials with respect to the grounded source. This is called *common source configuration*. The gate voltage required to switch the transistor from its “off” to its “on” state, i.e. to establish a conducting transistor channel, is called the threshold voltage. The threshold voltage along with the charge carrier mobility (μ) and the charge current modulation ratio between the “on” and “off” states (I_{on}/I_{off}) are the key properties of a transistor.

Typical materials for OSCs include polymers such as poly-(3-hexylthiophene) (P3HT),[49] poly(4,4’didecylbithiophene-co-2,5-thieno[2,3-b]thiophene) (PDTT),[50] alkyl-substituted triphenylamine polymers (PTAA),[51] and poly-DPOT and Poly-DDT,[52] but also oligomers such as pentacene (and its soluble derivatives), *α*-sexithiophene (*α*6T),[53] 5,5’-bis-(7-dodecyl-9H-fluoren-2-yl)-2,2’-bithiophene (DDFTTF)[54] as well as many other small molecule organic semiconductors.[55]

Ion-sensitive OFET (ISOFET)

Apart from classic OFETs operating in dry state, the most common architecture used in OFET-based biosensors is the so-called ion-sensitive OFET (ISOFET).[56,57] Here, the electrolyte containing the analyte is in contact with the insulator, and the gate electrode is immersed into the electrolyte. The source-drain current is modulated by field-effect doping due to the potential of the electrolyte–insulator interface (**Figure**

7) just as in conventional OFETs, but the electric field across the insulating gate dielectric is controlled by ions at the electrolyte/insulator interface. By making the insulator sensitive to a given analyte, it is possible to detect a wide range of biomolecules.

Electrolyte-gated OFET (EGOFET)

All the devices described above require dry conditions after the biorecognition step to enable electrical characterization. This makes them unsuitable for practical biosensors because they are all restricted to operation in a dry state. Furthermore, like ISOFETs, a high voltage is required to operate the device. Low-voltage transistor operation has attracted interest for reasons other than operation in aqueous media, particularly for low-power applications. Thus, tremendous efforts have been devoted in order to allow transistors to operate at low voltage; examples are devices exploiting high dielectric constant [58] or ultrathin gate dielectrics.[59]

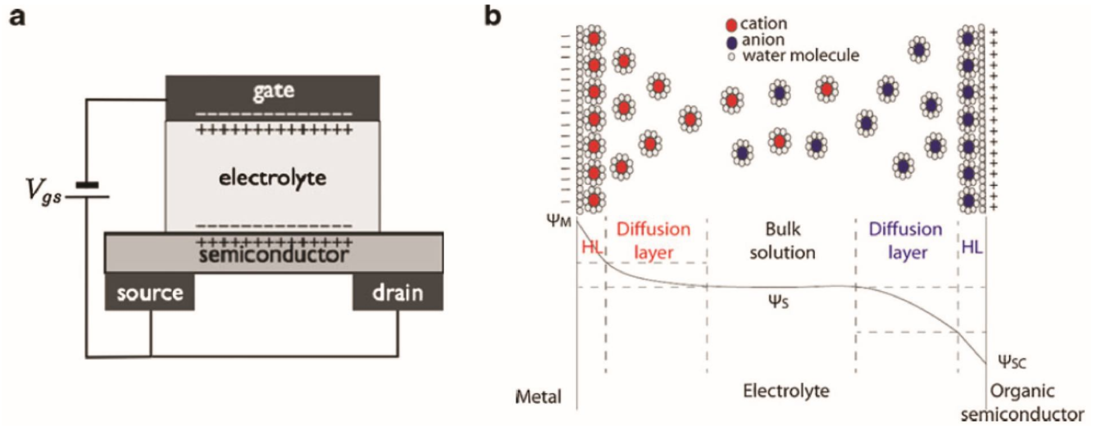

Figure 9 *(a) The conducting channel in an electrolyte-gated organic field-effect transistor. (b) Illustration of the ion distribution within the Helmholtz layer (HL), the diffuse layer and the bulk electrolyte (above), and spatial distribution of the potential between the gate and the semiconductor in an electrolyte-gated transistor (below). (Adapted with permission from L. Kergoat et al.,*[47] *© (2012) Springer).*

To this regard, another solution is represented by devices where the semiconducting layer is in direct contact with the electrolyte. One class of OFETs responding to these criteria are electrolyte-gated OFETs (EGOFETs),[60,47] that have recently attracted much attention because of low voltage operation compared with OFETs gated via solid dielectrics. EGOFETs are based on organic active materials that are not electrochemically active and differ from OFETs, as in OECTs, in that the gate is separated from the semiconductor by an electronically insulating, ionically conducting electrolyte (**Figure 9a**). By utilizing a ion-conducting electrolyte as an OFET gate dielectric, an electrostatic doping mechanism is achieved for the organic semiconductor. More in detail, when a negative bias (V_{gs}) is applied to the gate electrode, a negative surface charge produces on the metal that attracts mobile cations in the electrolyte and establishes an electrical double layer (EDL, a few nanometers thick) at the gate/electrolyte interface (**Figure 9b**).[61] Anions in the electrolyte are repelled from the gate and a layer of anionic charge is created at the opposite electrolyte/semiconductor interface. The resulting large local electric field at the electrolyte/semiconductor interface causes holes to accumulate on the organic semiconductor surface to balance the negative charge of the anionic layer. This process establishes the second EDL. The formation of the EDLs is responsible for the electrostatic doping of the organic semiconductor. The EDL at the electrolyte/semiconductor interface can have a very fast time response, as a result of a charge separation of only a few angstroms within the Helmholtz layers formed in a few tens of microseconds.[62] Furthermore, and more importantly, it can show extraordinarily high capacitance (typically a few to a few tens of $\mu F cm^{-2}$),[63,64] inducing a very large charge carrier density ($>10^{14}$ cm^{-2})[65] in the organic semiconducting channel at low (sub-volt) applied voltages.[66] If ions penetrate the semiconductor (or gate), however, the EDL model is not valid and an electrochemical transistor effect can be observed. A number of studies aimed at enlightening the exact working mechanism of EGOFETs have been reported. Although some studies would support the possible co-existence of the two doping mechanisms, electrostatic and electrochemical,[67] collective results point to an electrostatic (field-effect) doping mechanism.[68,69]

So far, a variety of electrolytes have been used: liquid electrolytes,[70] polymer electrolytes,[60,71,72] ionic liquids,[73] ionic gels,[74,66] and, finally, polyelectrolytes.[75] However, one drawback with electrolytes is that electrostatic and electrochemical doping can occur simultaneously, especially when semiconducting polymers with flexible and open structures are used. Such electrochemical doping would result in a higher switching time and in possible degradation of the semiconductor. Use of polyelectrolytes, in which anions are virtually immobile, has been shown to prevent this situation, because the anion groups are linked to the polymer backbone, and cannot enter the semiconductor bulk.[75]

Many EGOFET-based sensors have already been developed, such as DNA,[76,77] pH,[53,78] dopamine,[79] sensors. EGOFET have also been involved in recording the electrical activity of neuronal networks[80] and bio-functionalization for label-free electronic sensing.[81] More importantly, all printed EG-OFET devices can be easily integrated with microfluidic systems, implying broad potential applications in the future.[82]

1.1.4.2. OECT

Depending on the nature of the organic active material and the electrolyte, a similar transistor structure has been developed within the family of electrolyte-gated organic transistors, exploiting a different working mechanism. It is the case of organic electrochemical transistors (OECTs), based on electrochemically active conducting polymers, such as polypyrrole (PPy), polyaniline (PANI), PEDOT, poly(3-akylthiophene) (P3AT), polycarbazole. In OECTs, unlike the electrostatic doping of EGOFETs, the bulk conductivity of the semiconducting film is changed due to electrochemical doping combined by ion diffusion into the film.[83]

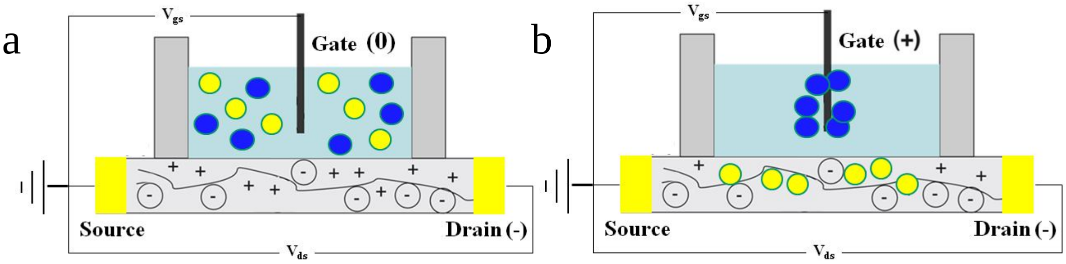

Figure 10 *Schematic cross section of an organic electrochemical transistor (OECT) based on a p-doped conducting polymer. a. When the gate electrode is not biased, the conducting polymer is in the doped state and the transistor is in the ON mode. b. When a positive bias is applied to the gate electrode, cations in the electrolyte (yellow circles) are injected into the polymer, causing it to be de-doped; anions (blue circles) are attracted toward the gate electrode.*

Within the family of electrolyte-gated organic transistors, OECTs, first developed in the 1980s by the group of Wrighton,[84–86] have attracted increasing interest.[87–89] In general an OECT consists of a conducting polymer film (transistor channel), whose extremities represent the source and drain electrodes. The gate electrode, separated from the polymer channel, is immersed in an electrolyte and controls the doping level of the conducting polymer. The channel current, flowing upon biasing of the transistor channel, is modulated by the gate due to the electrochemical doping/de-doping of the active layer. For the case of a *p-type* material such as PEDOT:PSS, the application of a positive V_g causes positive ions from the electrolyte to enter the organic film and de-dope it, decreasing the source–drain current (**Figure 10**). Charge neutrality implies that cation injection is balanced by hole extraction, meaning that as the sulfonate anions are compensated by the injected cations, the excess holes are swept away by the hole drift current. This mechanism is described by the reaction:[83]

$$\boldsymbol{PEDOT^{+}{:}PSS^{-} + M^{+} + e^{-} \leftrightarrow PEDOT^{0} + PSS^{-}M^{+}} \qquad \text{Eq. 2}$$

where M^{+} denotes the positively charged ion, e^{-} the electron and $PEDOT^{0}$ the reduced, poorly conductive form of PEDOT. Therefore, PEDOT:PSS OECTs operate in *depletion mode* (i.e. as gate voltage increases, source–drain current decreases). A device model to describe the transient behavior of the channel current of an OECT has been proposed by Bernards et al.:[87]

$$\boldsymbol{I_{ds} = \frac{q\mu p_0 tW}{LV_p}\left(V_p - V_g^{eff} + \frac{V_{ds}}{2}\right)V_{ds}} \qquad \text{Eq. 3}$$

$$\boldsymbol{V_p = \frac{qp_o t}{c_i}} \qquad \text{Eq. 4}$$

$$\boldsymbol{V_g^{eff} = V_G + V_{offset}} \qquad \text{Eq. 5}$$

where q is electronic charge, μ is the hole mobility, p_0 is the initial hole density in the organic semiconductor before the application of a gate voltage, t is the thickness of the organic semiconductor film, W and L are the width and length of the OECT device, respectively, V_p is the pinch-off voltage, V_g^{eff} is the effective gate voltage applied, and V_{offset} is an offset voltage caused by the potential drop at the two interfaces: gate/ electrolyte and electrolyte/channel. It is worth noting that c_i is the effective capacitance per unit area of the transistor, which is not only related to the capacitance of the interface between the electrolyte and organic semiconductor channel (C_d) but also to that of the interface between the electrolyte and the gate electrode (C_g). An electronic circuit combined with an ionic circuit was used to describe the device behavior. The electronic transport is influenced by the density and mobility of the holes, while the ionic transport is determined by the ions in the electrolyte. De-doping in these devices is reversible, and the source–drain current recovers when V_g is returned to zero. More aspects of the working mechanism of an OECT are described in section **2.3.1**.

OECTs show stable performance in aqueous environment and have low working voltages, which are tipically less than 1 V. Operation in electrolytes and exploitation of the electrochemical modification of the electrical response, make OECTs suitable for various sensing applications, such as chemical detection (ions,[89,90] pH,[86,85] hydrogen peroxide,[88,91] glucose,[92,93] and macromolecules[94,95]), humidity sensing,[96,97] and monitoring of nanosystems.[98,99]

EGOFETs and OECTs represent two devices apparently similar but substantially different. On one hand, they share common features, firstly the gate dielectric, consisting of an electrically insulating ionically conductive electrolyte, but also the ease and cost-effective of fabrication processes, compatible with printing technologies (roll-to-roll or inkjet printing). Moreover, both these devices show the ability to work in liquid environment while requiring very low voltages (hundreds of mV), which opens to their applications in biologic sensing. On the other hand, however, they present deep differences, mainly in the type of organic conductors they are based on and, more importantly, in their working mechanism. In particular, this last aspect has resulted decisive in the determination of OECTs as device of choice for the research carried out during this PhD. The electrochemical doping/de-doping mechanism mainly involved in OECTs operation, makes OECTs particularly well suited for applications where fluxes of ions are involved. This could, potentially, lead to higher sensitivities because of the direct implication of ions in modulating the conductive properties of conducting polymers.

1.1.5. Organic bioelectronics

The mixed electronic/ionic conductivity is of particular importance for devices that interface electronics with biology, and has led to the rise of a new and exciting field named Organic Bioelectronics, from the seminal paper by Magnus Berggren and Agneta Richter-Dahlfors[100] Organic bioelectronics deals with the interfacing of organic electronics with biology (**Figure 11**).[101,20] Due to their "soft" nature, organic electronic materials offer a range of advantages making this interface uniquely suitable. The advantages include a better mechanical compatibility with tissue than traditional "hard" electronic materials and, hence promising on improved compatibility with mechanically flexible substrates, which suits the non-planar form factors often required for implants. The ability of organic electronic materials to conduct ions, in addition to electrons and holes, enables a new communication channel with biology since the ion fluxes play a crucial role in biological systems. From this point of view, the amplified conversion of ionic currents into electronic ones that takes place in OECTs, provides a unique link between the worlds of biology and electronics.

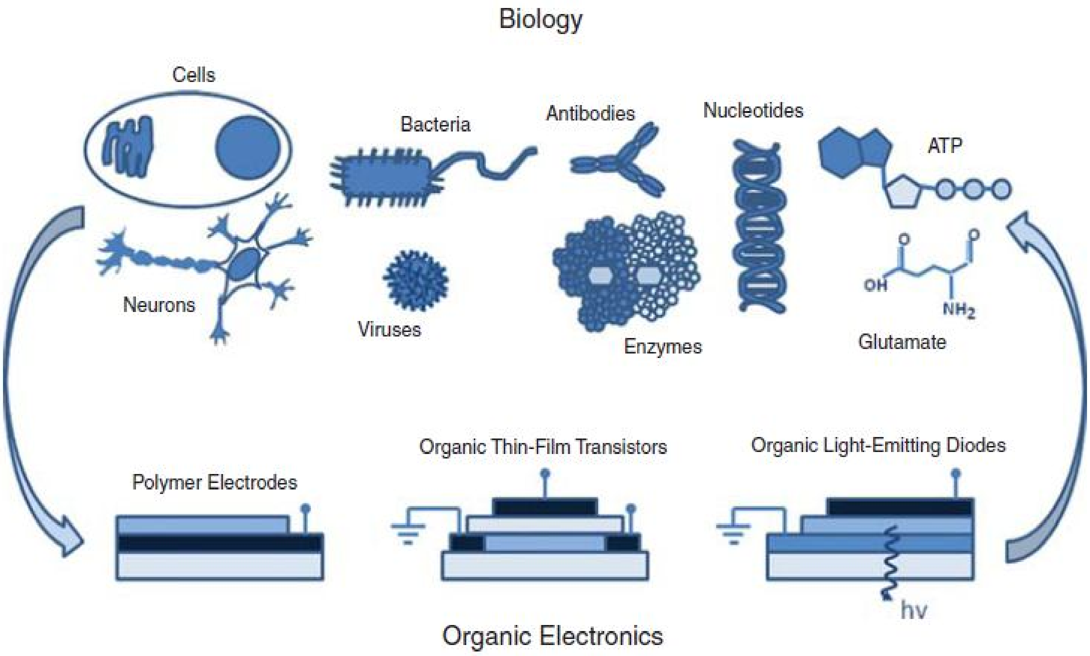

Figure 11 *A cartoon showing the scope of organic bioelectronics. Biological systems can be interfaced with organic electronic devices to yield biosensors, medical diagnostics, and tools with great impact in health care. (Reproduced with permission from R. Owens et al.,*[102] *© (2010) MRS).*

In the last decade, a considerable number of applications have already been developed by interfacing organic conductors to biology. Sensors for a wide range of biological molecules (neurotransmitters,[103] antibodies,[104] DNA[105]) and cell-based sensors[106–109] are only few examples. Recently, some emerging developments of organic electronics in neuroscience have also been reported,[110] consisting of the control of electronic ion signalling in individual cells,[111] monitoring of brain electrical activity[112] and delivery or detection of neurotransmitters.[113,114]

1.1.6. Aim and outline of this work

This Thesis sets within the context of organic bioelectronics described above. In particular, sensors and actuators based on organic conductors were interfaced with biological or biologically-relevant systems. On one hand, OECTs based on PEDOT:PSS were developed and studied for sensing and monitoring both eumelanin, an interesting biological molecule, and functionalized nano-particles, an example of nano-system for drug delivery. Aiming at paving the way of sensing, OECTs were also used for in vitro toxicology with the real-time detection of cellular stress induced by drugs. On the other hand, the conductive properties of organic conductors were exploited to study the influence of surface properties, such as the oxidation state, on the ability of bacterial cells to adhere, proliferate and form biofilms (see Section **1.4**).

This thesis is organized in 6 chapters. **Chapter 1** is intended to provide the motivation and the scientific background of the different topics treated in the next chapters, in order to offer a proper introduction to them. **Chapter 2** contains a first application of OECTs, that involved the sensing of pigment molecules, such as eumelanin. In **Chapter 3** a second application of OECTs is described, related to the detection and monitoring of magnetic nanoparticles functionalized with polymeric shell Control of bacterial adhesion and biofilm formation by means of conducting polymers is the central topic of **Chapter 4**. The topic of **Chapter 5** is the interfacing of OECTs with biological systems, such as mammalian cells, to develop a system for sensing the cellular stress induced by drugs. Finally, **Chapter 6** contains some conclusive remarks and perspective on the results achieved in this work.

1.2. Sensing biologically-relevant molecules

1.2.1. Biosensors and the demand for sensing of biomolecules

The most recent developments of medicine are increasingly oriented towards diagnostics based on molecular markers. In addition, highly specific therapies aimed at molecular targets and the necessity for high-throughput methods for the detection of biomolecules, concomitantly increases. Thus, technology platforms providing reliable, sensitive, rapid, quantitative, and cost-effective identification of biomolecules are becoming more and more important in clinical diagnostics and treatment.

Biosensors are, hence, receiving increasing interest for biomedical as well as environmental and industrial diagnostics.[115] A biosensor is an analytical device which integrates a biological recognition element with a physical transducer to generates a measurable signal proportional to the concentration of the analytes.[115] In such a device, the biological recognition element responds to the target compound and the transducer converts the biological response to a detectable signal, which can be measured electrochemically, optically, acoustically, mechanically, calorimetrically, or electronically, and then correlated with the analyte concentration. Various biological recognition elements, including cofactors, enzymes, antibodies, microorganisms, organelles, tissues, and cells from higher organisms, have been used in the fabrication of biosensors.[116] Biological sensing in aqueous solutions is particularly well suited.

1.2.2. Eumelanin: a test case of interesting biomolecule

Melanin is the most important class of chromophores in animals, plants, and microorganisms, and includes mainly eumelanin, pheomelanin, and neuromelanin. In the case of humans, the ability of specialized cells to synthesize the brown-black eumelanin and yellow-reddish pheomelanin dictates, to a large extent, the degree of pigmentation of skin, hair and eyes. Eumelanin is commonly accepted to be a heterogeneous macromolecule of 5,6-dihydroxyindole (DHI) and its 2-carboxylated form 5,6-dihydroxyindole-2-carboxylic acid (DHICA), and it is produced by oxidative polymerization of DHI and related metabolites.[117] The function of melanins is defined by their physical and chemical properties. For instance, the dynamic response of human skin and eyes to sun exposure and oxidative stress relies on the unique physicochemical properties of eumelanin.

The central role of eumelanin in skin and eye photoprotection, free radical scavenging and melanoma genesis[118–120] has prompted intense studies across biology, chemistry, and physics to gain insights into the intriguing mechanisms by which damaging UV radiation and reactive oxygen species are efficiently captured and quenched by this biopolymer. Parallel to the rapid advances in the elucidation of the primary structure and supramolecular architecture of natural eumelanin,[121,119] considerable attention has been focused over the past decade on the development of synthetic mimics for technological applications, including surface coating and thin films for organic electronics.[122]

1.3. Nano-particles and current detection techniques

1.3.1. Nano-particles: strong expectations and environmental concerns

One way to define our time could certainly be the nano-era, since nanoparticles (NPs) and nanosystems (NSs) are playing a growing overwhelming role in science and technology, and represent one of the driving forces toward the new paradigm of converging of sciences and technologies.

NSs are more and more multifunctional with application in a variety of fields, the list of which is everyday increasing.[123–127] Together with the enormous scientific and technological impact there is a fast and growing need of controlling and monitoring in real-time their presence, properties and evolution in different environmental conditions. This need comes from the interest in finely engineering their functions, and hence applications, but also from giving an adequate response to questions concerning pollution and health that are being raised and that could hamper the social acceptance of nano-based technologies.[128–131] Therefore, big efforts have been devoted to the development of techniques for sensing and characterization of NSs, especially in aqueous environment: to this end sensitivity, low-cost, feasibility and real-time response are considered key features.

NSs are being made by any kind of materials ranging from inorganic (i.e. carbon, silica, metals and oxides**),**[132–135,125,126] organic (phospholipids, lipids, chitosan, dextran, lactic acid),[136,137] hybrid organic/inorganic/biological,[138,139] including all possible combination and functionalization processes. Moreover, NSs with a large variety of structures have been developed in the past few decades: core-shell structures[140]; liposomes[141], which may enclose a magnetic core or act directly as drug-carrier; micelles[142,143]; fullerenes[144]; dendrimers[145]; and particles embedded within hydrogels.[146]

Most exploited properties of NSs include their surface to volume ratio, their quantum response arising when confinement takes place and their ability to adsorb and carry other compounds as, for example, in drug delivery applications.

The astonishing growth of this field is driven by the great added value of applications such as nanoelectronics[147], environmental remediation[127], cosmetics,[148,149] catalysis,[150] food packaging[151], medical healthcare[152] and consumer products[153] expected to give relevant social impact. Nevertheless, diffusion of engineered nanomaterials into commercial products and industrial solutions has inevitably generated the need of their easy, real-time and sensitive detection and monitoring at the different stages of synthesis, processing, product preparation and operation up to the end of their technological life. In fact, each of the needed scientific and technological steps strongly rely on the ability to sense and monitor in real-time the NSs, possibly recognizing the evolution of their properties under different environmental conditions.

Another crucial point is the social interest in environmental and health-related issues that could generate also social alarm. As it is well known, toxicity of fine and ultra-fine particles released by processes involving combustion have gained particular relevance [154]. Being those ultra-fine particles recognized as relevant environmental pollutants , manufactured NPs are suspected to have similar adverse effects. Many studies on eco- and bio-toxicology of NPs have been conducted to clarify the concerns about their risks and benefits[155,129,128] Studies about the real hazard of NPs are demonstrating a strong variability depending not only on size but also on specific properties such as crystal structure, morphology, functionalization and so on. For each nanosystem there is hence the need of a specific assessment of possible effects on the human health and the environment. As such effects became known, detection and monitoring devices as simple and cheap as possible become increasingly needed. Many methods have been used and specifically developed to detect and quantify manufactured NPs, each of which with its advantages and drawbacks. It should be mentioned that the largest part of the methods have been specifically described for metallic NPs (in particular gold NPs (Au-NPs) and silver NPs (Ag-NPs)), for metal oxides and for polystyrene. Au-NPs and Ag-NPs represent interesting nanosystems to be monitored because of their remarkable optical and antibacterial properties[156,157], respectively. Metal oxides NPs, and in particular those made of magnetic materials such as magnetite or maghemite, are more and more widespread in nanomedicine applications such as magnetic resonance imaging, hyperthermia and drug delivery.[158–160] The optical detection of microbiological agents, e.g. viruses, is difficult because of their small size, weak interaction with photons and low index contrast to the surrounding environment. Methods for detection and sizing of single low-index NPs that mimic microbiological agents (such as polystyrene NPs) are a promising route to develop suitable techniques for pathogen identification.[161]

In this part of **Chapter 1**, it is presented an overview of the methods for sensing nanostructured materials and some of their properties, discriminating between methods involving large or bulky instrumentations and methods based on small-scale devices. We then proceed to compare these techniques with the emerging capabilities of OECTs.

1.3.2. Sensing NPs by intrumental methods

Optical and microscopy methods require typically large or bulky systems and often are difficult to be used in real-time monitoring over different time-scales. On the other hand, they offer a very highly sophisticated level of information with details that are very relevant to understand properties of the nanosystems and possibly their dynamics.

NPs are typically below the diffraction limit of light in the visible range and, therefore, below the limit of detection of optical microscopy. Nevertheless, the performance of optical techniques such as confocal[162], near-field optical microscopy, Raman spectroscopy[163], and fluorescence microscopy[164] have been extended by strategies aiming at overcoming the diffraction limit of visible light, so that they have been widely used for single NP/molecule detection and studies. Microscopy techniques based on electron and scanning probes are ideally suited for the *nm* range. They are routinely used for visual imaging of NPs, but also for their physical characterization of shape, size, structure, and aggregation[165–167]. Unfortunately, sample preparation methods are very often required, with or without specifically tailored supports, that could give rise to artifacts or unwanted modification of the NS. This requires a skilled and careful knowledge of the methods used and of the NSs under studies, so that the artifacts could be minimized or avoided. The dynamics of NSs will then be derived by the sequence of snapshots obtained by studying the different stages of the evolution of the NS under study.

Dynamic Light Scattering (DLS) or UV-Vis spectrophotometry allow *in situ* studies and are commonly used for NPs sizing and physical characterization, as well as for label-free detection. It is very useful for measuring such basic properties, even for complex NSs, but it often requires other independent information on the NSs to give a definite understanding of the structure and evolution of the systems and of their interaction with the fluid environment in which they are immersed. Deconvolving the properties of the NSs from the DLS data is somewhat cumbersome, if ever possible, without information coming from other characterization methods. To overcome the problems related to the extremely small scattering cross-sections of single NPs, several adjustments to the original technique have been described. One example is laser-induced breakdown detection (LIBD), a novel, high sensitive and non-invasive method for the determination of both concentration and mean diameter of NPs in liquids. Compared with other methods, it has a much lower detection limit and is able to detect NPs down to the 10-nm range[168].

As mentioned, there are obvious drawbacks when bulky and expensive instrumentations are used, where often high vacuum and complex sample preparation are involved. Furthermore there is a strong demand of devices that would avoid long processing time, the need for labeling, that will make possible real-time detection and monitoring NSs in the environment or in situ for biomedical and industrial applications.. The aim of achieving portable, inexpensive and high-resolution devices capable of real-time and *in-situ* detection of particles, still requires strong efforts. In the following, we give an overview of some relevant techniques and devices developed so far.

In recent years, several studies have focused on detection of low index NPs by interferometric methods, which rely on interference of the scattered wave with a reference wave with the use of the same wavelength for detection and excitation (or probing). The main advantage of using interference in respect to usual scattering techniques is the increased sensitivity as the signal varies only with the third power of the particle size in contrast to Rayleigh scattering which scales with the sixth power limiting it to detection of particles larger than ~30 nm in diameter. Interferometric detection and characterization of low-index NPs has been shown to be highly sensitive[169] and capable of real-time detection[170,171]. Many works have already been published to this end, mainly on interferometry applied to the detection of polystyrene nanobeads[161,172] and metal NPs.[173,174]

Detection of metal NPs and ions, in particular silver, in solution has also been reported, where fluorogenic effects [175,176] or electrochemical oxidation[177] were involved.

Finally, magnetic fields were also used to detect super-paramagnetic NPs (Fe_3O_4), by detecting the little changes in the net magnetic induction induced by their presence.[178]

1.3.3. Sensing NPs by small-scale devices

Real-time, *in-situ* detection and sizing of single NPs, down to 30 nm in radius, was achieved by Zhu *et al.*[179] using scattering induced mode-splitting in an ultra-high Q whispering-gallery-mode (WGM) microtoroid resonator. This technique takes advantage of the strong light-matter interaction which allows for ultra-sensitive optical detection. Moreover, noise suppression, accurate size information, no need for NP labeling or *a priori* information on their presence in the medium are provided, as well as applicability to aqueous environment.

Detection of NPs is indirectly relevant also for biological diagnostics. For biomolecules detection, Wang *et al.*[180] used super-paramagnetic NPs as magnetic tags and detected by biochips based on giant magnetoresistance (GMR) spin valve

(SV) sensor arrays. The SV sensor array (detector), fabricated by optical or e-beam lithography, is bound with known biological probe (e.g., DNA); unknown DNA fragments are labeled by magnetic nanotags; finally, tagged DNA strands are selectively captured by complementary DNA probes, and the magnetic nanotags are read out by SV sensors. The peak-to-peak resistance change of SV sensors before and after capturing magnetic nanoparticle tags is defined as the signal. Sv structures based on GMR[181,182] was chosen as detector because of their high field sensitivity at room temperature, but also for many other technological and economic advantages. Detection of a single nanotag can be reached with molecular detection (of proteins or DNA, for instance) well below 10 pM in concentration. The combination of spin valve sensor arrays and magnetic nanotags allows for a sensitive, quantitative, non-optical detection system for many different biological assays. These devices revealed to be ideal for measuring multiple protein levels in a volume of only 10-50 μl of blood sample.

A microfluidics analyser for rapid electronic detection and volumetric analysis (concentration and size) of individual NPs in complex and unlabelled suspensions was presented by Fraikin *et al.*.[183] This device, combining microfluidic design with a high-throughput electrical readout, include some main features: two external voltage bias electrodes, a sensing electrode, a fluid resistor, a nanoconstriction, and some pressure-regulated fluidic ports. A ionic electrical current in the saline suspension containing NPs is generated by applying constant voltages to the two bias electrodes. NPs flow towards the nanoconstriction and changes in the electrical potential of the fluid adjacent to it are detected by the sensing electrode, through changes of the sensor electrode potential V_{out}. The voltage signal V_{out} is proportional to the NP volume, allowing particle sizing down to ~50 nm. Moreover, this analyser is capable of measuring directly the absolute concentration of particles in a multicomponent mixture. Transit times as small as 2-3 μs can be easily resolved, with a maximum particle count rate exceeding 500,000 particles per second. Low cost, high-throughput, scalable fabrication and simple readout electronics make this analyser well suited for several sensing applications, for instance dealing with viral detection in plasma.

1.4. Bacterial biofilms and biofouling

In liquid environments, bacteria and other microorganisms have developed a universal strategy for survival, which consists of the formation of sessile communities, enclosed into a self-produced polymeric matrix (EPS, extracellular polymeric substance), described as biofilms (**Figure 12**).[184] This natural colonization of most biological or non-biological submerged surfaces from microorganisms is known as biofouling. Biofilm forming bacteria display characteristic physiological traits that distinguish them from their planktonic counterparts. The structures that form in biofilms contain channels in which nutrients can circulate,[185] and a secreted matrix composed of a complex mix of chemical species; essentially water (97%), but also secreted/released exopolysaccharide polymers (cellulose, PGA, colanic acid),[186,187] proteins, nucleic acids, lipids/phospholipids, absorbed nutrients, and metabolites.[188,189] Mature biofilms correspond to three-dimensional structures, from which sessile biofilm communities can give rise to non-sessile individuals, planktonic bacteria that can rapidly multiply and disperse, colonizing new surfaces. Initial bacteria adhesion involves a reversible attachment process, which is strongly influenced both by environmental conditions such as pH and the ionic force of the medium or the temperature,[190] and by the nature of the surface itself (e.g. rugosity or hydrophilicity).[191] Moreover, cell surface structures of the fimbrial family, such as type I pili, type I fimbriae, curli, flagella, and conjugative pili, play also a relevant role in determining the bacteria-to-surface interaction.[192–195]

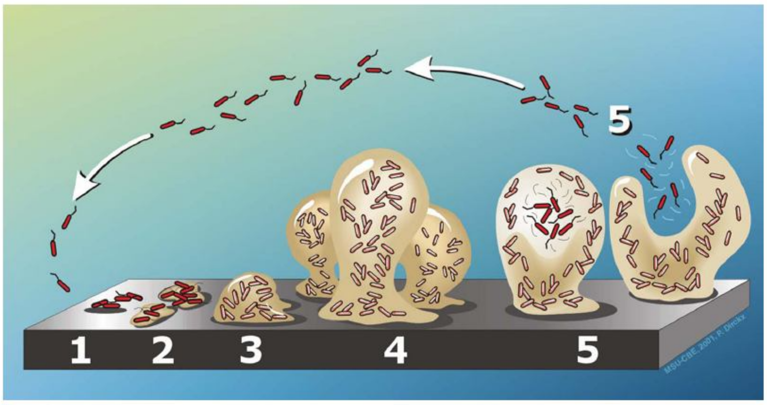

Figure 12 *Developmental stages of biofilm formation (Reproduced with permission from P. Stoodley et al,.*[196] *© (2002) Annual Reviews).*

Biofilms constitute a protected mode of growth that allows survival in a hostile environment. They are characterized by increased tolerance to stress, biocides (including antibiotics) and host immunological defences, which is at the origin of their resilience in most medical implants (catheters, prosthesis, stents, etc.),[197–199] food handling equipments[200] and industrial facilities.[201–203] The negative connotations of biofilms are manifold: from a medical perspective, bacterial biofilms on implants or catheters are of great concern because they can represent the source of recurrent or chronical infections. In many industrial activities, biofouling can reduce mass and heat transfer and increase corrosion. For the food industry, the formation of biofilms on food or food-contact surfaces and in potable water distribution systems constitutes an increased risk for product contamination.[204,200,205] The critical issues associated with biofouling include increased operational and maintenance costs and the degradation of abiotic materials. In addition, biofilm resistance has been subscribed to a variety of different mechanisms; mainly failure of an agent to penetrate the full depth of the biofilm, that retards the diffusion of biocides and slow-growing or starved state, which makes cells not very susceptible to many stress or biocide agents.[206–208] Although there are many negative connotations for biofilm formation, there are also successful cases in which biofilms are beneficial.[209] For instance, biofilms can be used in bioremediation, an emerging *in situ* technology for the clean-up of environmental pollutants (such as hydrocarbons or heavy metals) using microorganisms.[210] In some other cases, beneficial biofilms are capable of decreasing biological corrosion of mild steel, by means of several possible mechanisms (removal of corrosive agents by bacterial physiological activities, growth inhibition of corrosion-causing bacteria by antimicrobials generated within biofilms, and generation of protective layer by biofilms).[211] Other interesting applications of biofilms involve their use in bioreactors either for wastewater treatment or for the production of desired compounds, such as secretion enzymes, acetic acid or vinegar.[212]

Major approaches to controlling biofilm formation thus far have mostly concentrated on combating surface fouling by preventing biofouling agents from attaching or by degrading them.[213] The techniques employed to these purposes involve: the functionalization of surfaces with self-assembled monolayers (SAMs)[214] or polymer brushes based mostly on poly(ethylene glycol) (PEG) and its derivatives;[215–217] the design of coatings that release biocidal agents (silver, antibiotics, nanoparticles, polycations, enzymes, and antimicrobial peptides) into the surrounding aqueous environment;[218–222] and optimized surface topography.[223]

Most recent studies conducted on bacterial biofilms have used a limited selection of model bacteria, including *Escherichia coli.* (*E. coli*). In fact, this species being typically of faecal origin, *E. Coli* is used as an indicator of the sanitary quality of water and of the food-processing environment.[224,225]

1.5. Cellular stress and death

Monitoring cellular viability in response to drugs is of fundamental relevance for pharmaceutical research and for optimization of drugs treatments. Cell death can be classified according to: its morphological appearance (which may be apoptotic, necrotic, autophagic or associated with mitosis); enzymological criteria (with or without the involvement of nucleases or of distinct classes of proteases); functional aspects (programmed or accidental, physiological or pathological) or immunological characteristics (immunogenic or nonimmunogenic).[226] Cell death is typically discussed dichotomously as either apoptosis or necrosis. Apoptosis, expression coined by Kerr *et al*. In 1972,[227] is described as a programmed cell death and is an important mechanism of normal cellular population control. It is accompanied by several among the following morphological features: rounding-up of the cell, retraction of pseudopodes, reduction of cellular volume, chromatin condensation, nuclear fragmentation. Classically there are little or no ultrastructural modifications of cytoplasmic organelles, while there is plasma membrane blebbing but maintenance of its integrity until the final stages of the process.[228] Necrosis has been described as passive, accidental cell death resulting from environmental perturbations with uncontrolled release of inflammatory cellular contents. Apoptosis occurs normally during development and aging, and as a homeostatic mechanism that allows the organism to tightly control cell number and tissue size. Necrosis is morphologically characterized by a gain in cell volume (oncosis), swelling of organelles, plasma membrane rupture and subsequent loss of intracellular contents. Anticancer drugs, for instance, can inhibit proliferation and induce death in sensitive tumor cells.[229] Their cellular targets can be diverse, according to several cytological factors. Thus, anticancer drugs are classified as DNA-damaging agents (cyclophosphamide, cisplatin, doxorubicin), antimetabolites (methotrexate, 5-fluorouracil), mitotic inhibitors (vincristine), nucleotide analogs (6-mercaptopurine), or inhibitors of topoisomerases (etoposide). Doxorubicin is an anthracycline antibiotic possessing strong antineoplastic and antimetastatic activity, beyond cytotoxic and cytostatic effects.[230] It is one of 10 drugs which are the most frequent used in cancer chemotherapy[231] and is known to have an apoptotic-inducing effect on cancer cells.[232] A wide number of methods are commonly used for cell-death detection: agarose gel electrophoresis,[233] caspase-3 quantification,[234] Tunel (TdT-mediated dUTP nick-end labeling) assay,[235] morphological characterization on stained (Hoechst 33342, propidium iodide) or unstained cells using light-, phasecontrast- and fluorescence-microscopy, flow cytometry for DNA cleavage residuals.[236]

Chapter 2

2. Monitoring electrical activity of eumelanin

2.1. Introduction

Three peculiar yet highly elusive properties of eumelanin have especially intrigued physicists and materials scientists: their black chromophore, with a broad featureless optical absorption and near unity non-radiative conversion of absorbed photon energy; their paramagnetic character, revealed by a permanent signal in the electron paramagnetic (EPR) spectrum; and their electrical behaviour showing photoconductivity in the solid state.[118] Elucidation of these properties may provide new impetus towards application of eumelanin as soft, biocompatible and bioavailable functional polymer for organo-electronic devices and biointerfaces. Prospects in this field are exemplified by the burst of technological research on poly-dopamine, a peculiar eumelanin-like biopolymer resembling neuromelanin[237,238] produced by the auto-oxidation of dopamine at alkaline pH, which combines unique adhesion properties[239] with semiconductor-like behaviour.[240,122] Although early observations supported an amorphous semiconductor-like behaviour,[241] more recent studies demonstrated that optical and electrical properties of eumelanin can be better accounted for by alternative models, e.g. the chemical disorder model,[242] which takes into account a supposedly high molecular heterogeneity and the lack of a well defined optical gap. These concepts, together with the strong dependence of the electrical and EPR properties on the degree of hydration, support the idea that eumelanin behaves like an electronic–ionic hybrid conductor.[243] Electrical conductivity would thus be induced by hydration, which defines the balance of comproportionation/disproportionation equilibria between hydroxyquinone, semiquinone and quinine species so as to dope electrons and protons into the system, opening exciting possibilities for bioelectronic applications such as ion-to-electron transduction.

Despite the increasing recognition of both pro-oxidant and antioxidant behaviours of eumelanin with important medical implications, electrical characterization of this polymer has been carried out for the most part on thin films or bulk solids, since colloidal eumelanin particles have been reported to be typically electrochemically silent.[244]

On this basis, direct investigation of eumelanin electrical response in a more biomimetic aqueous suspension state is a challenging issue in view of the possible development of a biosensor aimed at assessing biopolymer concentration and redox state in its environment. Dysfunctions in eumelanin levels have been associated with different disorders, from melanoma (the most diffuse skin cancer) to neurodegenerative disorders, and the direct determination of eumelanin redox states and levels in a pathological setting is an ambitious yet highly desirable goal.

As already mentioned, we have chosen organic electrochemical transistors based on PEDOT:PSS as the device of choice, since they have emerged as an ideal platforms to interface bio-signalling with electronics.[245,246] These devices appear to be most suited for biosensing, due to their ability to work in liquid environments at low voltages (<1 V). In this respect, several studies dealing with OECTs as sensing devices for different species of analytes, such as hydrogen peroxide,[88,247] glucose[93,248] or ions,[90] have been published.

In this Chapter, we demonstrate that an organic electrochemical transistor based on PEDOT:PSS can be used as a biosensor device allowing for the first time detection and characterization of a colloidal suspension of a synthetic eumelanin from DHI. With detection sensitivity up to 10^{-6}M formal concentration, the OECT is the first purposeful device to detect insoluble redox-active materials and to provide insights into their electrical behaviour in aqueous suspensions by analysis of the gate current.

2.2. Experimental

2.2.1. Device fabrication and characterization

Design and fabrication of the OECTs followed the protocols already discussed by Malliaras' group in other papers[249,88]. A Parylene C layer was deposited on a glass slide of 2.5 x 7.5 cm by chemical vapour deposition. Standard photolithography was used to pattern this layer, followed by a dry etching using O_2 plasma. The degenerately doped semiconductor PEDOT:PSS was then spin-coated at 1500 RPM for 30 s from a commercially available dispersion (PH-500 from H.C. Stark). This dispersion was supplemented with ethylene glycol 20% (Sigma Aldrich) to enhance its electrical conductivity and with a 5% of dodecyl benzene sulfonic acid (DBSA) surfactant (Sigma Aldrich) to improve film formation.[250,251] The PEDOT:PSS film (100 μm thick) was briefly annealed at 120°C for 18 s and, subsequently, parylene was peeled-off. Finally, PEDOT:PSS was annealed at at 120°C for 60 min. The final device aspect ratio is L/W = 10 (channel width W = 1 mm, channel length L = 10 mm).

Sylgard 184, poly(dimethylsiloxane) (PDMS) mixed with a curing agent with a volume ratio 10:1 was used to fabricate a well (internal volume: 100 μL) for confining the electrolyte solution in contact with the polymer channel. The area of the polymer channel in contact with the electrolyte defines the active surface of the device.

A Pt metallic wire immersed into the electrolyte contained into the PDMS well was used as the gate electrode. **Figure 13** shows the schematic of an OECT device fabricated on a glass substrate.

2.2.2. Electrical measurements

Electrical measurements with the OECT device were obtained by a 2 channel source/measure precision unit (Agilent B2902A), controlled by a home-made LabView software.

The source electrode was grounded and the drain electrode was biased at -0.4 V (V_{ds}). The modulation measurements consisted basically in monitoring the drain current $I_{ds}(t)$ at increasing pulsed gate voltages (V_{gs}), in the range from 0 to 1 V with 0.2 V steps.

2.2.3. Synthetic eumelanin

Synthetic eumelanin was prepared by oxidative polymerization of 5,6-dihydroxyindole (DHI) with the orseradish peroxidase/ hydrogen peroxide system, as described previously.[252] Eumelanin concentration in aqueous suspensions is defined in terms of formal monomer concentration (DHI, Mw 149).

2.3. Results and discussion

2.3.1. The device

Figure 13 shows a schematic view of the OECT electrical circuit and the sensing mechanism in the case of eumelanin biopolymer dispersed at several concentrations in a Phosphate Buffered Saline (PBS) solution. The transistor channel is made of PEDOT:PSS. The gate electrode, aimed at inducing an electrochemical reaction in the presence of eumelanin, consists of a platinum wire, while source and drain electrodes are made of silver.

Figure 14a shows the output characteristics (I_{ds} vs. V_{ds}, at different gate voltages, V_{gs}) of the device measured in PBS 0.1 M with eumelanin at 10^{-9} M nominal concentration suspended in solution. The transfer characteristics (expressed as current modulation $\Delta I_{ds}/I_{ds,0}$ vs. V_{gs}, V_{ds} = -0.4 V) are shown in **Figure 14b** for the highest concentration of eumelanin (10^{-2} M) and for the PBS electrolyte solution based device, acting as a blank.

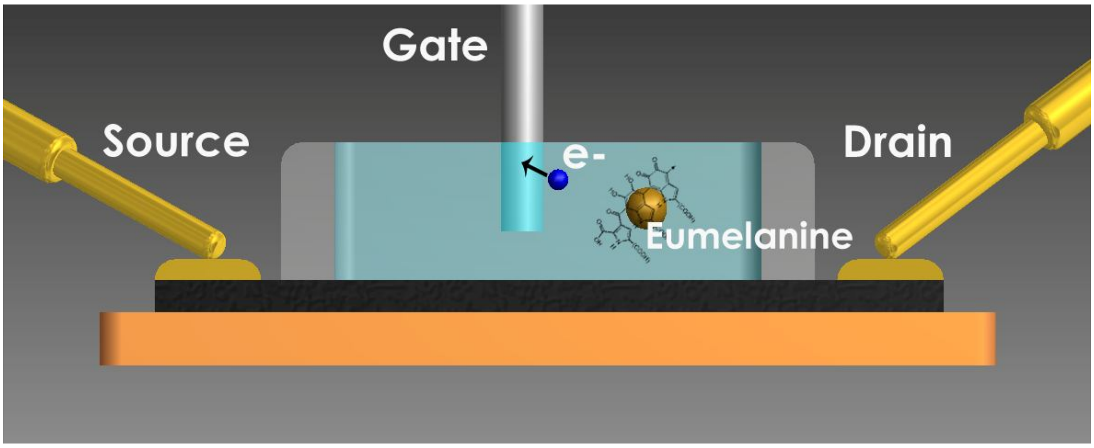

Figure 13 *Schematic diagram of the OECT-based biosensor for the detection of eumelanin pigment in colloidal suspension, here a saline electrolyte solution (PBS 0.1 M). The black stripe represents the active layer of PEDOT:PSS, the OECT channel being defined by the overlapping of the electrolyte with the polymer. The figure also represents the mechanism for the pigment detection, based on a redox reaction of eumelanin at the gate electrode. (Reproduced with permission from G. Tarabella et al.,*[95] *© (2013) Royal Society of Chemistry).*

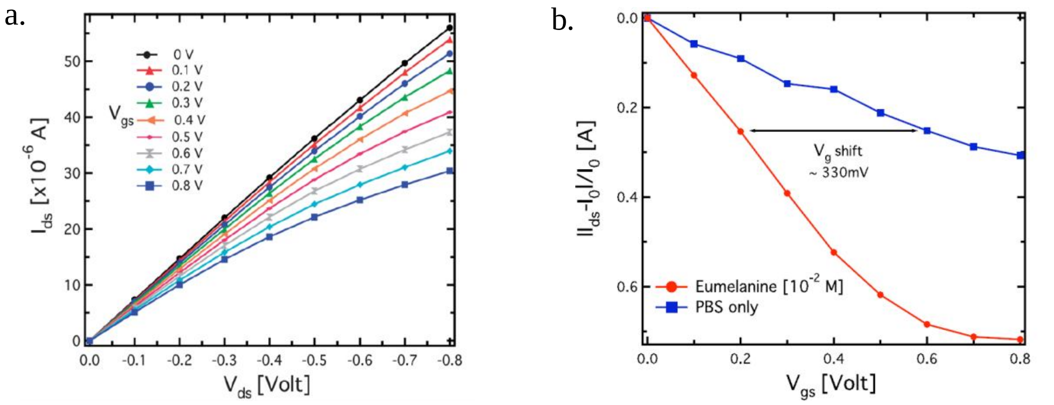

Figure 14 *a. Output characteristics of the OECT measured with eumelanin at the concentration of 10_9 M suspended in 0.1 M PBS. b. Transfer characteristics of the OECT with a Pt gate electrode characterized both with eumelanin in suspension and without (0.1 M PBS only),* V_{ds} *= 0.4 V. (Reproduced with permission from G. Tarabella et al.,*[95] *© (2013) Royal Society of Chemistry).*

Output curves were acquired by sweeping V_{ds} between 0 and -0.8 V, in steps of 0.1 V, at fixed V_{gs} between 0 and 0.8 V (V_g steps of 0.1 V). Transfer characteristics of OECT were acquired by measuring I_{ds} vs. time, fixing V_{ds} at -0.4 V and pulsing V_{gs} between 0 V and 0.8 V with a step of 0.2 V. The source–gate current (I_{gs}) was acquired simultaneously to I_{ds} in order to monitor the electron transfer reaction occurring at the gate electrode. The I_{gs} acquisition provides information both on the operational mode of the OECT, that is faradaic or non-faradaic mode,[90] and on the electrical and redox activity of the eumelanin components. It is assumed that catechol- type structures belonging to reduced DHI units undergo oxidation at the gate electrode providing electrons to the I_{gs} current of the gate circuit. For each step of the gate voltage applied across the gate electrolyte, the drain current was acquired for 60 s, e.g. a long time scale aimed at achieving a nearly steady drain current value for the related V_g, shown by a saturation of the channel current in time. The phosphate buffer solution (PBS) (pH = 7.2) was used as the electrolyte for all the measurements to ensure pH stabilization. The application of V_{ds} induces a drift of the holes along the PEDOT:PSS channel, generating a drain–source current (I_{ds}). As previously described, upon application of a positive gate voltage (V_{gs}), cations (M^+) from the electrolyte enter the PEDOT:PSS channel causing its de-doping according to Eq. 2. This is referred to as the de-doping process, as its effect causes a decrease in the modulus of drain current |Ids|.[87] This effect is due to the smaller number of holes available for conduction, as a consequence of incorporation of cations into the PEDOT:PSS backbone. Here, according to Eq. 2, cations tend to be adsorbed by the $PEDOT^+:PSS^-$ thin film causing a reduction of the oxidized $PEDOT^+$ and a consequent decrease of conductivity upon reduction to the reduced form $PEDOT^0$.

This process is reversible, in fact, when V_{gs} is switched off (V_{gs} = 0 V), ion diffusion occurs from the PEDOT:PSS to the electrolyte, increasing the number of conducting holes and, consequently, $|I_{ds}|$. Such a process is referred to as doping.[88] In this paper, the OECT current response is expressed as current modulation:

$$\frac{\Delta I}{I_0} = \frac{(I_{ds} - I_0)}{I_0}, \qquad \text{Eq. 6}$$

where I_{ds} is the drain current value measured for $V_{gs} > 0$ V and I_0 is the I_{ds} value for $V_{gs} = 0$ V.[88,90] The current values were determined from current transient measurements considering the quasi-steady state current level.

2.3.2. Eumelanin response in the OECT

Eumelanin sensing is based on the redox behaviour of the polymer in contact with the gate electrode. In more detail, oxidation of eumelanin units at the Pt gate electrode–electrolyte interface promotes electron injection into the gate electrical circuit. As a consequence, the OECT is said to work under a faradaic regime, characterized by a negligible potential dropping at the gate–electrolyte interface.[88,253] In this operating regime the applied gate voltage is almost entirely transferred as effective gate voltage (V_g^{eff}) acting at the electrolyte–polymer interface and the cations produced upon DHI oxidation in the electrolyte are forced to move toward the PEDOT:PSS by the gate voltage. The sensing mechanism would therefore be similar to the sensing of hydrogen peroxide,[253] halide,[90] or dopamine[254] previously reported with OECT devices operating in faradaic mode. However, in all the above cases the sensing process was aimed at monitoring soluble components, and the electrical behavior of insoluble polymer suspensions has been so far little explored.[118] **Figure 15**a shows the OECT response ($\Delta I/I_0$) as a function of the eumelanin concentration for two gate voltages (Vg = 0.3 V and Vg = 0.6 V). The dynamic sensing range spans between 1 x 10^{-6} M and 1 x 10^{-2} M, the signal becoming about 3-times larger for Vg = 0.6 V and reaching a modulation value close to 0.8 for the highest concentration of 10^{-2} M.

In detail, above 1.3 x 10^{-6} M the OECT response increases almost monotonically from a value of about 0.25 up to 0.79, indicating an increase of 0.54 in current modulation, corresponding to an increase of about 86% with respect to the base signal. In **Figure 14**b, showing the transfer curves of OECT characterized both without and with eumelanin suspension, the transfer curve shifts to a lower gate voltage (hundreds of mV), indicating that the effective gate voltage (V_g^{eff}) is increased due to the electro-oxidation of eumelanin at the Pt gate electrode. **Figure 15**b shows the expected gate current increase in the presence of eumelanin, such an increase being the fingerprint of the faradic mode of operation.[90,255]

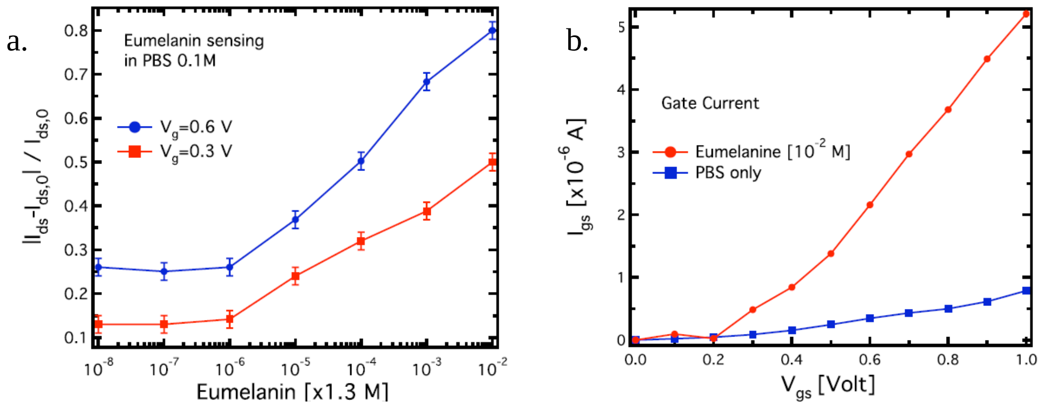

Figure 15 *a. Sensing plot (ΔI/I_0 vs. concentration) expressed as the OECT response at varying eumelanin concentrations. b. Corresponding OECT gate current flowing in the gate circuit, with (red curve) and without (blue curve, PBS electrolyte only) the eumelanin in suspension; when no pigment is present in solution, the OECT works in a capacitive (non-faradaic) regime. (Reproduced with permission from G. Tarabella et al.,[95] © (2013) Royal Society of Chemistry).*

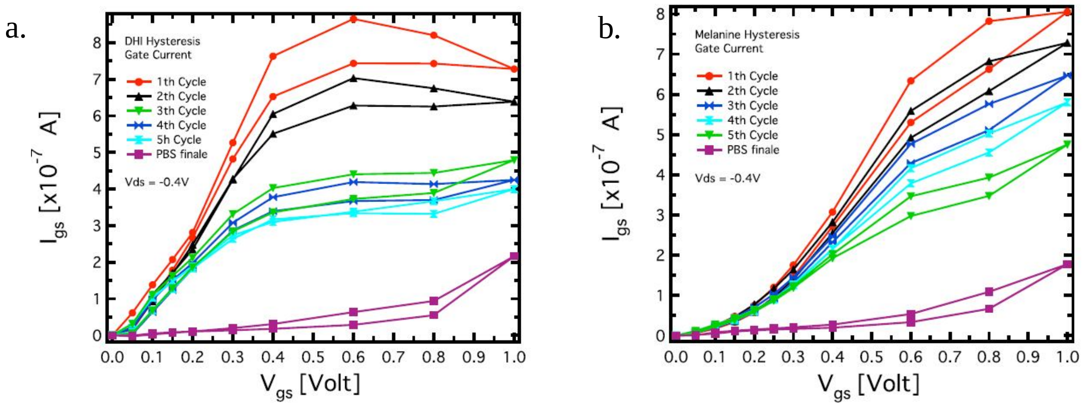

Figure 16 *Hysteresis loop cycles of the gate current acquired for DHI (a) and eumelanin pigment (b). V_{ds} = -0.4 V. (Reproduced with permission from G. Tarabella et al.,[95] © (2013) Royal Society of Chemistry).*

2.3.3. Eumelanin *vs.* DHI redox behaviour

A close analysis of the measured curves in the presence of eumelanin or DHI gave some qualitative insight into the effect of the ionic circuit (gate–source current, I_{gs}) on the underlying electronic circuit (drain–source current, I_{ds}). An initial consideration regards the PBS-based benchmark device, where the leakage through the gate related to the PBS solution provides the baseline for comparing eumelanin and DHI, since both I_{gs} (much lower than those exhibited by eumelanin and DHI) and the small hysteresis are preserved in different testing devices, denoting an excellent reproducibility. On this basis, analysis of OECT features may allow for a reliable comparison between the electrical properties of eumelanin and DHI.

Data in **Figure 16**a and b, obtained by recording cyclically (5 cycles) hysteretic I_{gs} loops in the presence of eumelanin- and DHI-based electrolytes, allowed for an insightful analysis of the ionic circuit. The data acquisition mode (i.e., long time scale between adjacent step voltages for the saturation of the polymer de-doping process) would ensure control of the hysteresis shape and minimization of memory effects[256] and/or trapping/de-trapping phenomena. Since a PBS based device does not display a faradaic behaviour in the presence of a Pt gate electrode, the observation that the initial gate current in the DHI- and eumelanin-based testing devices is almost 5 times higher than that recorded for the benchmark system would clearly provide a demonstration for the faradaic behaviour induced by the biopolymer and the indole monomer. Interestingly, the curves in **Figure 16**a and b show that both the gate current and the area subtended by each loop gradually decrease following each cycle, the latter approaching baseline behaviour.

Hysteresis is known to correlate to the mismatch between the scan rate and the time scale on which doping/de-doping occurs. On this basis, the hysteretic behaviour of eumelanin- and DHI-based devices would suggest a progressive and irreversible alteration of the samples associated with a decreased redox activity for both polymer and monomer following repeated modification of their redox states.[257] Consistent with this interpretation, a partial or complete loss of response was observed in the case of eumelanin samples that were allowed to stand for prolonged periods of time as suspensions without de-oxygenation or deep freezing.

The analysis of the shapes of the I_{gs} curves shows in the case of DHI a saturating behaviour starting at Vg = 0.6 V of gate bias, which is not apparent in the eumelanin-based devices, where a monotonic trend was visible in the spun gate voltage range. This behaviour could indicate that the redox activity of DHI is almost saturated at lower voltages compared to the eumelanin, in accord with a substantial conversion to less responsive polymeric components during the initial cycles. Generally, as mentioned above, a gate voltage shift is expected for faradaic like systems due to redox transformation of the analytes at the gate electrode, resulting thus in an effective gate bias drop at the dielectric– polymer interface. As a consequence, a more efficient ionic penetration inside the polymeric layer is induced and a stronger channel current modulation occurs at lower gate biases. This is observed as a shift toward lower gate voltage biases of transfer curves recorded in the presence of DHI or eumelanin relative to the PBS baseline prototype (see **Figure 14**b). Another important implication of the effective gate voltage can be shown by coupling the Bernard's equation of OECT source–drain current (Eq. 7) and the expression of the effective gate voltage (Eq. 8):[87]

$$\boldsymbol{I_{ds} = -\frac{G(V_g - V_p)^2}{2V_p}} \qquad \text{Eq. 7}$$

$$\boldsymbol{V_g^{eff} = V_g + (1+\gamma)\frac{kT}{2e}ln[M] + const.}, \qquad \text{Eq. 8}$$

where G is the conductance of the organic semiconductor, V_p is the pinch-off voltage, g is the ratio between the capacitances of the two interfaces (electrolyte–PEDOT:PSS and electrolyte– gate),[253] k is the Boltzmann's constant, T is the absolute temperature and e is the elementary charge. As a result, a linear dependence of the source–drain current on the logarithm of the concentration is predicted:

$$\boldsymbol{I_{ds}} = \frac{\boldsymbol{G}}{\boldsymbol{V_p}}\frac{\boldsymbol{kT}}{\boldsymbol{2e}}\ln\,[\boldsymbol{M}]] + \boldsymbol{cost}(\boldsymbol{V_g}, \boldsymbol{V_p}) \qquad \text{Eq. 9}$$

This linear relationship between I_{ds} and ln[M] was experimentally confirmed, as shown in **Figure 15**a, where the curves of the OECT response as a function of ln[M] are nearly linear in the dynamic range investigated (that is from 10^{-6} M up to 10^{-2} M).

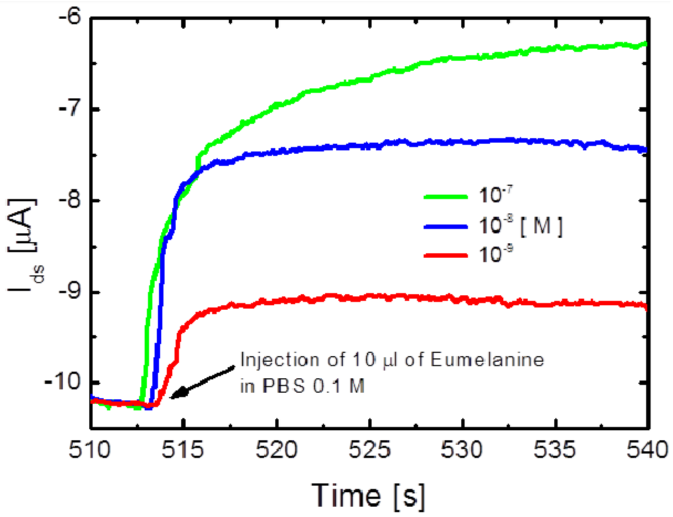

Figure 17 *Drain–source current vs. time of the OECT characterized upon addition of a 10 mL drop of eumelanin at different concentrations. It is found that the lowest eumelanin detection limit of OECT in real-time mode is 1 x 10^{-9} M. The black arrow represents the exact time of injection of the drop. (Reproduced with permission from G. Tarabella et al.,[95] © (2013) Royal Society of Chemistry).*

2.3.4. Real-time monitoring

In order to study the drain current evolution at fixed voltages, I_{ds} was monitored upon *in situ* addition of eumelanin. The OECT response was monitored in real-time (V_{gs} = 0.6 V, V_{ds} = -0.4 V) following injection of 10 mL eumelanin suspension during acquisition. **Figure 17** shows that in real-time mode the OECT sensor is eumelanin-sensitive down to the nM range, the sensor reacting almost instantaneously with a rapid relative change of the drain current (ΔI_{ds} ~1 mA) in less than 3 s. A more significant |Ids| decrease was observed at higher concentrations (10^{-8} to 10^{-7} M). Since the sensitivity of the OECT device is higher in the real-time monitoring mode compared to the dynamic range achieved by the modulation response, as previously observed with other bioanalytes,[254,99] it can be concluded that we could achieve a10^{-9} M detection limit for the eumelanin pigment in the present device configuration.

2.3.5. Towards a chemical model for eumelanin electrical response

Eumelanin formation from DHI is known to involve oxidative polymerization of indole via the 2-, 4- and 7-positions of the indole ring to give mixtures of oligomeric/polymeric chains at various levels of oxidation (Scheme 1). Depending on the reaction conditions, the redox characteristics of the environment and the extent of polymer exposure to oxygen and other oxidizing agents (i.e. the extent of "aging"), the relative proportion of reduced (catechol, DHI) versus oxidized (indolequinone) units may vary significantly.

Both the key features of the curves in **Figure 16**b, i.e. the progressive decrease in gate current and hysteretic loop areas, would suggest that in fresh eumelanin samples the catechol– quinone units are initially "frozen" by the mode of aggregation of the molecular components into a redox state that is far from the equilibrium and that the repeated redox interaction with the gate electrode provides the input for a progressive redistribution of the redox centres within the polymer, leading eventually to a more stable, overall less responsive electronic arrangement.

In line with this view, the low or null response of “aged” eumelanin samples might suggest either a higher degree of oxidation of indole units or the slow spontaneous attainment of the final equilibrium conditions between the interacting redox centres of the polymer aggregates.

On the other hand, the analogous behaviour of DHI in solution may be interpreted by assuming that the initial oxidation product, 5,6-indolequinone, as soon as it is generated, is immediately trapped by the excess reduced indole present in solution to give eumelanin-like intermediates that irreversibly alter the analyte electric response after each cycle.

Since injection of electrons from the eumelanin into the gate electrode can occur only from reduced DHI units (Scheme 2), the voltage values determined by the OECT device may be taken as roughly reflecting the proportion of reduced indole units in the polymer. It is noted that DHI unit oxidation results in the generation of protons in the medium, which may be involved in the ionic circuit.

An interesting implication is that, taking the OECT response of monomer DHI in solution as the maximum response of a hypothetical, fully reduced eumelanin sample, with the null response of an oxidized (aged) eumelanin sample at the opposite extreme, it could be possible in principle to gain information about the average redox state of a given polymer sample simply by determining its onset voltage relative to that of DHI. From the data in **Figure 15**, for example, it can be concluded that the oxidation potential of the investigated eumelanin samples approaches a value that is around 200 mV, suggesting a similar proportion of reduced catechol units. This is a rough estimation and a more accurate evaluation requires the application of narrower gate bias steps below 200 mV. It would be interesting to compare these data with those obtained in a previous study on the electrochemical behaviour of DHI polymer films,[258] which gave an oxidation potential $E_{1/2}$ of 150 mV. Therefore our interpretation of the threshold oxidation potential could be reasonable.

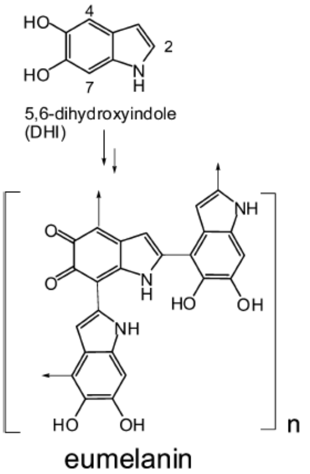

Scheme 1 *Simplified view of eumelanin formation by oxidative polymerization of DHI. A representative structural motif is highlighted, showing the coexistence in the polymer of oxidized (quinone) and reduced (catechol) units. (Reproduced with permission from G. Tarabella et al.,*[95] *© (2013) Royal Society of Chemistry).*

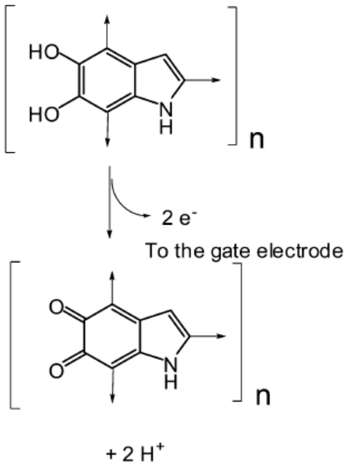

Scheme 2 *Schematic illustration of eumelanin oxidation at the gate electrode. Reduced DHI units release two electrons and two protons to generate oxidized quinone units. (Reproduced with permission from G. Tarabella et al..*[95] *© (2013) Royal Society of*

2.4. Conclusions

In this chapter it has been described the characterization of the electrical properties of an insoluble eumelanin sample as an aqueous suspension using OECT technology. The most interesting finding of this study, that deserves further investigation, is the high sensitivity of the device response to eumelanin, supporting a hitherto unrecognized versatility of the OECT for sensing insoluble redox active materials. In this respect, gate current analysis underscored the ability of the dynamic DHI– quinone system in the fresh eumelanin biopolymers to exchange electrons with the gate even under heterogeneous phase conditions by shuttling between accessible redox states.

Noteworthy is also the observed abatement in current intensity with decreased hysteretic loop area after each cycle suggesting irreversible conversion of eumelanin from an originally unstable electronic arrangement toward a p-equilibrated state less responsive to the gate electrode. Elucidation of the processes underlying gate current characteristics and hysteretic behaviour of eumelanin may not only guide ongoing efforts toward the rational design and implementation of bio-inspired devices with tailored electrical behaviour for bio-electronics, but may yield new insights into the redox properties of the biopolymer that have otherwise escaped previous investigations.

Chapter 3

3. Sensing functionalized nano-particles

3.1. Introduction

3.1.1. Functionalised Super Paramagnetic Iron Oxide NPs

In this chapter it is described and discussed for the first time the efficient detection of polymer-coated Super Paramagnetic Iron Oxide NPs (SPION) by means of OECTs.

Magnetic NPs (MNPs) have a relevant role especially for biomedical applications. They have been widely used in medicine[259,260] and existing applications include magnetic resonance imaging (MRI)[261,262], drug delivery[263], hyperthermia treatment of cancerous tumors[264], and production of improved biocompatible materials. The biocompatible coating is important in order to hide SPION to the host immune system, and can be loaded with drugs or chemicals to be addressed to specific regions of the body.

Dealing with drug delivery applications, functionalized SPION have been increasingly used in pharmaceutical sciences to reduce toxicity and side effects of drugs. Indeed, chemotherapic drugs delivered by NPs show reduced systemic distribution and also allow to use lower but more accurately targeted doses of chemical compounds. Nevertheless, only recently it has been realized that the carrier systems themselves may address safety issues to the patient due to their nanometric size. The development of a fast, low cost, portable and sensitive technique for sensing functionalized NPs is highly required as a tool for point-of-care diagnostics. The detection of such NPs would allow to obtain information on the concentration of drug and, of course, of the MNPs themselves, providing an estimation of risk related to the local concentrations of nano-carriers.

3.1.2. A novel method for NSs detection: OECTs

Despite the large number of techniques used for NPs detection, the development of sensors capable of direct and portable detection and quantification of functionalized NPs is still limited and remains a challenging scientific goal. Some of the techniques mentioned in sections **1.3.2** and **1.3.3**, in fact, represent useful tools only for Ag-NPs detection. Some others, more suitable for MNPs, often do not show portability and easy-processability features, being constituted by space-consuming and some time complicated instrumentation.

This work aims at developing a low cost, easy-processable, portable, sensitive, rapid and disposable device for *in-vivo* and *in-vitro* detection of functionalized NPs in aqueous environment. A final aim was that such a device could be eventually applied locally in human body, through an opportune microfluidic structure, to monitor reliably and in detail the effective presence of NPs.

OECTs are suitable devices that can reliably operate in aqueous solutions, providing low-cost, portability and easy-processability. The innovative OECT technology has already been applied to NSs sensing in aqueous environment, as described by Tarabella *et al.*[98] and Toccoli *et al.*[265]. In these works, OECTs were used for sensing of NSs applicable as drug nanocarriers: structures made of amphiphilic molecules, as micelles and Au-NPs functionalized with polymeric shells (f-Au-NPs), respectively. In the first case, micelles made of the cationic surfactant CTAB were effectively detected by OECTs between 1 x 10^{-6} and 1 x 10^{-2} M by monitoring the current modulation of OECT close to the critical micellar concentration. The OECT modulation increased above the CMC of CTAB, revealing that positively charged CTA^+ micelles de-dope PEDOT:PSS more efficiently than CTA^+ dissociated ions, as confirmed by spectroscopy measurements. Thus, OECTs were shown to be a simple and fast method to detect the formation of micelles from dissociated ions. In the second case, the device response was correlated to the concentration of polymer loaded on the f-Au-NPs, ascribing the detection to an electrostatic interaction of the negatively charged polymeric shell and the cations in the electrolyte. This opens to the possibility to determine the quantity of drugs that could be loaded inside the functionalized shells and also to detect the kinetics of drug delivery.

3.2. Materials and methods

3.2.1. SPION preparation

SPION had a crystalline iron-oxide core, as described in the Results section, and have been functionalized with two different polymeric coating (polyethylene glycol (PEG)-modified phospholipids and poly-acrilic acid (PAA), respectively). In the first case (PEG-NPs), the standard protocol described elsewhere was followed[266]. Iron oxide cores were synthesized by thermodecomposition of Iron complex in a mixture of oleic acid and oleylamine. These cores were suspended in toluene and added to a solution of 1,2-Distearoyl-sn-glycero-3-phosphoethanolamine-N-methoxy(polyethylene glycol) (DSPE-mPEG) and 1,2-Distearoyl-sn-glycero-3-phosphoethanolamine-N-[amino(polyethylene glycol) (DSPE-PEG amine) in chloroform. The mixture was then dried and resuspended in deionized water, filtering with a 0.2-μm inorganic membrane syringe filter. The so-obtained PEG-NPs show both a methoxy group and an amine group at the ends of the polymer coating. In the second case (PAA-NPs), Iron oxide cores were synthesized by Massart's method[267], i.e. alkaline co-precipitation from Fe^{2+} and Fe^{3+} aqueous solution at room temperature. The cores were then coated with PAA under mechanical stirring or ultrasonication.

3.2.2. SPION characterization

SPION were studied by Transmission Electron Microscopy (TEM), Dynamic Light Scattering (DLS) and laser Doppler velocimetry (LDV). For electron microscopy samples were prepared by sonication and drop-casting of the NPs solution onto a carbon coated copper grid. Images were acquired in a 200kV JEOL 2200FS field-emission microscope, working both in high resolution TEM mode (HRTEM) and in High Angle Annular Dark Field scanning TEM mode (HAADF-STEM), the latter with a nominal probe size of 0.5 nm. Information on the mean size was obtained from measuring over 100 NPs in random fields of the grid.

DLS and LDV, for characterization of size and zeta potential of the NPs in solution, were performed on a Brookhaven Zeta Potential Analyser 3.3 with a He-Ne laser source at 633 nm. For the DLS characterization, the original solutions were used to get information about the hydrodynamic radius of the polymer-coated NPs in liquid since the polymeric coating is not observable by TEM. Moreover, information about the net surface charge of the polymeric coating of the NPs has been obtained analyzing the zeta-potential. Solutions from the as-received sample were made at a concentration of 1 mg/ml for the device to acquire enough counts per second. 1.5 ml and 1 ml of sample were transferred to a square cuvette for DLS measurements and LDV, respectively.

3.2.3. OECT experiments

Electrical measurements were carried out using a couple of Keithley 2400 SourceMeters, controlled via home-made Labview software. The source electrode was grounded and the drain electrode was biased at -0.4 V (V_{ds}). The modulation measurements consisted basically in monitoring the drain current $I_{ds}(t)$ at increasing pulsed gate voltages (V_{gs}), in the range from 0 to 1 V with 0.2 V steps. The OECT response is expressed as $(I_{ds}-I_{ds,0})/I_{ds,0}$ *vs.* V_{gs}, where $I_{ds,0}$ is the drain current with gate bias $V_{gs} = 0$ and I_{ds} is the drain current when the gate is turned on.

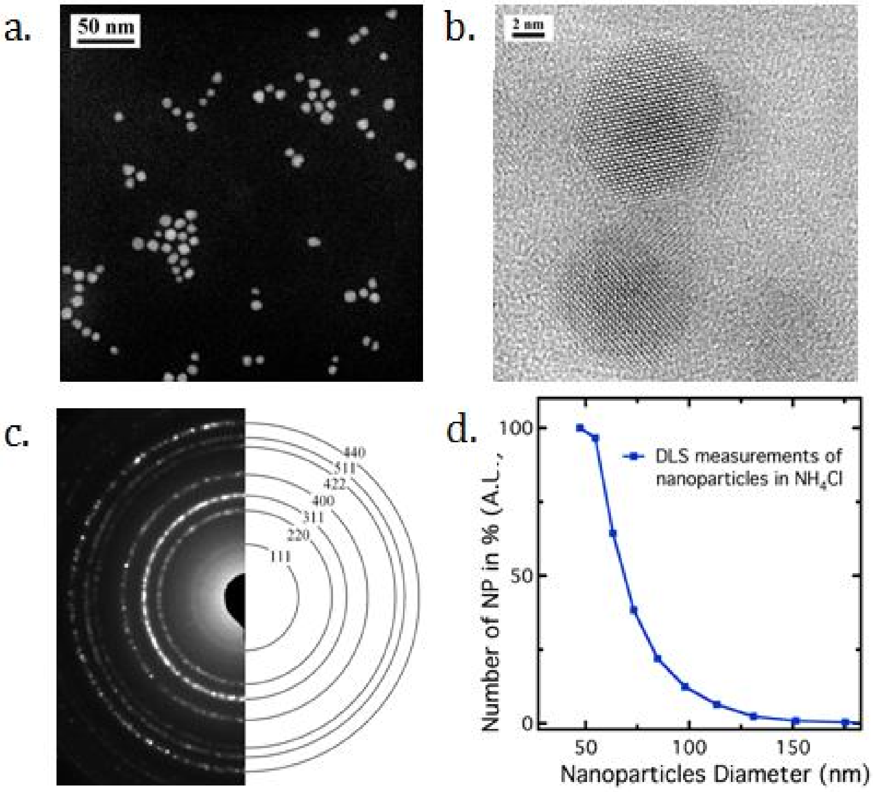

Figure 18 *a. HAADF-STEM image. Nanoparticles have a quite narrow size distribution centred around 10 nm. b. HRTEM image of two neighbour nanoparticles, showing each being single-crystalline. c. SAEDP, with indexing scheme, taken in a region of the TEM grid containing about a hundred nanoparticles. d. Average size distribution of magnetic nanoparticles, coated with polyethylene glycol, and measured by Dynamic Light Scattering. The hydrodynamics diameter of the NPs is about 45nm for almost 50% of particles. Before DLS the nanoparticles solution has been treated by ultrasonication for a few minutes.*

3.3. Results and discussion

3.3.1. SPION characterization

In **Figure 18** the core size and crystalline structure of the uncoated NPs, as studied by TEM, are shown. Since the HAADF intensity depends on the atomic number as Z^{α} with $\alpha \sim 2$[68], the NPs cores are clearly identified in HAADF-STEM imaging as bright objects on a dark background corresponding to the carbon support film

(**Figure 18a**). The core size average diameter results to be about 10 nm. Atomic resolution structural studies (**Figure 18b**) confirm that each iron oxide core has a single-crystalline cubic structure, which can be imaged in HRTEM along different zone axes (e.g. found experimentally <114>, <111> and <112>-type viewing directions). Selected-area electron diffraction patterns (SAEDP, see **Figure 18**c) turn out to be ring patterns, since they stem from many NPs randomly oriented with respect to each other. Each ring corresponds to a set of lattice planes and can be indexed according to the scheme in **Figure 18c** on the right. The cubic symmetry and the experimental lattice parameters d, as found both by HRTEM analysis of single NP and SAEDP, are consistent with a Fe_3O_4 (magnetite) or α-Fe_2O_3 (maghemite) structure of the nanoparticles core. To get an estimation of the size of the PEG covered NPs in solution, **Figure 18d** reports the average hydrodynamic size distribution of the PEG-NPs in liquid, in this case NH_4Cl 0.1M.

The DLS measurements show that about 57% of NPs have a size between 45 nm and 55 nm, representing the estimated radius of isolated coated NPs. About 38% fall between 63 nm and 98 nm, representing a estimated degree of aggregation of about 2 coated NPs, while the other 5% have a size above 100 nm. A minor percentage of particles have a mean size greater that 100 nm, so that the overall size-distribution represents a good degree of dispersion and separation in solution.

The results from reading the zeta potential of PEG-NPs and PAA-NPs show that the former with have net negative charge of -38 mV while the latter have no appreciable net surface charge.

3.3.2. Sensing of SPION by OECT

After DLS and LDV characterizations, the PAA-NPs were injected into the OECTreservoir, to investigate NPs detection in water. In order to continuously monitor the response of the OECT under the NPs effect, a real-time I_{ds} measurement has been performed with fixed gate voltage (V_{gs} = 0.4 and 0.6 V), as reported in **Figure 19.**

All the measurements have been performed in water with a Ag-wire as gate electrode. At the time of injection (at 360 sec.), in the first plot (red curve, V_{gs} = 0.4 V) 50μL of electrolyte alone has been injected into the solution and no signal change is recorded. The same amount (50μL) of an aqueous solution of PAA-NPs (1mg/ml) has been injected after the same time (green curve, V_{gs} = 0.4 V). Upon NPs injection we see a clear variation in the drain current, which reveals the presence of coated NPs. At higher gate voltage the effect results enhanced, as reported in the third injection after the same time (blue curve, V_{gs} = 0.6 V), confirming an effective detection of the PAA-NPs.

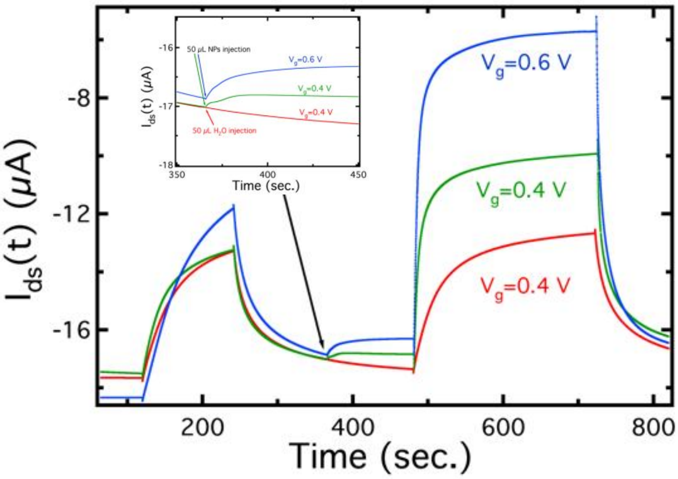

Figure 19 *Typical real time detection of the PAA-NPs. At the time of 360 s, a drop of 50μL of electrolyte only (red curve) or electrolyte with nanoparticles (green curve at Vg 0.4, blue curve at Vg 0.6) has been injected into the electrolyte-reservoir of the OECT. The inset shows a close up of the effect induced by adding extra solvent.*

Then PAA-NPs have been investigated as a function of different concentrations (0.1, 1 and 10 mg/ml) by OECT sensing with an Ag-wire used as gate electrodes (**Figure 20**). Here the OECT response is expressed in modulation current units (ΔI

$=|I_{ds} - I_{ds,0}| / I_{ds,0}$). The current signal for the lowest concentration (0.1 mg/ml) achieves the value of 0.44 at V_{gs} = 0.8 V, and increases till about 0.5 for the concentration of 1 mg/ml. The maximum value of 0.61 is reached for the highest concentration (10 mg/ml). The modulation spans over a range of 0.17 modulation units, which is much higher than the experimental error limit (0.05 units). The intensity of the current modulation is proportional to the concentration of coated-NPs in solution.

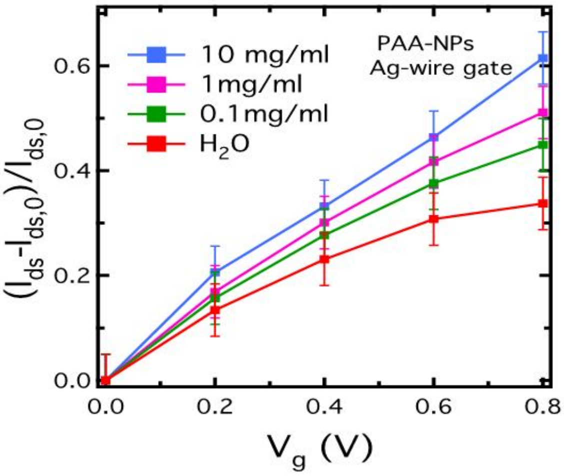

Figure 20 *Normalized response of the OECT as a function of the gate voltage for different concentration of PAA-coated NPs.*

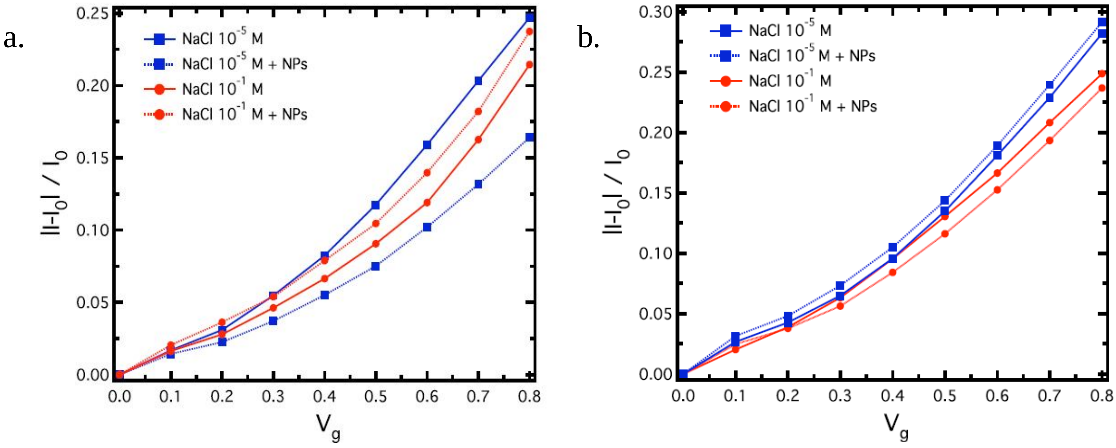

Figure 21 *a. normalized OECT response as function of gate voltage for* 10^{-5} *M and* 10^{-1} *M NaCl solution with and without PAA-coated NPs (solid and dotted line, respectively). b. normalized OECT response for* 10^{-1} *M NaCl solution with and without PEG-coated NPs (red solid and dotted line, respectively) and for* 10^{-5} *M NaCl solution with and without PEG-coated NPs (blue solid and dotted line, respectively).*

3.4. Discussion

The origin of the different response of OECT in presence of NPs can be attributed to the way NPs affect the electrolyte solution potential (V_{sol}), that is the potential acting on the OECT channel and which ultimately determines the OECT current modulation. In the OECTs-based sensors the effective gate voltage (V_g^{eff}) is sensitive to the potential drops at the electrolyte/semiconductor and electrolyte/gate interfaces. The equations representing the channel current of an OECT, as reported by the Bernards' model [45] is described by Eq. 3, Eq.4, and Eq. 5.[45, 49] c_i in Eq. 4 is also related to the capacitance of the interface between the electrolyte and the gate electrode (C_g). Hence, the net surface charge of PAA-NPs, due to the polymer coating plays a primary role in their detection by OECTs. The mechanism proposed here to explain the NPs sensing is the solvatation of cations around the negatively-charged PAA-NPs. The solvatation of cations would reduce their amount in the electrolyte available for de-doping of PEDOT:PSS, modifing the I_{ds} current and revealing the presence of the NPs. To understand the role of cation solvatation in the charged NPs, we perform a series of meaurements with different concentration of NaCl in solution. Different electrolyte concentrations containing charged coated NPs (PAA) or uncharged coated NPs (PEG), allows to show the effective role of solvatation with respect to the sensing measurements. **Figure 21a** shows current modulation of the OECT in NaCl aqueous solution at concentration of 10^{-1} M with and without PAA-NPs at 1 mg/ml. The difference between the two curves of modulation could be discriminated, being over the limit of the device resolution. Then, modulation curves for PAA-NPs were recorded in NaCl solution at 10^{-5} M (**Figure 21a**), showing an evidently larger difference in the modulation responses. This result can be explained taking into account that higher concentrations of salt (and, therefore, of Na^+ ions) in the eletrolyte are likely to shield more the PAA-NPs surface charge, reducing the capability of the OECT to detect them. On the other hand, lower concentrations of cations induce less shielding of the PAA-NPs charge, allowing the device to detect more effectively the NPs. Our hypothesis was further confirmed repeating the same measurement with PEG- NPs (with no net surface charge). In this case (**Figure 21b**), no evident difference in the modulation responses, and, hence, in the sensing ability of the device was found, independently from the salt concentration. This indicates both that the surface charge of SPION plays a primary role in their detection by OECTs and that a solvatation process is likely to take place at the outermost surface of the charged NPs.

An alternative mechanism that could possibly take place (also simoultaneusly to that described above) could be a direct interaction of charged SPION with PEDOT:PSS. Indeed, little shielding of PAA-NPs surface charge in low concentrated eletrolyte could cause NPs to enter more efficiently into the PEDOT:PSS channel as result of the eletctrostatic action of the positively biased gate. SPION would act as cations, inducing an efficient de-doping of PEDOT:PSS easily detectable from the electrical response of the OECT.

3.5. Conclusions

The large number of applications of NPs in modern technology and also the high variety of naturally occurring NPs with size less than 100 nm, has boosted great interest in the development of techniques for NPs sensing and characterization. Among the different methods introduced for sensing nanostructured materials and their nanoscale properties, a new class of devices, based on organic conductors, we have proposed and demonstrated that OECTs, based on conducting polymers, are well suited for sensing of nanoparticles and nanosystems. In fact, we have monitored polymer-coated SPION by OECTs. SPION were first characterized by TEM and their hydrodynamic radius and zeta potential in aqueous solution was analysed by DLS and LDV. OECTs based on PEDOT:PSS were used as a NPs sensor with different polymeric-coating. PAA-NPs in water were detected in real-time respect to the pure electrolyte. Finally it was found that the device is able to discriminate different concentrations of PAA-NPs at different gate voltages. The sensing mechanism is mainly imputable to the electrostatic interaction of electrically charged SPION with cations in the electrolyte and, possibly, to a direct de-doping effect of PEDOT:PSS by SPION. A deeper understating of the phenomena is under investigation. The real-time monitoring of these nanosystems is part of the overall thesis project, being the aim to demonstrate the ability of OECTs to study drug-delivery nanosystems and their dynamics with respect to their interaction with living cells.

Chapter 4

4. Conducting polymers: a route towards biofouling control

4.1. Introduction

As previously discussed, smart materials, whose surface properties can change with an external stimulus, are emerging as a means to achieve differential adhesion of microorganisms and cells.[269] One example of a smart material, is conducting polymers (CPs), which have recently received renewed attention due to their potential applications in bioelectronics.[20] One commonly used CP is PEDOT, commonly degenerately p-type doped with PSS anion. Different anions can be used in order to dope PEDOT, the most common alternative to PSS being the Tosylate anion (TOS). When a conducting polymer is in contact with an electrolyte and is negatively biased, positive ions from the electrolyte enter the polymer; the local hole density decreases in order to maintain charge balance and the film is reduced. In a similar fashion, oxidation takes place when the polymer is positively biased.

Previous work has established that the redox status of conducting polymer films influences the adhesion and function of mammalian cells.[270–272] Studies on conducting polymer devices interfaced with mammalian cell layers open new directions in biomedical applications such as drug development and toxicology.[109,106,273] Of particular relevance for this study, conducting polymer devices have been used to sense the presence of bacteria.[274] Although smart surfaces that electrically control the formation of biofilms have been recently reported,[269,275] the use of conducting polymers would provide great added value because of the ability to eventually yield smart systems that combine control of biofilm formation with sensing and actuation.

In this Chapter the first step in such a concept is demonstrated, namely that the redox status of a conducting polymer film controls biofilm formation. It was found that oxidation of a conducting polymer thin film encourages the growth of an *E. coli* biofilm. Two conducting polymers, PEDOT:PSS and PEDOT:Tos, were compared here. The former was studied more in detail, since it is the most common used conducting polymer and it can be easily and effectively patterned by means of photolithographic techniques. The latter was also used because its synthetic flexibility that allows to modify its composition by incorporating molecules; this paves the possibility to enhance the influence of redox status on biofilm development by adding appropriate chemicals that can interact with bacteria.

4.2. Materials and methods

4.2.1. Microtiter plate fabrication

Both patterns for gold and PEDOT:PSS were designed using CleWin 4 software

(MESA+ Research Institute and DeltaMAsk, NL), and chromium masks were prepared using standard photolithography and wet etch techniques.[276] Briefly, glass substrates were coated by thermal deposition with chromium (100 nm). A 1.9 µm-thick layer of Microposit S1813-G2 (Rohm and Haas, Philadelphia, PA) positive photoresist was spin-coated and soft-baked (115 °C, 1 min). Photomasks were generated by laser lithography (Laserwriter LW405B, Microtech, Palermo, Italy), in which mask patterns were transferred to the photoresist by exposing it to UV-range laser at 80 mJ/cm^2. After exposure, the photoresist was developed with MF-26A developer. Exposed chrome was finally etched with chromium etchant solution (Sigma Aldrich). Glass substrates were extensively cleaned with a diluted industrial cleaner (Micro-90), acetone and isopropanol followed by plasma cleaning. The fabrication process, outlined in **Figure 22**a, included the deposition and patterning of metal and PEDOT:PSS. For the gold patterning, Microposit S1813-G2 was spin-coated and exposed to UV light using a SUSS MBJ4 contact aligner, and then developed using MF-26 developer. This was followed by the deposition of 4 nm of chromium and 50 nm of gold using a metal evaporator. Lift-off was performed by immersion of the samples in acetone for 30 minutes with sonication. For the preparation of the PEDOT:PSS films, 20 mL of aqueous dispersion (Heraeus Holding GmbH, Clevios PH-1000), were supplemented with 5 mL ethylene glycol (Sigma Aldrich), 50 µL dodecylbenzenesulfonic acid (DBSA; Sigma Aldrich), and 1% of (3-glycidoxypropyl)trimethoxysilane (GOPS).[277] Ethylene glycol was added in order to enhance the conductivity of PEDOT:PSS, DBSA helps to adjust the surface tension and thus the coating properties of the suspension, while GOPS is a surface adhesion promoter as well as a heat activated polymer cross-linker to enhance film stability in aqueous solutions. The resulting dispersion was spun onto the substrates at 600 rpm for 30 s (resulting in a ~250 nm thick film), and then soft baked at 110°C for 1 min in atmospheric conditions.

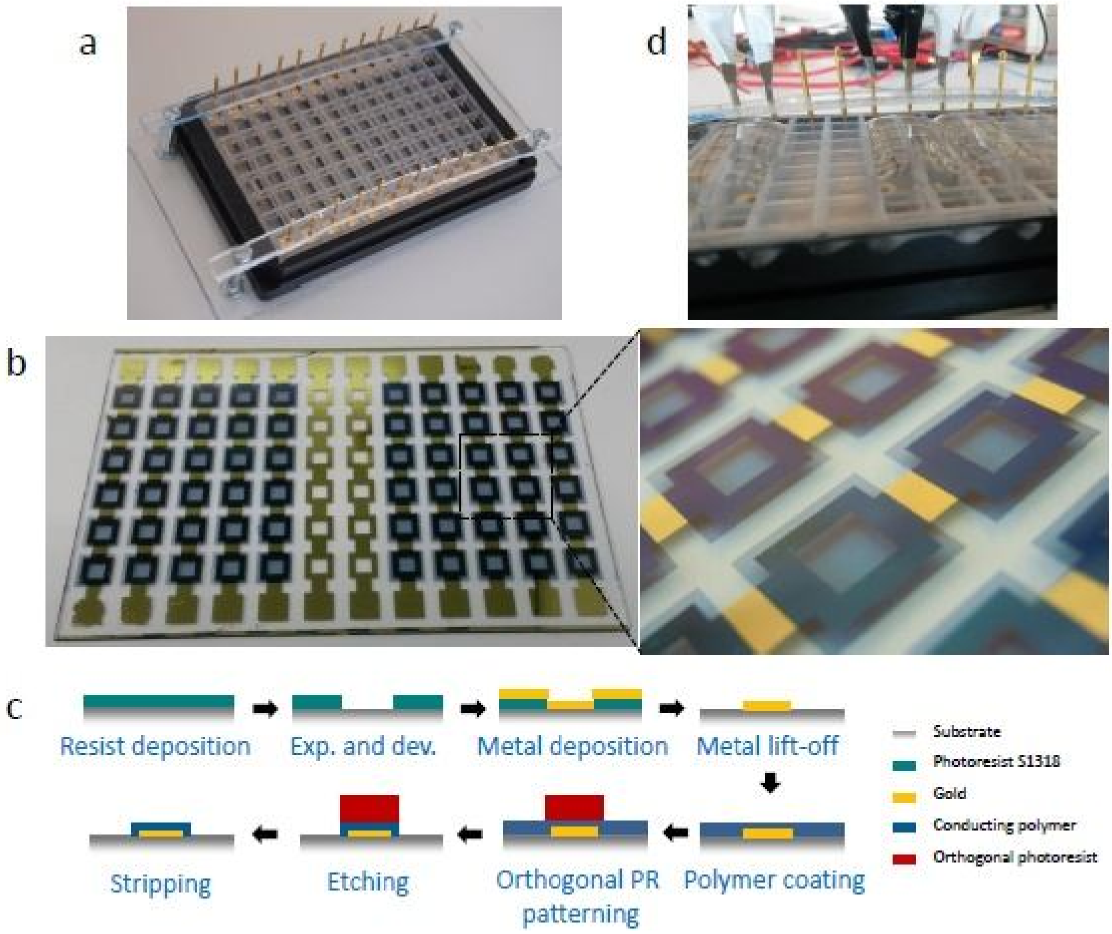

Figure 22 *a. Overview of the assembled device with lower plastic tray, patterned glass substrate, silicone superstructure and spring-loaded connectors. b. Gold contacts and PEDOT:PSS pattern deposited on a 74 mm x 110 mm x 1 mm glass substrate. c. Scheme of the main photolithographic steps used for device fabrication. d. Meniscus made with bacteria growth medium for PEDOT:PSS biasing.*

PEDOT:TOS was prepared via VPP directly onto the glass substrates.[26,28] Prior to VPP, 3,4-ethylenedixoythiophene (EDOT) monomer (H.C. Starck) was pre-heated for at least one hour in a glass polymerization chamber kept in an oven at 70°C at ambient pressure. An oxidant solution was prepared, mixing 1 ml Fe(III)tosylate (40 wt% in solution with butanol, Yacoo Chemical Company), used as the oxidant, with 22 µl pyridine (Sigma; used as received) as a weak base[27] and 1 ml ethanol (99.9%, Sigma) for conductivity enhancement[35]. The oxidant solution was spun onto the substrates at 1500 rpm for 30 s and placed directly in the vapour phase polymerisation chamber without a drying step, in order to avoid formation of crystallites from air humidity.[29] EDOT was allowed to polymerise on the coated substrates for 30–40 minutes, until when the film turned into a dark blue colour. At this point samples were removed from the polymerisation chamber and rinsed twice in ethanol to remove excess Fe(III)Tos and unpolymerised EDOT monomer. The resulting film was ~130 nm thick.

The conducting polymer film was patterned using fluorinated chemicals from Orthogonal, Inc.. The photoresist OSCoR 4000 was spin-coated onto the PEDOT:PSS film, exposed to UV light and developed in Orthogonal Developer 105; the remaining image was then transferred onto the PEDOT:PSS film by O_2:CHF_3 (50:10 sccm) plasma etch. The resist film was then washed away with Orthogonal Stripper solution, and the samples were rinsed in de-ionized water to remove any excess of low molecular weight compounds. Prior to use for experiments, devices were immersed in a 70% ethanol solution for sterilization. Bias was applied using spring-loaded connector with leads to a three-channel power supply (Hameg HMP 2030, Hameg Instr., Mainhausen, DE).

4.2.2. Biofilm culture

Laboratory *E. coli* BL21(DE3) strain was purchased from Invitrogen (Carlsbad, CA). M63 minimal medium (glucose 0.2%)[190] was prepared in-house and supplemented with 1% LB medium (indicated as M63%). Bacteria were grown overnight in Luria-Bertani (LB) medium at 37 °C without shaking. Several aliquots (20 µL each) of overnight culture were subcultured in 200 µL M63% medium in different wells of a 96-well flat-bottom polystyrene microtiter plate (Corning 3595, New York, NY).[278] Subsequently 20 µL of each culture were subcultured again in 200 µl M63% medium and inoculated into the device.

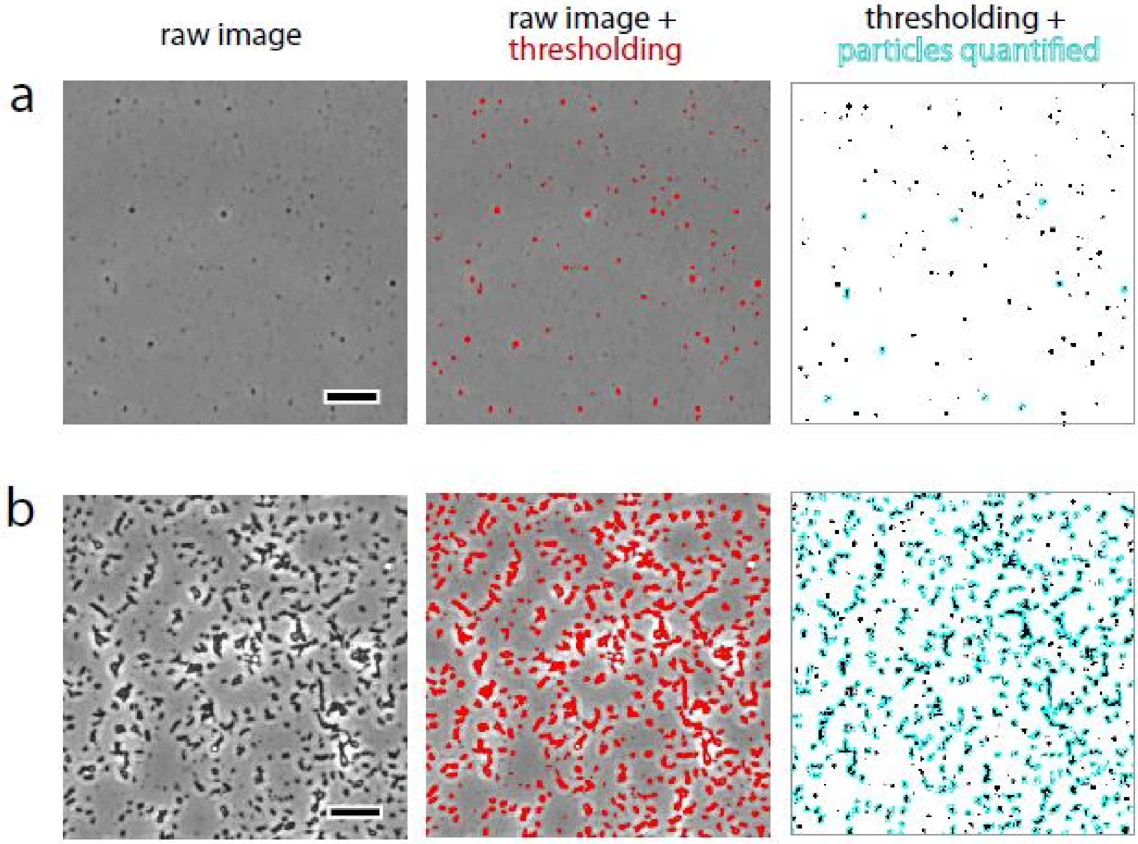

Figure 23 *Illustrative example of image processing/analysis to extract the % coverage of bacterial biofilm. (a) A control sample of PEDOT:PSS in media, un-biased and without bacteria, and (b) oxidized PEDOT:PSS film with bacteria, after 22 hours. Raw images are shown on the left. In the middle, the raw images after default automatic thresholding in ImageJ software overlayed on the raw image. On the right, the thresholded binary image (black/white), with cyan outlines indicating the "particle" that are counted and included for determination of area coverage percentage. Scale bars are 20µm.*

4.2.3. Quantification of biofilm formation

After removing the electrical bias, planktonic cells were discarded from each well and the biofilm which had developed on the pixel (both PEDOT:TOS and PEDOT:PSS) was washed twice with de-ionized water.

The biofilm formed on PEDOT:TOS pixels was firstly observed by bright-field optical microscopy with a Carl Zeiss Primo Vert Inverted Microscope (Carl Zeiss, Oberkochen, GE), equipped with a Zeiss Axiocam MR, using Carl Zeiss LD-Plan ACHROMAT 10 x / 0.25, 20 x / 0.30 and 40 x / 0.50 objectives.

The biofilm formed on PEDOT:PSS pixels was observed in bright-field optical microscopy on an inverted Carl Zeiss Axio Observer Z1 Microscope (Carl Zeiss, Jena, GE), equipped with a Zeiss Axiocam MR, using a Carl Zeiss EC-Plan NEOFLUAR 10 x / 0.3 objective and AxioVision 4.8 digital imaging software. Biofilm was quantified using ImageJ software[279] by estimating the percentage of coverage in each picture. Thresholding of the images was first performed by applying the default (modified IsoData algorithm) automatic thresholding in ImageJ, resulting in a binary image (**Figure 23**). This image is then quantified using the Analyze Particles tool in ImageJ, yielding a %Area of particulate coverage, where a lower particle size limit of $10px^2$ was applied (features smaller than this size are most frequently attributed to particulates in PEDOT films in the control), and circularity of 0 to 1 is selected. Error bars in %Area coverage represent the standard deviation of N=4 samples per condition, this error value is consistently larger than the variations due to a ~5% variation in the automatic thresholding value.

Quantification of biofilm was also performed, when possible, by staining biofilm with 100 μL of 0.1% Crystal Violet (CV) aqueous solution. Absorbance signals was measured at λ=590 nm (A_{590}) in an Infinite® M1000 PRO microplate reader (Tecan, Lyon, France), and corrected both for blanks and contribution of the CP.

4.2.4. Fluorescence staining

When Syto 9 (Invitrogen) was used, the bacteria on each pixel were stained with 100 μL 500 nM Syto 9 in 0.9% NaCl for 20 minutes, followed by three washes with 0.9% NaCl and deionized water. Fluorescence emission was measured at 498 nm using a Carl Zeiss Observer Z1 Inverted Microscope, equipped with a HXP 120 C mercury lamp. When PKH26 staining (Sigma Aldrich) was used, 30 μL of dye/diluent C solution (dil. 1:300) were added to each well, and incubated for 10 min; then 50 μL fetal bovine serum (FBS) were added for 1 minute for removing excess of stain; finally, the biofilm was washed with 10% FBS RPMI cell culture medium and deionized water. All fluorescence observations were performed immediately after staining.

4.2.5. CPs characterization

The thickness of the PEDOT:PSS layer was measured on an Ambios XP2 mechanical profilometer (Ambios Techonolgy, Santa Cruz, CA).

The characterization of the surface properties of the PEDOT:PSS thin film was performed on samples biased in M63 growth medium but without inoculation of bacteria. Absorbance was measured on an Infinite® M1000 PRO microplate reader. Absorbance scans over the wavelength range 230 - 8800 nm and 400 - 800 nm were recorded for PEDOT:PSS and PEDOT:TOS, respectively; absorbance at 590 nm was more finely recorded for PEDOT:TOS. Contact angle was measured at room temperature (T ~ 22 °C) and ambient humidity after 1 hour from removing the bias and drying the samples. An Apollo OCA200 contact angle meter (Apollo Instr., Compiègne, FR) was used for the measurements, in sessile drop mode and with water as working liquid.

4.2.6. Statistical analysis

Data obtained from characterization of the conducting polymer films and from biofilm assay are averages generated from multiple reading on four pixels along each column. The error bars represent the standard deviation from these averages. Statistical analysis was performed using one-way analysis of variance (ANOVA), followed by Tukey’s post-test). P-values of 0.05 or less were considered to indicate statistical significance. OriginPro 8.1 (OriginLab, Northampton, MA) was used to perform ANOVA and to create graphics.

Note that it is difficult to compare absolute values of CV staining from experiment to experiment. Although the relative values within each controlled experiment are reproducible, the absolute values of CV staining vary depending on numerous factors, including the batch of CV used and the age of the CV solution. Thus, comparisons between experiments are not meaningful, and only comparisons between the relative levels of CV staining provide meaningful results.

4.3. Results and discussion

4.3.1. Design of the device and its working principle

To study the effects of the oxidation state of a conducting polymer on *E. coli* biofilm formation, it was developed a device compatible with current biological laboratory techniques such as microscopy and spectroscopy, and which allows the assessment of large numbers of samples required for statistical biological analysis, while keeping volumes down to reduce cost of expensive biological assay reagents. A 96 well plate format was chosen, which fits these requirements. Devices consisted of a rigid polycarbonate microtiter frame, supporting a glass substrate and a 96-well silicone superstructure, with a transparent cover (Schott, Jena, GE) (**Figure 22**a). An array of 72 pixels of conducting polymer, with dimensions of 6 x 6 mm, was patterned on the glass substrate (**Figure 22**b). Pixels within one column were electrically addressed by a square ring-like Au electrode and connected with each other with Au lines. This configuration leads to up to 6 replicates of the same experimental variables within each column, allowing the collection of statistics, while the remaining two contained a bare gold electrode for connections. The details of the fabrication, shown in **Figure 22**c, are discussed in the experimental section. Briefly, the Au lines were deposited and patterned first using traditional photolithography and lift-off, followed by the deposition and subtractive patterning of the conducting polymer pixels (made of PEDOT:PSS or PEDOT:Tos) using orthogonal lithography.[280,281] Columns are addressed electrically using spring-loaded connectors. To change the redox state of the conducting polymer pixels, a bias of ±1V was applied to two neighbouring columns while they were overfilled with bacterial growth medium (used as the electrolyte), exploiting surface tension to create a meniscus (**Figure 22d**). This allowed the electronic/ionic circuit to be closed between the two columns and to oxidize the pixels of one while simultaneously reducing the pixels of the other column.

4.3.2. Biofilm formation and microtiter assay

4.3.2.1. Oxidation state of PEDOT:TOS and bacterial biofilms

The effect of the oxidation status of the surface on the ability of *E. coli* to form biofilm was preliminarily investigated using PEDOT:Tos as electrically switchable surface layer. Bacteria were seeded and left to sediment on the conducting polymer surface for 8 hours, *before any bias was applied*. After the initial 8 hours, an electrical bias (±1V) was applied continuatively for 16 hours, modifying the redox status of PEDOT:Tos. Thus, in this experiment a condition corresponding to 24 hours of total growth time was investigated.

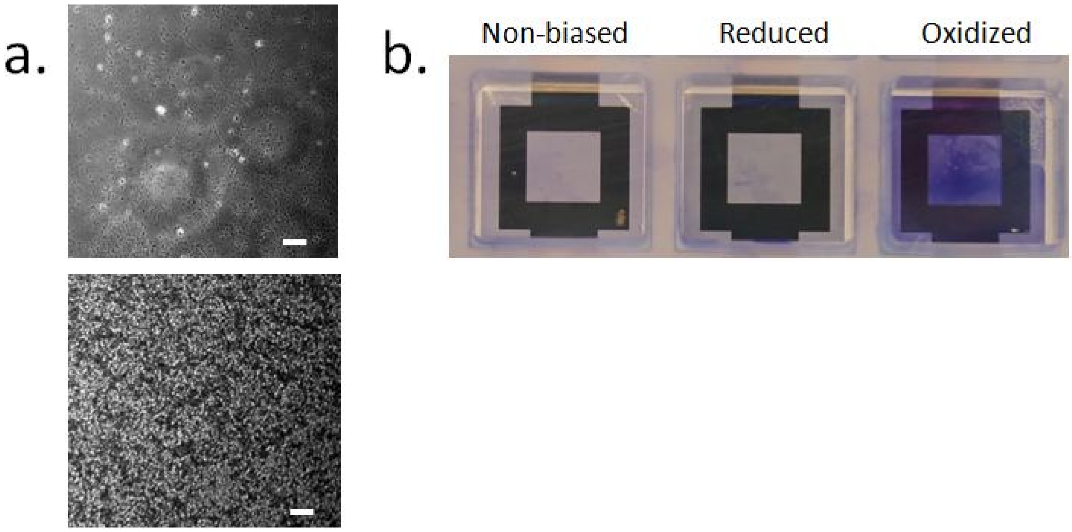

Figure 24 *a. Bright-field micrographs of bacterial biofilm adhered to the surface of reduced (top) and oxidized (bottom) PEDOT:TOS. Scale bars are 50 µm. b. PEDOT:TOS pixels after CV staining, clearly showing the higher amount biofilm formed on the oxidized pixel.*

Figure 24a shows the bright-field micrographs recorded from reduced and oxidized pixels at the end of the experiment, after the pixels being washed twice with distilled water to remove planktonic un-adhered cells. The amount of structures that can be associated to biofilm formed on and adhered to the oxidized pixel (bottom) was clearly higher than on the reduced pixel. Subsequently, the biofilm was stained using CV, as shown in **Figure 24b**. Here a sample pixel is shown for each bias condition (oxidized, reduced, and non-biased), and the higher amount of stain fixed to the biomass on the oxidized pixel comparing with the other pixels allowed to visualize the effect of the redox status on the biofilm formation. The biofilm formed on the various pixels was quantified by measuring the absorbance signal, that for oxidised, reduced and non-biased pixels was 1.00 ± 0.14, 0.40 ± 0.05, and 0.3 ± 0.02, respectively.

It can be concluded that, after 8 hours sedimentation of bacteria, oxidizing PEDOT:Tos and increasing its surface energy encourages biofilm formation. On the other hand, reduction of the conducting polymer after the same amount of sedimentation time does not allow the development of biofilm, showing that lower surface energy and, possibly, the presence of a negative electrical field, affects negatively the ability of bacteria to form biofilm. Noteworthy, bacteria seeded on a non-biased PEDOT:Tos film were not able to form biofilm either. This could stand for a possible natural antifouling effect of PEDOT:Tos, that avoids bacteria to organize in favourable structures such as biofilms.

4.3.2.2. Oxidation state of PEDOT:PSS and bacterial biofilms

In order to investigate the influence of the PEDOT:PSS redox status on biofilm formation, bacteria were inoculated into the wells of a freshly fabricated plate, following a protocol designed to promote biofilm formation.[282] Typically, bacteria are allowed to grow for more than 24 hours for formation of biofilms on surfaces such as glass or polystyrene.[278] Lab *E. coli* strains such as the one used here tend to favour the planktonic state, however they can be induced to form biofilms by culture in limiting growth medium.[283] We decided to study the effect of the redox status on already established biofilms with differing levels of maturity; so, in a first phase of the experiment, bacteria were allowed to grow for various time intervals (T_1 = 0, 8, and 22 hours) *before any bias was applied*. In a second phase of the experiment, the bias was switched on to change the redox status of some columns. For each condition (each time interval T_1), three columns were used: one that was biased to become oxidized, one that was biased to become reduced, and one that was not biased, representing a control. The duration of this second phase was the same for all pixels and equal to T_2 = 22 hours. This experiment, therefore, probed various conditions corresponding to (1) 22 hours, (2) 30 hours, and (3) 44 hours of total growth time. Finally, one column was filled with bacterial growth medium (for 44 hours) but not inoculated with bacteria, representing a global blank for all the samples. At the end of the experiment, the pixels were washed twice with distilled water. These wash steps removed a significant portion of un-adhered/planktonic bacteria which were not embedded into a biofilm structure.

a.

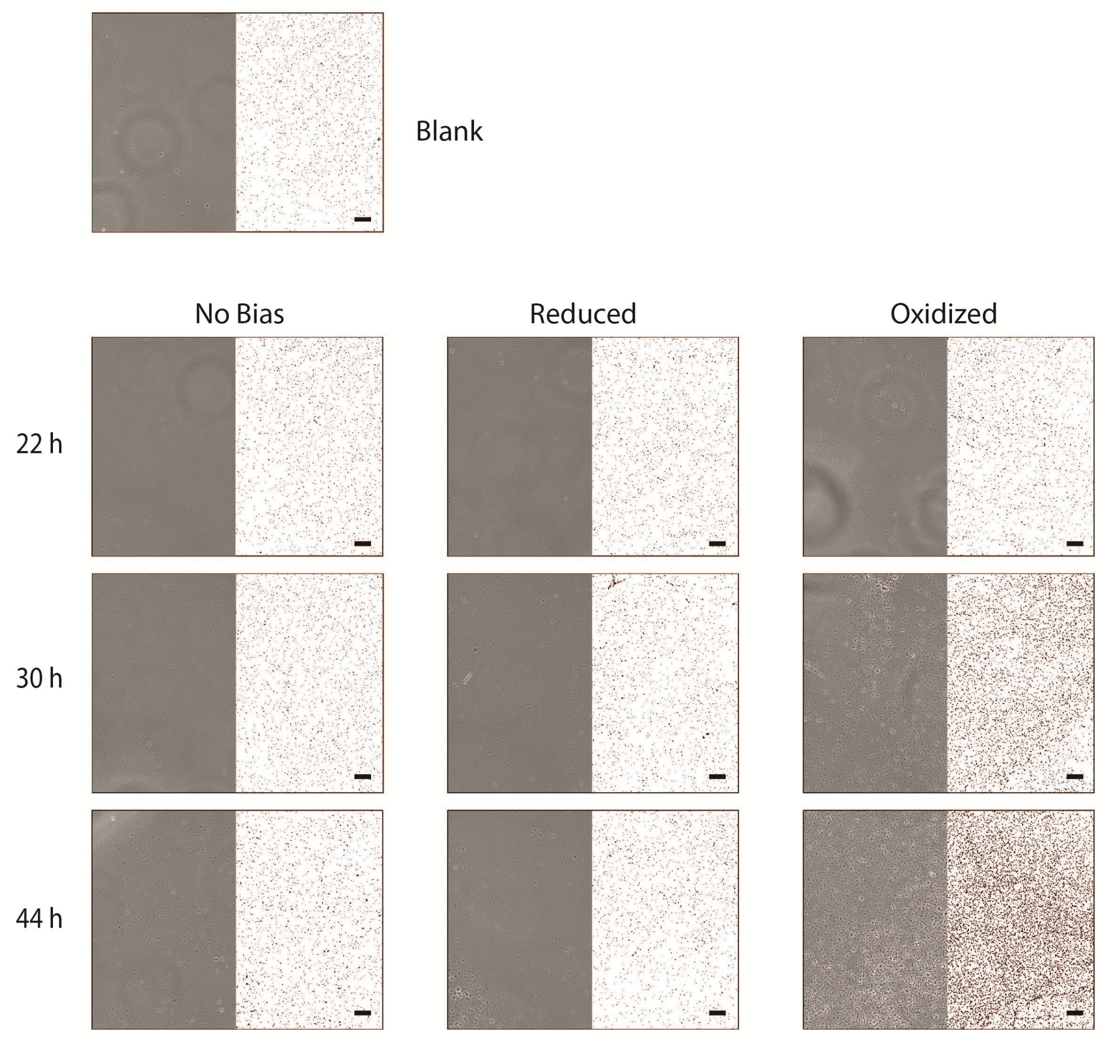

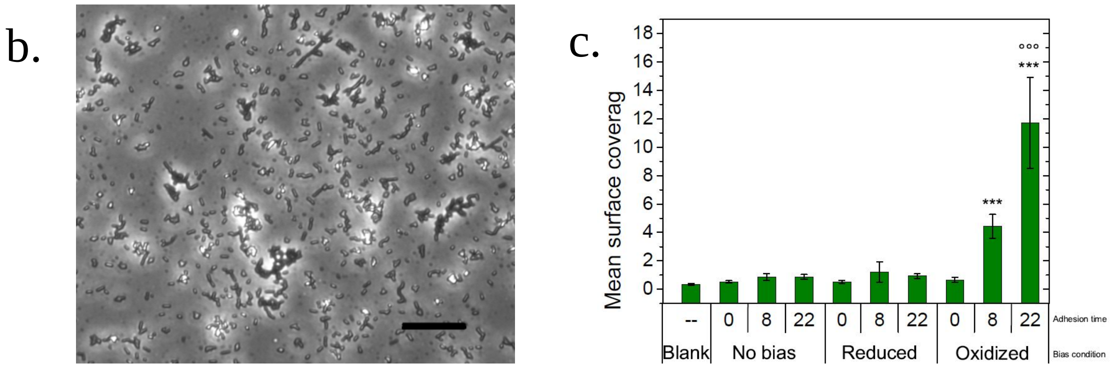

Figure 25 *a. Bright-field microscopy of bacteria biofilm on the surface of PEDOT:PSS (left-hand side of the pictures) and processed binary image used for surface coverage counting (right-hand side). Scale bars are 50 µm b. Close up of the capsule around bacteria adhered to oxidized PEDOT:PSS after 22 hours biasing. Scale bar is 20 µm. c. Mean surface coverage calculated by image processing from bright-field pictures of E. coli bacteria grown on the surface of PEDOT:PSS (*** p<0.001 vs blank, °°° p<0.001 vs oxi 8h).*

Figure 25a shows the bright-field micrographs recorded from non-biased, reduced and oxidized pixels corresponding to the three conditions required above, plus the global blank. In each micrograph, the total area of biofilm coverage was quantified via image processing, (for more details, see **Figure 23**), and is shown as the right-half of the image. All images, including the blank (no bacteria), show a uniform distribution of round-shaped spots with size between 1 and 3 µm, which we attribute to aggregates in the PEDOT:PSS film. In addition, and more importantly, structures ascribable to biofilm (rod-shaped objects, consistent with *E. coli*, **Figure 25b**), were present on the oxidized pixel corresponding to condition 2 (30 hours) and were even more pronounced on the oxidized pixel corresponding to condition 3 (44 hours). The histogram of **Figure 25c**, which shows mean surface coverage values averaged over nominally identical six pixels corresponding to each column, reveals a definite trend: the biofilm coverage on the oxidized pixel increases with the growth time, from 0.7% ± 0.2% for 22 hours of growth, to 4.4% ± 0.8% for 30 hours of growth, to 11.7% ± 3.2% for 44 hours of growth. In contrast, on the reduced sample no increase in biofilm formation is observed, even at 44 hours. The same was true of the non-biased sample, and of course of the blank, which was used as a control to ensure that the biofilm formation was due to the inoculated bacteria, and not to environmental bacteria. Interestingly, the micrographs show what appears to be a polysaccharide capsule localized outside the outer membrane of the cell.[284] Indeed, in all the pictures where biofilm could be detected, a transparent “halo” surrounded the cells and their aggregates (**Figure 25**b). We postulate that this halo is the polysaccharide capsule often found covering the bacterial membrane.[284,285] The latter represents an organelle mainly composed of hydrophilic polysaccharides that, among several other functions, serves to protect encapsulated organisms from phagocytosis, enhancing their virulence, and helping them to adhere to a variety of substrates.[286] It should be noted that attempts to use fluorescent stains (Syto 9 and PKH26) were not successful, probably due to the presence of this capsule that shielded the bacteria from the dyes. In addition, crystal violet staining, commonly used for quantification of biofilms, was not possible, as this stain binds to PEDOT:PSS forming a uniform layer on the surface of the polymer.

The following conclusions can be drawn from the experiment shown in **Figure 25**: First, the fact that little biofilm growth could be detected on the surface of the control sample, even after 44 hours of continuous growth, indicates that PEDOT:PSS has an intrinsic antifouling effect, yet resulting non-antibacterial. Indeed, liquid flow induced in each well by pipetting was enough to dislodge the majority of the bacteria from the surface of the polymer, showing that they are able to sediment and proliferate on the surface of the polymer but they are not able to form a biofilm resistant to mechanical stress (**Figure 26**, images *c* and *d*). This result, together with low cost and high conformability of PEDOT:PSS, makes this conducting polymer a promising candidate as a so-called “foul release coating”, one of several approaches developed in the last decades to combat biofouling. Second, these experiments demonstrate that oxidation of PEDOT:PSS encourages biofilm formation.

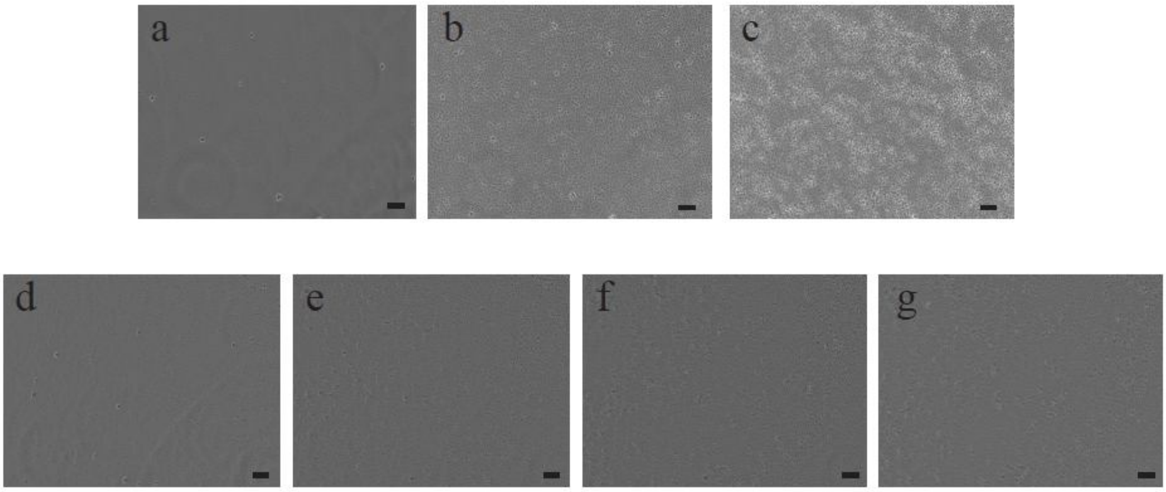

Figure 26 *Bright-field microscopy images of E. coli bacteria on reduced PEDOT:PSS taken prior and post biasing (a: inoculation of bacteria; b and c: 4 and 8 hours after sedimentation, respectively; d: addition of extra M63 medium and bias; e, f and g: 6, 12 and 17 hours after biasing, respectively).*

As pointed out in the introduction, prevention of biofouling is not the only requirement when biofilms are involved. Indeed, several examples of beneficial biofilms also exist, such as in bioreactors, bioremediation and anti-corrosive systems. In this optics, our finding that an oxidized surface enhances biofilm formation represents an important step in the comprehension of the factors that facilitate obtaining biofilms. Furthermore, on the side of conducting polymer applications, the possibility to make three-dimensional structures of PEDOT:PSS[287] could possibly allow to study the effect of the oxidation environment on more complex and lifelike cell systems.

4.3.3. CP characterization

4.3.3.1. Absorbance

When considering electrochromic materials, such as PEDOT:PSS or PEDOT:TOS, it is useful to characterize them through their color. Therefore, colorimetric measurements (absorbance) were performed in order to assess the optical properties of PEDOT:PSS and PEDOT:TOS thin films, depending on their electrically induced oxidation state.

As shown in **Figure 27a**, as expected for a cathodically colouring polymer, the luminance of PEDOT:PSS increased upon oxidation, as the intensity of the π - π^* diminishes. The polymer switched very fast in time (hundreds of millisecond) from a dark blue neutral state to a transmissive gray-sky blue oxidized state, while the reduced state switched to an even darker colour; to ensure stability of the redox change, bias was kept active for 1 hour. In spite of this, PEDOT:PSS did not show a detectable absorbance in all the range studied, regardless of the oxidation state of the polymer. This result is in good agreement with previous results in literature,[288,289] where PEDOT:PSS was shown to exhibit a sharp absorbance peak at 225 nm and a leading edge of broad absorption in the near-IR wavelength region around 3000 nm, ascribed to PSS and to a polaron or bipolaron band of PEDOT, respectively.[290,291] Both these wavelengths being out of the wavelength range of the equipment used here, optical characterization of this CP was not achieved here.

On the other hand, optical characterization of PEDOT:TOS was more effective. As shown in **Figure 27b**, colour switch of the polymer along with the oxidation state change (bias time of 1 hour) was easily detectable, the reduced state presenting an absorbance peak at 590 nm. Oxidized and neutral samples showed lower absorbance in the visible range, differing from each other appreciably only above

~650 nm. Also in this case, a luminance increase accompanied the oxidized state of the polymer, with the reduced state showing a darker colour (**Figure 27c**). Interestingly, the absorbance of a non-biased sample immersed into the electrolyte for 16 hours showed the same signal of the two reduced samples (data not shown). This not-induced reduction could be related to a weak bond of TOS^- ions into the polymer bulk, which could allow them to leave the film easily with an ionic exchange with the electrolyte.

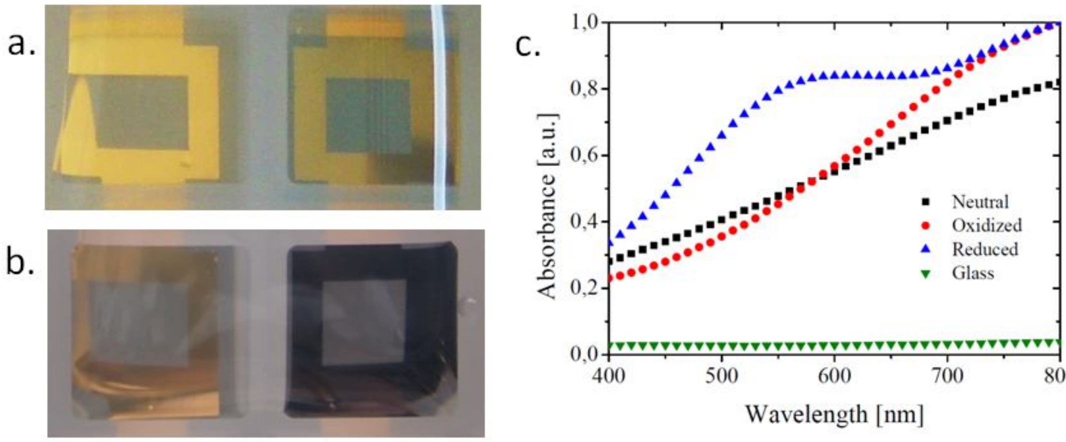

Figure 27 *a. Colour change of PEDOT:PSS associated to the electrochemical change of oxidation state, following the application of an electrical bias (reduced pixel on the right, oxidized on the left) b. Colour change of PEDOT:TOS following the application of an electrical bias (reduced pixel on the right, oxidized on the left) c. Absorbance spectra of PEDOT:TOS after applying an electrical bias.*

4.3.3.2. Contact angle

Surface properties, not only of the substrate, but also of the bacteria themselves, including the chemical nature and the morphology, are expected to play a role in the adhesion of bacteria and subsequent formation of a biofilm. The primary adhesion of bacteria involves a reversible attachment which is known to be highly dependent on the physicochemical and electrostatic interactions between the bacterial membrane and the substrate. Although the exact mechanism of biofilm formation is still unclear, it is thought that in general hydrophobicity and negative charge promote bacterial adhesion.[292] Assessing the nature of the surface submerged in liquid is technically very challenging, and so surface characterization is most often done on dry samples. Nevertheless, to attempt to explain the increased biofilm formation seen here on oxidized surfaces, we characterized the films with respect to contact angle and roughness. For the contact angle experiment, the films were biased as in the previous experiment; two columns were filled with bacterial growth media and were oxidized and reduced, respectively, as discussed above, for different periods of time (1, 8, 16, and 22 hours of bias applied). Two controls were also used, one column that was filled with bacterial culture medium and not biased, and another one that was neither filled with medium, nor biased. **Figure 28** shows the contact angle of the PEDOT:PSS pixels corresponding to these columns. The results are summarized in **Table 1**. The contact angle of the reduced pixels was found no to be dependent on bias time, and have an average value of 98°. The contact angle of the oxidized pixels, on the other hand, was found to decrease with bias time and reach an average value of 80° after 22 hours of bias. The control, left in bacterial growth medium for 30 hours without bias had an average contact angle of 89°. The second control (not exposed to bacterial growth medium, nor biased) was the most hydrophobic, with an average contact angle of 106°. The data shows that upon oxidation PEDOT:PSS becomes relatively more hydrophilic. The high overall contact angles observed here are thought to be partly due to the conducting polymer formulation used here, which includes GOPS, and also the use of fluorinated compounds during the patterning steps, which may, together or individually render the surface more hydrophobic. In addition to contact angle, the roughness of PEDOT:PSS films was also measured, in order to exclude the contribution of this surface property to the control of bacterial adhesion. Representative films (non-biased, but exposed to aqueous solutions) were typically smooth, with a roughness of approximately 2 nm, well below the range previously shown to influence bacterial adhesion.[293] Further data shows that there is no significant difference between oxidized and reduced samples in terms of roughness.[294]

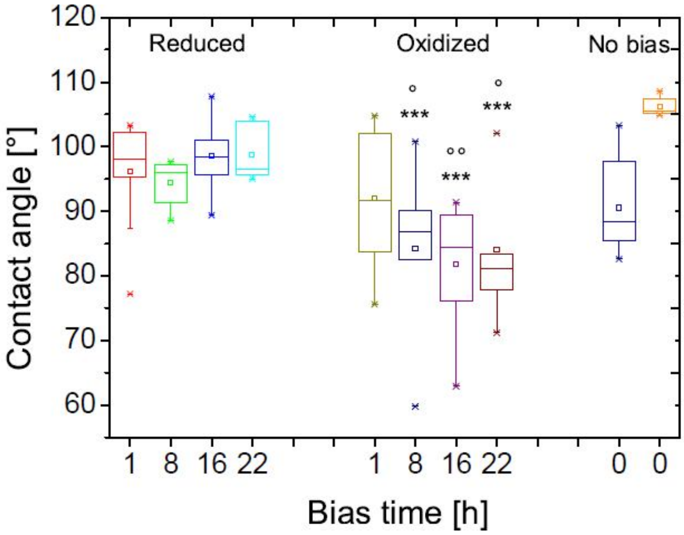

Figure 28 *The contact angle of water on the surfaces of PEDOT:PSS at different bias times (the two non-biased samples have been exposed or not to M63 growth medium, from left to right) (*** $p<0.001$ vs dry non-biased; ° $p<0.05$, °° $p<0.01$ vs 16h red). The lines in the boxes from bottom to top present the 1st, 2nd (median), and 3rd quartile values. The squares in the boxes are mean values, and the symbols below and above the boxes connected by lines represent the highest and the lowest values. Stand-alone symbols represent outliers, that lie more than one and a half times the length of the box either end of the box.*

Bias time [h]	**PEDOT:PSS**		**PEDOT:TOS**	
	Red	Oxi	Red	Oxi
1	98.3°±5.0°	92.8°±8.0°		
8	94.5°±3.7°	87.7°±9.5°		
16	98.6°±4.0°	83.0°±8.4°	109.6°±3.2°	89.6°±6.7°
22	98.7°±4.4°	78.9°±4.2°		
0 **(wet)**	89.5°±4.9°		95.5° ± 3.7°	
0 **(dry)**	106.2°±1.5°			

Table 1 Contact angle of water measured on reduced, oxidized and non-biased PEDOT:PSS and PEDOT:Tos.

These data indicate that there are changes in the chemical nature of the surface between the oxidised and reduced pixels. One explanation is that in the oxidised form of PEDOT:PSS there is increased biofilm formation due to a favourable conformation of the molecules involved in the early stages of bacteria adhesion, analogous to that seen with mammalians cells.[272] Previous studies on different redox states of PEDOT doped with tosylate (an alternative small molecule dopant) showed local changes in the pH of the electrolyte close to the surface of the film occur, due to release (oxidized) of or uptake of protons (reduced) from the film, which may alter the conformation of proteins mediating cell adhesion.[295] By analogy, a similar process may be occurring during bacterial adhesion, however, more detailed studies, beyond the aim of this work, will be required in order to understand at molecular level the surface property changes induced by electrochemical switch in these films. It should be noted that comparisons of surface characterization between PEDOT:PSS and PEDOT:Tos are complicated due to the polymeric nature of the dopant anion PSS, which is not able to rotate as freely as DBSA or Tosylate anions upon electrochemical switch resulting in different conformational rearrangement of the molecules on the outermost layer.

Based on these experiments, 22 hours was chosen as the bias time to study bacterial biofilm formation on PEDOT:PSS in subsequent tests, to ensure more stability on the surface energy change induced.

Contact angle was measured also on PEDOT:TOS after 16 hours bias, revealing it to be more hydrophobic than PEDOT:PSS in overall. Moreover, once more the reduced polymer was found to be more hydrophobic than the oxidized one, with an average contact angle of 96°, 89.5° and 110° for the non-biased, oxidized and reduced films, respectively.

4.4. Conclusions and outlook

In conclusion, evidence was provided that the redox status of a conducting polymer film affects the ability of bacteria to adhere and form a biofilm. In particular, a 96-well microtiter plate, compatible with high throughput screening, was developed. A thin layer of conducting polymer (PEDOT:PSS or PEDOT:TOS) was deposited on the bottom of the wells yielding pixels that could be electrochemically reduced or oxidized. Here it was showed that oxidation of the conducting polymer resulted in increased *E. coli* biofilm formation compared to reduced or non-biased samples. A secondary conclusion is that one contribution to the increased biofilm formation on oxidized pixels is the relatively more hydrophilic nature of these films. A negligible amount of biofilm was observed on reduced film, and on film that was not biased. This work paves the way for the development of smart systems that control and sense biofilm growth.

Future developments will focus on using the versatility of the 96-well plate combined with the transparency of the polymer to conduct time-lapse experiments to follow the establishment (or not) of biofilms. Preliminary evidence (**Figure 26**) indicates that the proliferation of bacteria on the surface of the negatively biased polymer is slower than that on the same polymer without bias. This confirms that a reduced environment, and possibly also the presence of an electrical field, affect not only the ability of bacteria to form biofilm, but also their growth kinetics.

Finally, several routes could be followed for further improvements of the technology developed. This could involve:

- use of different methods for biofilm quantification (such as carbohydrates, lipid or slime assays) and better targeted fluorescence stainings;
- study of the effect of the oxidation state of the adhesion surface on fully

established bacterial biofilms;

- direct comparison of oxidized and reduced surface in the same well of the device (alternative patterning layout required);
- doping the polymer with natural antifouling extracts, in order to associate the effect of the oxidation state to the chemical antifouling effect of the extracts.

Chapter 5

5. Monitoring cell stress and death by OECTs

5.1. Introduction

As already mentioned in section **1.1.5**, organic electronics, due to the unique ability of conducting polymers to conduct both electronic and ionic carriers, has gained a highly relevant role in interfacing sensors with biological systems.[100,20] In particular, Organic Electrochemical Transistors (OECTs) are a class of organic-based sensors, where the active material of the transistor channel is made of a conducting polymer, the most popular being PEDOT:PSS. Furthermore, the latter is an excellent material for studying cells, but also proteins, since its demonstrated biocompatibility.[296]

Due to their ability to work in aqueous environment, the low working voltages and the ability to convert ion-to-electron signals, OECTs result to be particularly well suited for applications with cells. In fact, recent biological applications of OECTs deal with: delivering neurotransmitters in vivo;[113] electronically controlling of ion signaling;[297] cell adhesion[271,298] and migration;[299] measuring neuronal activity in vivo,[110] and fabricating ion-based logic circuits.[83] Various examples of conducting polymer devices interfacing layers of mammalian cells have been recently described, with applications in toxicology and diagnostic monitoring. [109,300,106,273]

Jimison et al.[107] have reported the integration of an organic electrochemical transistor with a trans-well (T-well) semipermeable membrane support (hereafter referred to as a Twell-OECT). Cells monolayers were cultivated and let form a barrier tissue on the T-well membrane. The Twell-OECT was used to monitor the barrier tissue integrity by analysing the variation of the ions flux through the membrane. The ionic current in an OECT has been modelled using a combination of linear circuit elements,[87] where the T-well membrane contribution is represented by a resistor and capacitor in parallel.[301] T-well as a support for the cultivation of cells is quite useful because avoids cultivation of cells directly on the PEDOT:PSS surface. Despite the high biocompatibility and electrical stability of PEDOT:PSS, our experiments show that when exposed to a very-high ionic density electrolyte, such as culture mediums, PEDOT:PSS achieve a state of saturation, that make it insensitive to further change in ionic-concentration. For this reason in the following a freshly fabricated device was used for each measurement.

One of the major aims of this work was to demonstrate and qualify organic electronics as an efficient and viable method for monitoring cellular dynamics including stress and death. In this chapter it is investigated and demonstrated the possibility to develop a low-cost, portable and disposable organic sensor for *in-vitro* detection of drug-induced cell death. In order to do so, a T-well was integrated with an OECT to monitor the viability of A549 cell line when cells are exposed to Doxorubicin. The time-evolution of cell death was studied upon exposure of cells to a fixed dose of Doxorubicin, as well as the effect of different doses of drug at a fixed time. The results obtained using OECTs were validated by more traditional methods, such as optical microscopy and fluorescence staining.

5.2. Experimental

5.2.1. Cell culture

Human non-small-cell lung carcinoma cell line A549 was purchased from ATCC (Manassas, VA, USA). Human HCC827 NSCLC cell line was kindly provided by Dr P. Jänne (Dana-Farber Cancer Institute, Boston MA).

All cells were cultured in RMPI-1640 containing 10 % FBS (Gibco, Life Technologies) 1 % penicillin/streptomycin (Sigma Aldrich) solution and 2mM glutamine (Sigma Aldrich). Cells were maintained under standard cell culture conditions at 37°C in a water-saturated atmosphere of 5% CO_2 in air.

5.2.2. Drug treatment

Stock doxorubicin (Sigma Aldrich) solutions were prepared using dymethilsulfoxide (DMSO, Sigma Aldrich) as solvent, and diluted in fresh medium before use. Final DMSO concentration in medium never exceeded 0.1% (v/v) and equal amounts of the solvent were added to control cells.

5.2.3. Surface coverage assessment

After electrical measurements, micro-porous membranes of T-wells were detached from the support. Cells adhered on the membrane were fixed with 100% methanol, and stained with hematoxylin to assess the surface coverage of the cells.

5.2.4. Cell death quantification by staining

After electrical measurements on the OECTs T-well, cell death was assessed using fluorescence microscopy after staining with Hoechst 33342 (3 μg/ml) and Propidium Iodide (2.5 μg/ml). The nuclear morphology of doxorubicin-treated and untreated A549 cells was examined as previously described.[302]

5.2.5. OECT fabrication and characterization

For the fabrication of OECT devices a standard protocol was used, [249] as already described in section **2.2.1**. Transistor channels, made of PEDOT:PSS supplemented with ethylene glycol 20% and DBSA 5%, were patterned on a glass slides using standard photolithographic techniques. The resulting transistor channel was 1 mm width and ~100 nm thick.

Wells for the lodgement of T-well were made of PDMS mixed with a curing agent (volume ratio 10:1) and designed with internal volume of ~200μL.

Electrical measurements with OECT device have been performed by a 2 channels source/measure precision unit (Agilent B2902A), controlled by a home-made LabView software**.**

5.3. Results

5.3.1. Working principle of the device

Figure 29 shows the schematic view of the experimental setup used here, with the T-well support integrated in the OECT device through a dedicated PDMS-well. The PDMS-well was designed with a 1 mm high step at the base, so that the T-well could be gently placed on it but avoiding it to directly touch the transistor channel.. De-ionized water (DI water) was used to fill the gap between the channel and the bottom part of the micro-porous membrane of the T-well, while cell culture medium, used as the electrolyte, was confined in the upper part of the membrane. The area of the polymer channel in contact with water defined the active surface of the device. Cells were cultivated on the T-well membrane before incorporation into the OECT. The main advantage to use such a setup is that cells are cultivated on the membrane of the T-well support and do not enter directly in contact with the polymer channel; therefore, the polymer is free to register any variation in ionic concentration of the liquid (water) with which is in contact. The Ag gate was immersed in the water batch, and not directly in contact with the culture medium. The DI water in contact with PEDOT:PSS could be considered as an electrolyte at zero ionic concentration with respect to the overlying medium culture. This embraces the ability of the OECT to detect even very small changes in the concentration of ions in water.

The working principle designed for our device is that, when the drug comes into action, the cell stress and death, with the inherent changes in morphology and biochemistry, will end up in a progressive disruption of the cell layer cultivated on the T-well. In fact, the exposure to the drug is expected to modify the cell-cell and cell-substrate interactions, causing the cell layer to untight and cells to detach from the T-well membrane, resulting in a decreased barrier effect towards ions from the electrolyte. As a consequence, the cell layer on the T-well membrane would be less effective in shielding cations in the electrolyte from crossing the membrane . by diffusion and reaching the DI water on the bottom.

Due to the chosen position and geometry of the gate electrode, immersed into the water batch on the side of the T-well, cations in the electrolyte could sense directly the electrostatic effect deriving from the positive bias applied to the gate. Therefore, only cations drifted into the water would be injected into the PEDOT:PSS channel by the gate voltage applied. The geometry described here represents one the major innovation elements of this work, since in OECTs both the gate electrode and the conducting polymer are commonly placed in direct contact with the electrolyte. This innovative configuration could provide a higher sensitivity to processes involving ion fluxes.

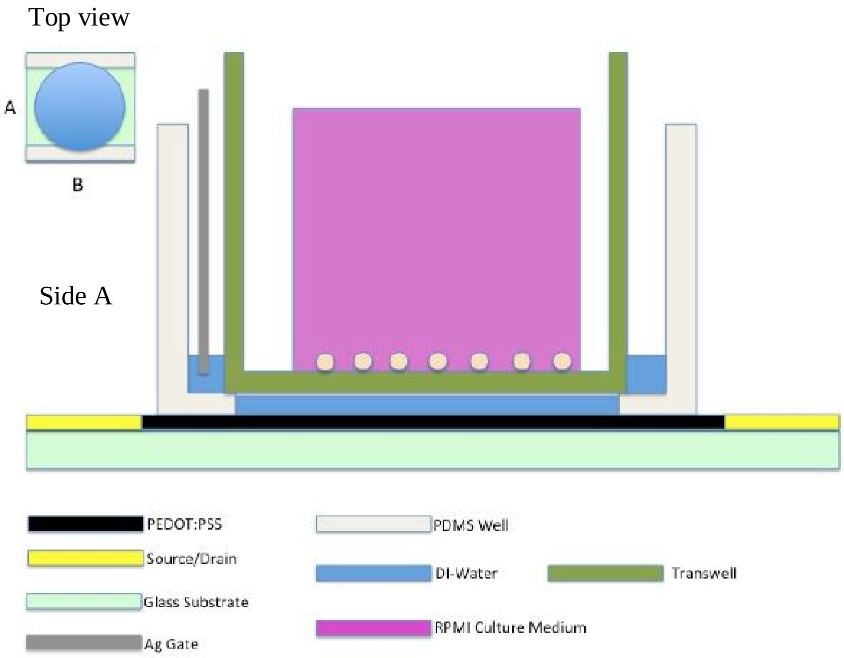

Figure 29 *Experimental setup with the T-well support integrated in the OECT device through the dedicated PDMS-well, the T-well in inserted into the PDMS-well, the T-well membrane is suspended in the electrolyte without touching the PEDOT:PSS.*

It is important to remember here that PEDOT:PSS is a degenerately *p-type* organic semiconductor, therefore its conductivity can be changed upon incorporation of cations into its polymer backbone. In fact, cations coming from the electrolyte can enter the channel and de-dope it, hence decreasing the source-drain current (I_{ds}) flowing across the channel, in accordance with the reaction in Eq. 2. Since the change in I_{ds} is proportional to the ionic force of the electrolyte, OECTs can advantageously act as sensing devices.

In the following the *in vitro* detection of cell stress and death is discussed, achieved by monitoring the cell response in time upon the effect of a fixed dose of doxorubicin and the cell response at fixed incubation time upon exposure to different doses of the same drug. A549 cells were used, representing a well-known cell-line with a good sensitivity to doxorubicin.[303,304] The OECT electrical response was correlated to optical imaging of the cell death/viability, in order to confirm that the device response can be reliably ascribed to the modifications in cell viability. All measurements were carried out inside the cell-incubator in a water-saturated atmosphere of 5% CO_2 in air at 37 °C.

5.3.2. Device characterization

As a first step of the experiment we monitored the passage of cations from the RPMI culture medium electrolyte through a clean T-Well membrane, that is without cells cultivated on its surface. The T-well was integrated in the OECT, as shown in **Figure 29**: the inner part of the T-well was left empty, while the gap-area between the bottom of the T-well and the OECT channel was filled with DI-water. The use of DI-water is important because it embraces the ability of the OECTto detect the effects of cations diffusing from the overlying electrolyte. We expected that the change in ionic density should be proportional to the available free area of the membrane. Since the RPMI culture medium is a very-high ionic density electrolyte, water should be considered as a quasi-zero ionic density electrolyte with respect to the RPMI.

Figure 30 shows the plot of the OECT drain current (I_{ds}) *vs.* time, upon injection of 150µL RPMI culture medium into the T-well, without cells cultured on the membrane of the T-Well. The plot highlights the evidence of the RPMI cations crossing the T-well membrane. The blue-curve is the reference measurement (indicated as “blank”), that is the current signal of the OECT recorded with a dry T-Well and only DI water at the interface between the membrane and the PEDOT:PSS channel, while no culture medium was injected during the measurement. The red-curve shows the same measurement carried out on the same device immediately after the previous one. In this case, 150µL of electrolyte were injected ~40 seconds after the gate voltage was turned on, the injection done with a positive gate voltage applied (V_{gs} = +0.4 V). The resulting signal is observed with a delay of about 50s, representing the time ions need to diffuse from the electrolyte into the underlying water, passing through the pores of the membrane. Once crossed the porous membrane, the cations feel the positive potential V_{gs} that force them to enter into the PEDOT:PSS channel, de-doping it and decreasing its conductivity. The observed signal represents the evidence that cations effectively cross the microporous membrane and can be efficiently and reliably detected by our OECT setup.

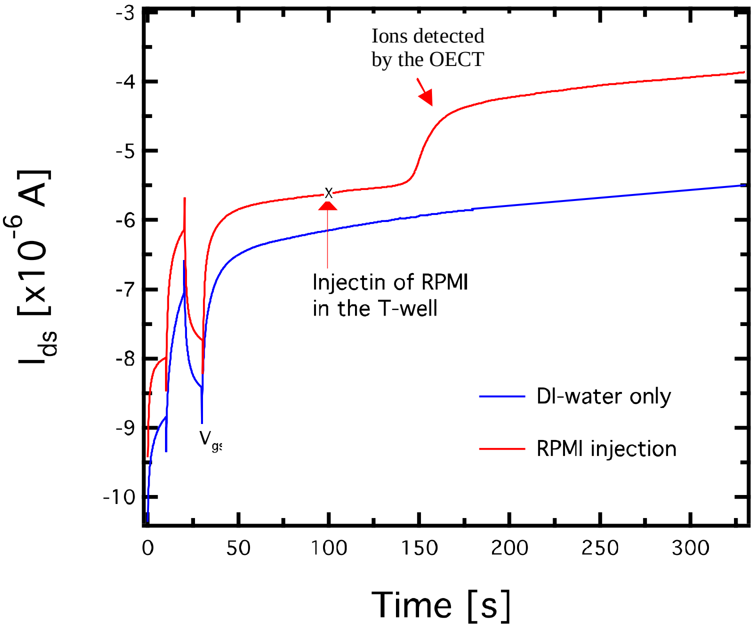

Figure 30 *Plot of the source-drain current versus time (transient current measurement) recorded at* V_{gs} *= +0.4V and* V_{ds} *= -0.4V, with (red curve) and without (blue curve) injection of an electrolyte (RPMI culture medium) in the T-well.*

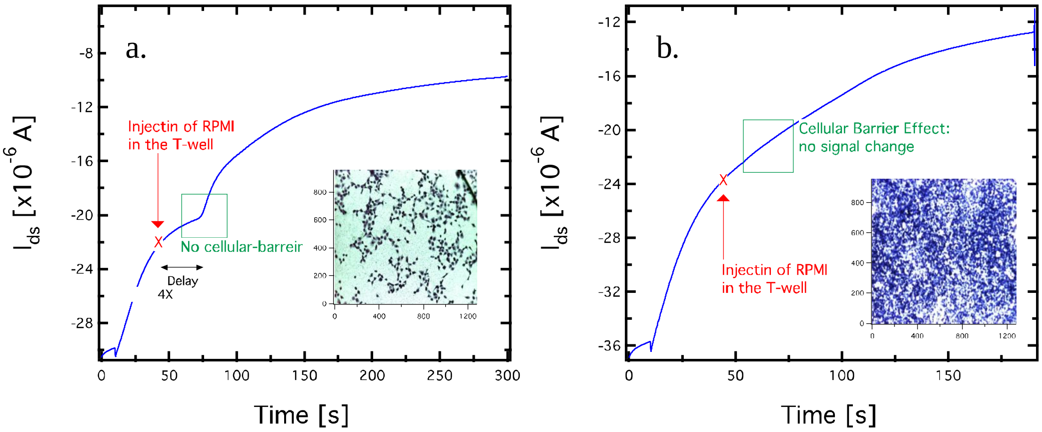

Figure 31 *Electric response of the OECT in presence of 0.5 x 105 (a.) and 1 x 105 (b.) cells cultivated on the micro-porous membrane of the T-well. The insets show the different surface coverage of the membrane in the end of the electrical measurements, observed by optical microscopy after staining with hematoxylin.*

5.3.3. Cell barrier formation and threshold cell number

The second task was to find the threshold number of cells that could generate cellular-barrier on the surface of the T-well membrane and hence test the integrity of the barrier. We expected that a good cellular-barrier would block completely the migration of cations from the RPMI culture medium through the microporous membrane.

A549 cells were seeded at different densities (*a*: 0.25 x 10^5 cells and *b*: 1 x 10^5 cells) on the membrane of the T-well, and cultivated in 150µL of medium for 24h. Immediately before the OECT measurement, the medium was removed from the T-well, leaving only a superficial thin-film of culture medium on the micro-porous membrane surface. The T-well was then coupled to the OECT and the combined device stored inside the incubator for the electrical measurement. **Figure 31** shows I_{ds} *vs.* time acquired in condition *a* and *b* (**Figure 31a** and **Figure 31b**, respectively). After ~60s the gate voltage was turned on and the T-well refilled with 150 µL of RPMI. Cells remained in a state of semi-dry condition only during the measurement time (2-3 minutes), before refilling with RPMI. This time was short enough to avoid that cells would feel any significant stress. **Figure 31a** shows that a full cellular barrier was not formed in condition *a*. Indeed, after RPMI injection, the OECT shows a decrease of the I_{ds} current (in absolute value), induced by the passage of cations through the T-well membrane. **Figure 31b** identifies the threshold number of cells able to form a full cellular-barrier. In fact, under condition *b*, after injection of extra-electrolyte into the T-well, no variations of the electrical signal could be detected, indicating that no cations were able to cross the T-well membrane, or at least, that the flow of cations was below the detection limit of the OECT. Therefore we identified the threshold number of cell to form a cellular-barrier on the T-well surface, corresponding to 1 x 10^5 cells cultivated for 24 hours.

After the OECT measurements, cells were stained with hematoxilin. This staining showed that a wide area of the T-well membrane was still uncovered by cells with condition a, while a surface coverage > 90% was observed in condition b, which is consistent with the electrical measurements.

5.3.4. Viability assessment of doxorubicin-treated A549 cells

The effect of a fixed dose (2 μM) of doxorubicin was monitored at different times from 0 to 24h on A549 cells. The dose-response assay was performed on cells cultivated on a standard 96-wells plate. This test is important to monitor the effect of doxorubicin on cell viability and to know the timescale through which the drug can induce cell death. Noteworthy, in our case it is also a complementary standard biological technique useful to correlate the OECT electrical signal with a visual imaging of cell viability.

Cell viability was expressed as percentage of alive, apoptotic and necrotic cells over the total number of counted cells. Considering, in particular, the noxious effect induced by the drug, the results related to dead cells (resumed in **Table 2**) were the following: apoptotic cells increased monotonically from 7.7% ± 4.1% at 4 hours exposure to doxorubicin to 62.3% ± 12% at 24 hours exposure; conversely, necrotic cells decreased from 20.7% ± 8.6% at 4 hours exposure to 12.7± 5.7% at 24 hours exposure, but showing a maximum of 39.1% ± 3.7% at 8 hours exposure.

Exposure time [h]	Apoptosis	Necrosis	Total
4	7.7% ± 4.1%	20.7% ± 8.6%	28.5% ± 12.7%
8	43.8% ± 12%	39.1% ± 3.7%	82.9% ± 14.1%
24	62.3% ± 12%	12.7± 3.7%	75.02± 15.8%

Table 2 *Cell viability assessment by staining with Hoechst 33342and Propidium Iodide. Cell viability is expressed as percentage of dead cells over the total number of counted cells. Apoptotically and necrotically dead cells are indicated, as well as the total number of dead cells.*

5.3.5. OECT experiments on doxorubicin-treated A549 cells

The aim here was testing whether our setup could detect the evolution of cell death upon drug effect by monitoring the OECT electrical response. A549 cells were cultivated on the micro-porous membrane of the T-well, and exposed to doxorubicin 2µM added to the RPMI culture medium. The concentration of 2µM is the reference value we find both from the dose-response assay and from the literature data. Control experiments confirmed that the doxorubicin alone at the concentration used (max 4µM, for a total volume of less than 4µL), does not affect the OECT response.

5.3.5.1. Monitoring in time, fixed drug-dose

A549 cells were exposed to a fixed dose of doxorubicin (2µM). We monitored the cellular barrier status at three time intervals (4, 8, and 24 hours) after the injection of the drug in two different conditions. RPMI not supplemented with doxorubicin was used for reference measurement (control). A second measurement RPMI where RPMI was not supplemented with doxorubicin was used as control. The control measurement is important to exclude that cell growth to confluence induce effects that can alter the cellular barrier integrity. For both the control and the measurement where doxorubicin was used, a preliminary measurement was performed, without injection of the RMPI medium in the T-well (the blank measurement). As an exemplification we report the measurements carried out on the cell culture exposed to doxorubicin for 4h.

Figure 32a shows the plot of I_{ds} recorded from A549 cells cultivated on a T-well and not exposed to doxorubicin, while **Figure 32b** shows the same plot recorded with cells cultivated under the effect of doxorubicin.

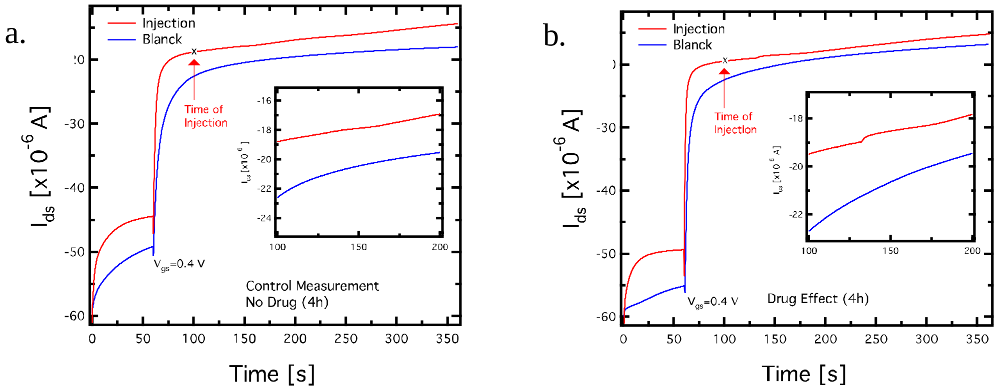

Figure 32 *Current signal of OECT recorded from control (a.) and doxorubicin-treated (4 hours) samples (b.). Blue curves represent the measurements without injection of electrolyte in the T-well; red curves represent measurements where electrolyte was injected into the T-well during the recording. Insets highlight the range between 100 and 200 seconds, where it can be observed the step induced by the flux of cations that, passing through the holes left by dead cells in the cellular layer, de-dope the PEDOT:PSS channel.*

After 4 hours from doxorubicin addition, T-well was integrated into the OECT: the culture medium in the inner part of the T-well was removed and electrical measurements acquired. The blue plot in **Figure 32a** represents the blank, that is the current acquisition without injection of electrolyte on the control T-Well, while the red curve represents the current signal recorded with injection of electrolyte in the T-well. The electrolyte was injected ~40s after the gate voltage was turned on. In the inset the time range from 100 to 200 seconds has been enlarged, representing the time where we expect a change in the I_{ds} due to a partial disruption of the cellular barrier induced by cell death: the inset highlights that no changes occurred, showing that the cellular barrier was still fully intact. This control indicated and confirmed that the change in I_{ds} recorded in **Figure 32b,** and highlighted in the corresponding inset, is directly correlated to a partial disruption of the cellular barrier as a consequence of exposure to doxorubicin.

According to the method previously described, cells were analysed also after 8h and 24h of exposure to doxorubicin. **Figure 33a** summarizes these results: the change in I_{ds} due to the cellular barrier disruption was found to be dependent on the time of exposure to the drug, with increasing effect over the 24 hours treatment. For each measurement the control measurements confirn that signals are imputable to the effect of the drug. Fluorescence pictures were recorded from the dose-response test at times of exposure to the drug corresponding to the times studied with the OECT. Photos in **Figure 33b** show that the number of apoptotic cells (shiny blue coloured) increased with time, as expected.

The correlation between the electrical signals and the images of dead A549 cells seem to be in agreement with our hypothesis. Therefore, it could be reasonable to ascribe the detected electrical signals to a disruption of the cellular barrier correlated to the number of stressed/dead cell.

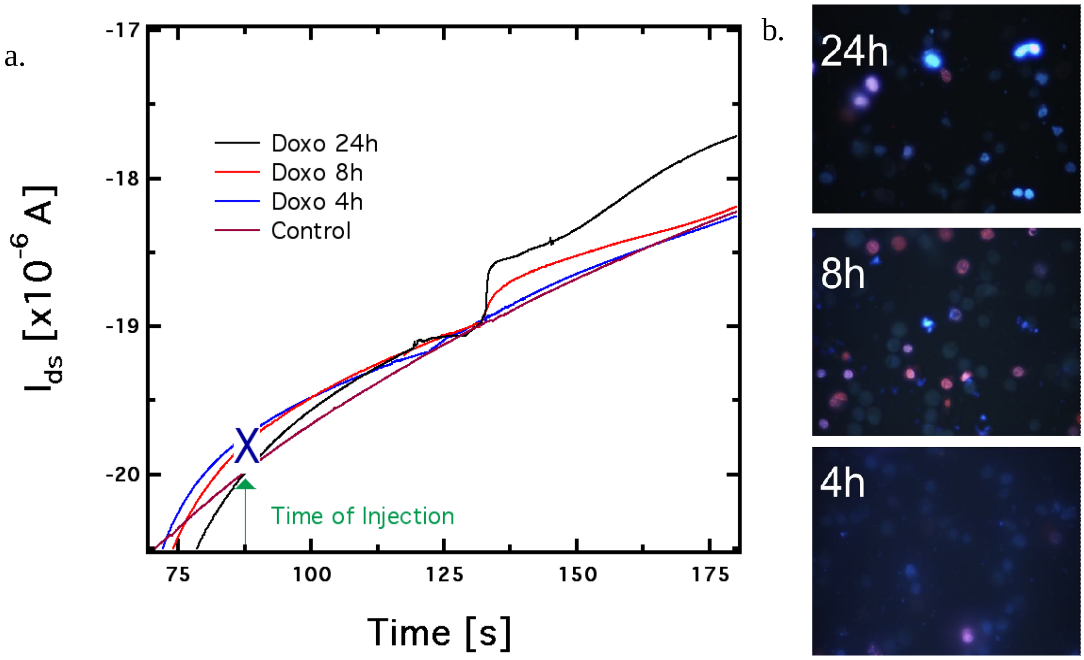

Figure 33 *a. OECT response at several times of exposure to doxorubicin. b. Results from the dose-response test performed on A549 cells exposed to doxorubicin 2 µM.*

5.3.5.2. Monitoring drug-dose at a fixed time

Finally, we exploited the ability of OECT as a biosensor for monitoring cell death upon exposure to drugs by performing tests on another lung-cancer cell line, the HCC cells, a model system in the lung-cancer research. In this experiment we analysed the cellular barrier integrity at fixed incubation time, upon exposure to a standard (2µM) and to a double dose of doxorubicin (double is intended with respect to the standard). Two cell cultures were cultivated on two different T-wells in RPMI and left to adhere for 24h. Then doxorubicin was added with concentration of 2µM and 4µM, respectively and the T-wells were left in incubation for other 48h (that is the total cultivation time was 72 hours). Following the same method previously described, after 48h the addiction of doxorubicin, immediately before the electrical measurement, the medium inside the T-well was removed and the T-well integrated in the OECT inside the incubator. **Figure 34** shows the OECT response (I_{ds} *vs.* time) acquired for the two cell cultures. The blue-curve is the water-benchmark, that is I_{ds} recorded with water alone leaving the T-well dry, without injection of electrolyte (RPMI). The green-curve is the OECT-response recorded from the cell culture exposed to 2µM doxorubicin, upon refilling the T-well with electrolyte; the red-curve is the same type of measurement recorded from the cell culture exposed to 4µM doxorubicin. The curves give evidence of cations crossing through the micro-porous membrane. Since increasing the concentration of drug (from 2 µM to 4 µM) causes a higher number of cells to die, the higher signal observed in the red-curve (4µM) is correlated to the higher surface available on the T-well membrane.

Although our findings are still preliminary, they provided us insights about the opportunity to exploit organic devices, such as OECTs, as useful tool for point-of-care, low cost and portable diagnostics.

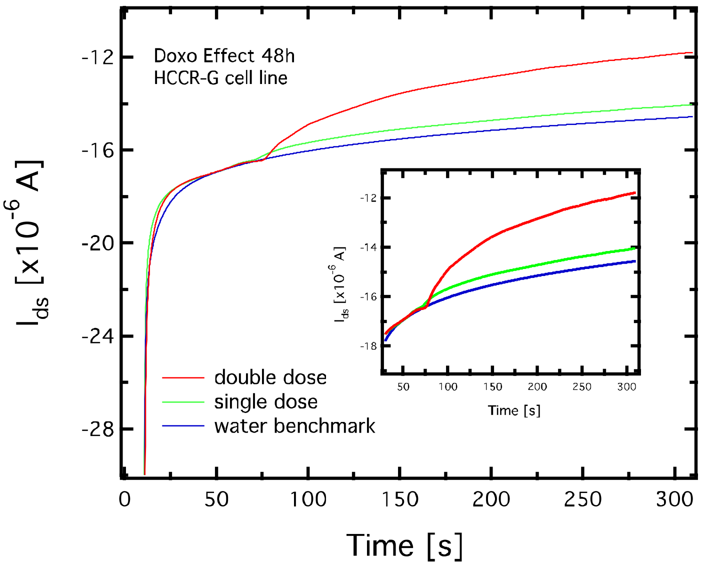

Figure 34 *Electric signal of the OECT showing the effect of the exposure of HCC cells to doxorubicin for 48 hours. The electric outputs reported compare single (2 μM) and double dose doxorubicin to the water-benchmark.*

5.4. Discussion

In order to achieve a better understanding of the results obtained by OECT signals and cell viability assessment, an effective parameter was introduced, being conceived as the combination of the drug concentration and the incubation time in presence of the drug (*D* = drug concentration x exposure time). The choice of this parameter was useful to have a first insight on the type of processes that our OECT system is sensitive to. Indeed, we hypothesized that the OECT response correlates to the viability of cells with the effect of the drug concentration at fixed time being comparable to that of time of exposure to drug at fixed concentration, in a somewhat similar fashion to what dictates the time–temperature superposition principle applied in polymer physics.[305] Thus, we decided to plot the OECT response, expressed as modulation of I_{ds} current steps observed in **Figure 33** and **Figure 34** according to Eq. 6, as function of the parameter D.

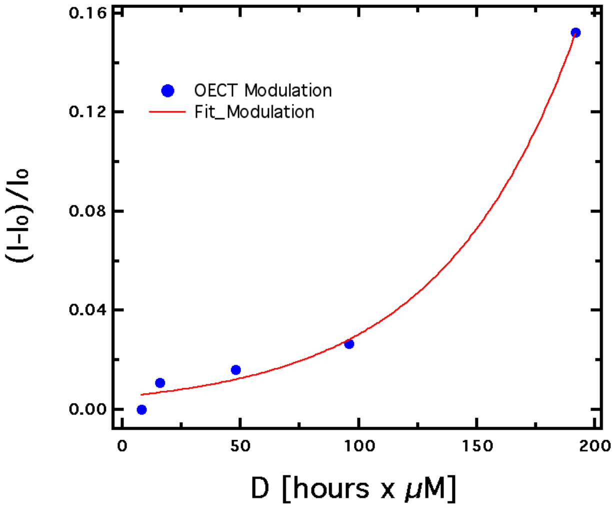

Figure 35 *I_{ds} current modulation of OECT expressed as function of the effective parameter D. The trend can be described with an exponential function.*

The data points, resulting from the drug concentrations (2 μM and 4 μM) and the times of exposure to drug (4, 8, and 24 hours) used here, are shown in **Figure 35**. The figure depicts the dependence of the OECT measured signals on the parameter D. The trend obtained could be reproduced as a typical exponential behaviour, that is shown in the figure. This allowed to temptatively correlate the electrical signals observed to the cell death, and possibly to differentiate the death mechanism (apoptosis *vs.* necrosis). To this regard, a direct comparison of the $\Delta I/I_0$ *vs. D* curve with the trends in cell death obtained from the viability assessment described in section **5.3.4** was carried out, as shown in **Figure 36**. Here, to facilitate the comparison between cell viability trends and current modulation, the former were scaled of a factor 8. Even though these are preliminary data, one can distinguish a different trend as function of the parameter D of necrotic cells compared to the apoptotic ones and to the total dead cells. As can be observed in the **Figure 36**, the necrotic trend shows a maximum at about D = 16 *h*μM,* followed by a significant reduction at higher *D*. The apoptotic percentage, instead, shows an increase that is similar to that observed by OECT, being this the major expected effect of doxorubicin. The total dead cells (apoptotic + necrotic) shows a trend that seems to have again a trend not exactly reproducing the one obtained by OECT.

Even though this interpretation is quite temptative, there seems to be the evidence that our OECT systems are effectively able to monitor the apoptotic portion of dead cells. This is quite encouraging but has to be confirmed by further and more statistically significant experiments.

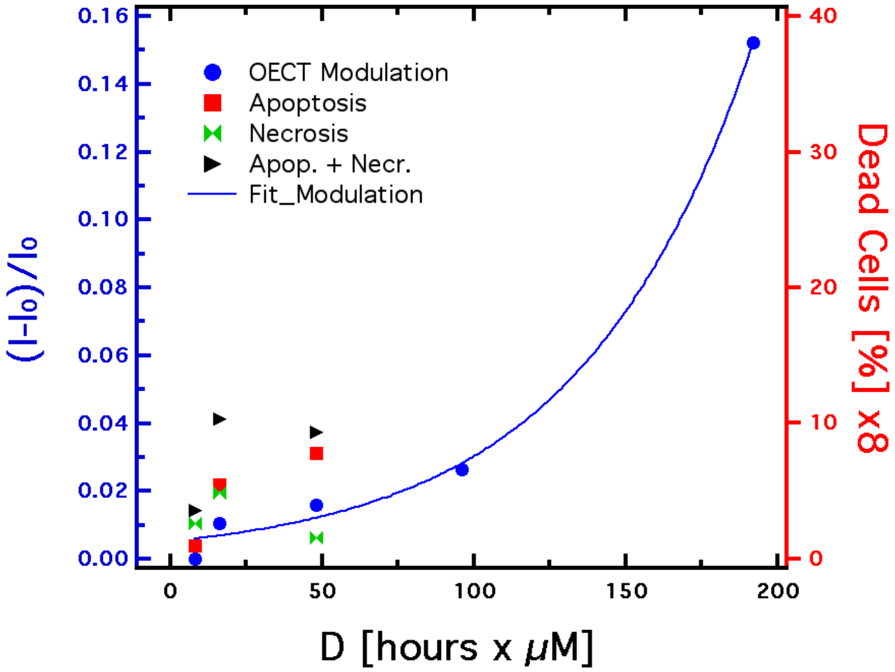

Figure 36 *Comparison of the OECT modulation with the cell viability curve, both as function of the effective parameter D. Percentage of dead cells was divided by a factor 8 for a easier comparison with OECT modulation.*

5.5. Conclusions

In conclusion, in this chapter a cell-based biosensor has been presented. An OECT was applied to electrochemically detect cell death in A549 cell line induced by exposure to doxorubicin. Cells forming a barrier tissue were treated with doxorubicin and the disruption of the barrier tissue was monitored as function of time for a fixed dose of drug (2µM) and. Results show that the OECT is able to detect the disruption of the barrier tissue through the electrochemical de-doping that takes place due to an appropriately designed measurement setup.

Future developments of this technology will involve the integration of the OECT in microfluidic systems in order to finely control liquid flows and more efficiently emulate living organisms. A further goal will be represented by the ability to distinguish different cell death mechanisms, such as apoptosis from necrosis.

Chapter 6

6. Conclusions and perspectives

Conducting polymers, represent a class of materials of increasing relevance paving the way to a growing number of applications ranging from photovoltaic to nerve regeneration. The research work of this Thesis deals with the ability, and the deriving possibilities, of some polymers to have an electrical response to both ionic and electronic transport. Properties such as the mixed ionic/electronic conductivity, together with high flexibility, conformability, and “softness” make conducting polymers uniquely suitable for interfacing the world of electronics to biological systems where ions play a dominant role. As confirmed with our work, devices based on these materials offer improved compatibility with cells and tissues and represent an ideal amplification system to transduce ionic to electronic signals, giving a fundamental contribution to the growth of the innovative field of Organic Bioelectronics. Organic Bioelectronics has been defined by and has benefited from a high interdisciplinarity, engaging expertise in materials science, chemistry, physics, electronics, engineering and life science. In spite of its high level of complexity, the cross-fertilization between the worlds of organic electronics and biology is increasingly evolving, and has already provided successful examples of integration of micro- and nano-technological applications of organic electronics with techniques of cell biology. Biosensors, medical diagnostics, tools for biomedical research, and bioelectronic implants are only few examples of the achievements attained. These results will have a undoubted effect on healthcare and quality of our lives.

This Thesis falls in the track of these great achievements and expectations for Organic Bioelectronics. In particular, the contribution of this work has been highlighting the eminent role of organic conductors in diagnostics and actuator applications. The main type of device developed and used here is the OECT, and our general aim has been to demonstrate the potential of such devices in real-time and in-situ monitoring elements and dynamic processes involved in biological systems. It has been demonstrated for the first time that OECTs can effectively and reliably sense and monitor biomolecules (eumelanin), nano-systems for drug-delivery (functionalized paramagnetic NPs) and drug-induced cellular stress. In all the different experiments reported, the analysis of the electrical output of the device allowed to successfully monitor the concentration of the analyte (eumelanin and functionalized NPs) and the evolution of the system studied (i.e., cells). The conductive properties of organic semiconductors were also exploited to control and study the surface factors that influence the adhesion of biological systems, such as bacterial cells. In this case, the organic-based actuators that were developed allowed controlling the formation of bacterial biofilms according to the redox status of the surface.

Future developments of the present work will address the optimization of the devices developed here, aiming at reaching unprecedented levels of accuracy and sensitivity in monitoring and studying biological processes. A first application will deal with monitoring the cellular stress induced by drugs, released *in situ* by nano-carrier systems, such as liposomes, functionalized NPs, micelles, etc. To this regard, the results pursued here on the detection and monitoring biological molecules, drug-delivery systems and cellular stress by organic electronic devices are pieces of a big puzzle being represented by an ambitious project. The latter is aimed at integrating the outstanding capabilities of OECTs demonstrated here towards an highly-sensitive, reliably and easy-to-use organic technology for in situ and real- time monitoring of drug-induced cellular stress. Monitoring drug-induced cellular stress is of great relevance since today this often requires cumbersome and somewhat complicated procedures. This application will run close to a more fine and precise detection of the cell death, with discrimination between apoptotic and necrotic cell death pathways. On the side of diagnostics and food safety, the sensing capabilities of OECTs will be applied for monitoring the bacterial content present in liquid environment.

It should be emphasized that, while many efforts have been already done in order to comprehend the physics underlying organic conductors and organic-based devices, plenty of work needs to be done yet.

The first area of fundamental physics that should receive attention is ion transport in organic electronic materials. The presence of both electronic and ionic carriers represents the key challenge, which renders classical methods such as conductivity measurements and impedance spectroscopy difficult to interpret. Thus, new techniques are needed in order to help decouple the contributions of electronic and ionic charges. To this end, recent experiments on charge transport in PEDOT:PSS revealed that ion mobilities were as high as those found in water, demonstrating the key role of water uptake in the polymer for increasing transport properties.

Relatively little work has been done on the synthetic side of organic bioelectronics compared to the more traditional organic electronic devices. Most materials used in bioelectronics are fundamentally unchanged since one or two decades, and are often used simply because they are commercially available. More work, therefore, needs to be done, in order to further improve chemical, physical and biocompatible properties of organic semiconductors and enlarge their functionalities and applications.

Dealing more specifically with biocompatibility, a deeper understanding of the structure of the interface between organics and electrolytes is needed. Surface properties, such as morphology and composition, greatly influence how ions, proteins, macromolecules and cells interact and conform to the surface.

Finally, *in vitro* diagnostics represents a major opportunity for future applications of organics in biomedicine. Systems with higher degree of similarity to living tissues will represent the perfect basis for the achievement of new application with high social impact.

In summary, the research work described in this Thesis has given a contribution to further demonstrate the relevance of organic electronic devices and, in particular, of OECTs in the increasingly relevant field of bioelectronics.

References

1. H. Shirakawa, E. J. Louis, A. G. MacDiarmid, C. K. Chiang, and A. J. Heeger, *J. Chem. Soc. Chem. Commun.*, 1977, 578.

2. W. R. Salaneck, I. Lundström, and B. Ranby, in *Proceedings of the Eighty-first Nobel Symposium*, Oxford University Press, Oxford, UK, 1993.

3. A. J. Heeger, *Angew. Chem. Int. Ed. Engl.*, 2001, **40**, 2591–2611.

4. J. H. Burroughes, D. D. C. Bradley, A. R. Brown, R. N. Marks, K. Mackay, R. H. Friend, P. L. Burns, and A. B. Holmes, *Nature*, 1990, **347**, 539–541.

5. A. J. Heeger, N. S. Sariciftci, and E. B. Namdas, *Semiconducting and Metallic Polymers*, OUP Oxford, 2010.

6. E. M. Conwell, in *Handbook of Conductive Molecules and Polymers*, ed. H. S. Nalwa, John Wiley & Sons, Chichester, England, 1997, pp. 1–45.

7. V. N. Prigodin and a. J. Epstein, *Phys. B Condens. Matter*, 2003, **338**, 310–317.

8. S. S. Zade and M. Bendikov, *Org. Lett.*, 2006, **8**, 5243–6.

9. M. Jaiswal and R. Menon, *Polymer (Guildf).*, 2006, **55**, 1371–1384.

10. A. G. Bayer, 1988.

11. F. Jonas and L. Schrader, *Synth. Met. Met.*, 1991, **831**, 41–43.

12. G. Heywang and F. Jonas, *Adv. Mater.*, 1992, **4**, 116.

13. L. A. A. Pettersson, F. Carlsson, O. Inganäs, and H. Arwin, *Thin Solid Films*, 1998, **313**, 356–361.

14. A. N. Aleshin, S. R. Williams, and A. J. Heeger, *Synth. Met.*, 1998, **94**, 173–177.

15. Y. Chang, K. Lee, R. Kiebooms, A. Aleshin, and A. . Heeger, *Synth. Met.*, 1999, **105**, 203–206.

16. B. L. Groenendaal, F. Jonas, D. Freitag, H. Pielartzik, and J. R. Reynolds, *Adv. Mater.*, 2000, **7**, 481–494.

17. Q. Pei, G. Zuccarello, M. Ahlskog, and O. Inganäs, *Polymer (Guildf).*, 1994, **35**, 1347–1351.

18. M. Dietrich, J. Heinze, G. Heywang, and F. Jonas, *J. Electroanal. Chem.*, 1994, **369**, 87–92.

19. A. Elschner, S. Kirchmeyer, W. Lövenich, U. Merker, and K. Reuter, *PEDOT, Principles and Applications of an Intrinsically Conductive Polymer,* CRC Press, Boca Raton, FL, USA, 2010.

20. J. Rivnay, R. M. Owens, and G. G. Malliaras, *Chem. Mater.*, 2013, **in press**.

21. H. Okuzaki, in *19th International Workshop on Active-Matrix Flatpanel Displays and Devices (AM-FPD),* Kyoto, Japan.

22. X. Crispin, S. Marciniak, W. Osikowicz, G. Zotti, A. W. D. van der Gon, F. Louwet, M. Fahlman, L. Groenendaal, F. D. E. Schryver, and W. R. Salaneck, *J. Polym. Sci. Part B Polym. Phys.*, 2003, **41**, 2561–2583.

23. A. Mantovani Nardes, M. Kemerink, R. A. J. Janssen, J. A. M. Bastiaansen, N. M. M. Kiggen, B. M. W. Langeveld, A. J. J. M. Van Breemen, and M. M. De Kok, *Adv. Mater.*, 2007, **19**, 1196–1200.

24. G. Greczynski, T. Kugler, M. Keil, W. Osikwicz, M. Fahlman, and W. R. Salaneck, *J. Electron Spectrosc. Relat. Phenom*, 2001, **121**, 1.

25. J. Hwang, F. Amy, and A. Kahn, *Org. Electron.*, 2006, **7**, 387–396.

26. B. Winther-Jensen and K. West, *Macromolecules*, 2004, **37**, 4538–4543.

27. B. Winther-Jensen, D. W. Breiby, and K. West, *Synth. Met.*, 2005, **152**, 1–4.

28. L. H. Jimison, A. Hama, X. Strakosas, V. Armel, D. Khodagholy, E. Ismailova, G. G. Malliaras, B. Winther-Jensen, and R. M. Owens, *J. Mater. Chem.*, 2012, **22**, 19498.

29. K. Zuber, M. Fabretto, C. Hall, and P. Murphy, *Macromol. Rapid Commun.*, 2008, **29**, 1503–1508.

30. K. E. Aasmundtveit, E. J. Samuelsen, L. A. A. Pettersson, O. Inganas, T. Johansson, and R. Feidenhans, *Synth. Met.*, 1999, **101**, 561–564.

31. S. Ashizawa, R. Horikawa, and H. Okuzaki, *Synth. Met.*, 2005, **153**, 5–8.

32. S. K. . Jönsson, J. Birgerson, X. Crispin, G. Greczynski, W. Osikowicz, a. . Denier van der Gon, W. . Salaneck, and M. Fahlman, *Synth. Met.*, 2003, **139**, 1–10.

33. J. Y. Kim, J. H. Jung, D. E. Lee, and J. Joo, *Synth. Met.*, 2002, **126**, 311–316.

34. A. M. Nardes, R. a. J. Janssen, and M. Kemerink, *Adv. Funct. Mater.*, 2008, **18**, 865–871.

35. T. Y. Kim, J. E. Kim, and K. S. Suh, *Polym. Int.*, 2006, **55**, 80–86.

36. R. H. Friend, R. W. Gymer, A. B. Holmes, J. H. Burroughes, R. N. Marks, C. Taliani, D. D. C. Bradley, D. A. Dos Santos, J. L. Bredas, M. Logdlund, and W. R. Salaneck, *Nature*, 1999, **397**, 121–128.

37. J.-M. Nunzi, *Comptes Rendus Phys.*, 2002, **3**, 523–542.

38. H. Klauk, *Chem. Soc. Rev.*, 2010, **39**, 2643–2666.

39. H. Sirringhaus, N. Tessler, and R. Friend, *Science (80-.).*, 1998, **280**, 1741–4.

40. G. H. Gelinck, H. E. a Huitema, E. van Veenendaal, E. Cantatore, L. Schrijnemakers, J. B. P. H. van der Putten, T. C. T. Geuns, M. Beenhakkers, J. B. Giesbers, B.-H. Huisman, E. J. Meijer, E. M. Benito, F. J. Touwslager, A. W. Marsman, B. J. E. van Rens, and D. M. de Leeuw, *Nat. Mater.*, 2004, **3**, 106–10.

41. L. Zhou, A. Wanga, S.-C. Wu, J. Sun, S. Park, and T. N. Jackson, *Appl. Phys. Lett.*, 2006, **88**, 083502.

42. P. Andersson, R. Forchheimer, P. Tehrani, and M. Berggren, *Adv. Funct. Mater.*, 2007, **17**, 3074–3082.

43. P. F. Baude, D. A. Ender, M. A. Haase, T. W. Kelley, D. V. Muyres, and S. D. Theiss, *Appl. Phys. Lett.*, 2003, **82**, 3964.

44. S. Steudel, K. Myny, V. Arkhipov, C. Deibel, S. De Vusser, J. Genoe, and P. Heremans, *Nat. Mater.*, 2005, **4**, 597–600.

45. J. T. Mabeck and G. G. Malliaras, *Anal. Bioanal. Chem.*, 2006, **384**, 343–53.

46. P. Lin and F. Yan, *Adv. Mater.*, 2012, **24**, 34–51.

47. L. Kergoat, B. Piro, M. Berggren, G. Horowitz, and M.-C. Pham, *Anal. Bioanal. Chem.*, 2012, **402**, 1813–26.

48. L. Torsi, M. Magliulo, K. Manoli, and G. Palazzo, *Chem. Soc. Rev.*, 2013, **42**, 8612–28.

49. Z. Bao, A. Dodabalapur, and A. J. Lovinger, *Appl. Phys. Lett.*, 1996, **69**, 4108.

50. F. Maddalena, M. J. Kuiper, B. Poolman, F. Brouwer, J. C. Hummelen, D. M. de Leeuw, B. De Boer, and P. W. M. Blom, *J. Appl. Phys.*, 2010, **108**, 124501.

51. M.-J. Spijkman, J. J. Brondijk, T. C. T. Geuns, E. C. P. Smits, T. Cramer, F. Zerbetto, P. Stoliar, F. Biscarini, P. W. M. Blom, and D. M. de Leeuw, *Adv. Funct. Mater.*, 2010, **20**, 898–905.

52. L. Torsi, M. C. Tanese, N. Cioffi, M. C. Gallazzi, L. Sabbatini, P. G. Zambonin, G. Raos, S. V. Meille, and M. M. Giangregorio, *J. Phys. Chem. B*, 2003, **107**, 7589–7594.

53. F. Buth, D. Kumar, M. Stutzmann, and J. a. Garrido, *Appl. Phys. Lett.*, 2011, **98**, 153302.

54. M. E. Roberts, S. C. B. Mannsfeld, N. Queraltó, C. Reese, J. Locklin, W. Knoll, and Z. Bao, *Proc. Natl. Acad. Sci. U. S. A.*, 2008, **105**, 12134–9.

55. C. Liao and F. Yan, *Polym. Rev.*, 2013, **53**, 352–406.

56. P. Bergveld, *IEEE Trans. Biomed. Eng.*, 1970, **BME-17**, 70–71.

57. P. Bergveld, *Sensors Actuators B*, 2003, **88**, 1–20.

58. R. Ponce Ortiz, A. Facchetti, and T. J. Marks, *Chem. Rev.*, 2010, **110**, 205–39.

59. S. Ju, K. Lee, D. B. Janes, M.-H. Yoon, A. Facchetti, and T. J. Marks, *Nano Lett.*, 2005, **5**, 2281–6.

60. M. J. Panzer, C. R. Newman, and C. D. Frisbie, *Appl. Phys. Lett.*, 2005, **86**, 103503.

61. M. J. Panzer and C. D. Frisbie, *Adv. Mater.*, 2008, **20**, 3177–3180.

62. J. H. Cho, J. Lee, Y. He, B. S. Kim, T. P. Lodge, and C. D. Frisbie, *Adv. Mater.*, 2008, **20**, 686–690.

63. S. Mitra, A. . Shukla, and S. Sampath, *J. Power Sources*, 2001, **101**, 213–218.

64. T. Cramer, a. Kyndiah, M. Murgia, F. Leonardi, S. Casalini, and F. Biscarini, *Appl. Phys. Lett.*, 2012, **100**, 143302.

65. M. J. Panzer and C. D. Frisbie, *Adv. Funct. Mater.*, 2006, **16**, 1051–1056.

66. J. H. Cho, J. Lee, Y. Xia, B. Kim, Y. He, M. J. Renn, T. P. Lodge, and C. D. Frisbie, *Nat. Mater.*, 2008, **7**, 900–6.

67. M. Hamedi, L. Herlogsson, X. Crispin, R. Marcilla, M. Berggren, and O. Inganäs, *Adv. Mater.*, 2009, **21**, 573–7.

68. M. J. Panzer and C. D. Frisbie, *J. Am. Chem. Soc.*, 2007, **129**, 6599–607.

69. L. Herlogsson, M. Cölle, S. Tierney, X. Crispin, and M. Berggren, *Adv. Mater.*, 2010, **22**, 72–6.

70. L. Kergoat, L. Herlogsson, D. Braga, B. Piro, M.-C. Pham, X. Crispin, M. Berggren, and G. Horowitz, *Adv. Mater.*, 2010, **22**, 2565–9.

71. M. J. Panzer and C. D. Frisbie, *J. Am. Chem. Soc.*, 2005, **127**, 6960–1.

72. H. Shimotani, H. Asanuma, J. Takeya, and Y. Iwasa, *Appl. Phys. Lett.*, 2006, **89**, 203501.

73. S. Ono, K. Miwa, S. Seki, and J. Takeya, *Appl. Phys. Lett.*, 2009, **94**, 063301.

74. J. Lee, M. J. Panzer, Y. He, T. P. Lodge, and C. D. Frisbie, *J. Am. Chem. Soc.*, 2007, **129**, 4532–3.

75. E. Said, X. Crispin, L. Herlogsson, S. Elhag, N. D. Robinson, and M. Berggren, *Appl. Phys. Lett.*, 2006, **89**, 143507.

76. L. Kergoat, B. Piro, M. Berggren, M.-C. Pham, A. Yassar, and G. Horowitz, *Org. Electron.*, 2012, **13**, 1–6.

77. P. Stoliar, E. Bystrenova, S. D. Quiroga, P. Annibale, M. Facchini, M. Spijkman, S. Setayesh, D. de Leeuw, and F. Biscarini, *Biosens. Bioelectron.*, 2009, **24**, 2935–8.

78. F. Buth, A. Donner, M. Sachsenhauser, M. Stutzmann, and J. a Garrido, *Adv. Mater.*, 2012, **24**, 4511–7.

79. S. Casalini, F. Leonardi, T. Cramer, and F. Biscarini, *Org. Electron.*, 2013, **14**, 156–163.

80. T. Cramer, B. Chelli, M. Murgia, M. Barbalinardo, E. Bystrenova, D. M. de Leeuw, and F. Biscarini, *Phys. Chem. Chem. Phys.*, 2013, **15**, 3897–905.

81. M. Magliulo, A. Mallardi, M. Y. Mulla, S. Cotrone, B. R. Pistillo, P. Favia, I. Vikholm-Lundin, G. Palazzo, and L. Torsi, *Adv. Mater.*, 2013, **25**, 2090–4.

82. T. Someya, A. Dodabalapur, A. Gelperin, H. E. Katz, and Z. Bao, *Langmuir*, 2002, **18**, 5299–5302.

83. D. Nilsson, N. Robinson, M. Berggren, and R. Forchheimer, *Adv. Mater.*, 2005, **17**, 353–358.

84. H. S. White, G. P. Kittlesen, and M. S. Wrighton, *J. Am. Chem. Soc*, 1984, **106**, 5375–5377.

85. J. W. Thackeray, H. S. White, and M. S. Wrighton, *J. Phys. Chem.*, 1985, **89**, 5133–5140.

86. E. W. Paul, A. J. Ricco, and M. S. Wrighton, *J. Phys. Chem.*, 1985, **89**, 1441–1447.

87. D. a. Bernards and G. G. Malliaras, *Adv. Funct. Mater.*, 2007, **17**, 3538–3544.

88. F. Cicoira, M. Sessolo, O. Yaghmazadeh, J. a DeFranco, S. Y. Yang, and G. G. Malliaras, *Adv. Mater.*, 2010, **22**, 1012–6.

89. P. Lin, F. Yan, and H. L. W. Chan, *ACS Appl. Mater. Interfaces*, 2010, **2**, 1637–41.

90. G. Tarabella, C. Santato, S. Y. Yang, S. Iannotta, G. G. Malliaras, and F. Cicoira, *Appl. Phys. Lett.*, 2010, **97**, 123304.

91. P. N. Bartlett and Y. Astier, *Chem. Comm.*, 2000, 105–112.

92. H. Tang, F. Yan, P. Lin, J. Xu, and H. L. W. Chan, *Adv. Funct. Mater.*, 2011, **21**, 2264–2272.

93. S. Y. Yang, F. Cicoira, R. Byrne, F. Benito-Lopez, D. Diamond, R. M. Owens, and G. G. Malliaras, *Chem. Comm.*, 2010, **46**, 7972–4.

94. H. Tang, P. Lin, H. L. W. Chan, and F. Yan, *Biosens. Bioelectron.*, 2011, **26**, 4559–63.

95. G. Tarabella, A. Pezzella, A. Romeo, P. D'Angelo, N. Coppedè, M. Calicchio, M. d'Ischia, R. Mosca, and S. Iannotta, *J. Mater. Chem. B*, 2013, **1**, 3843.

96. S. Chao and M. S. Wrighton, *J. Am. Chem. Soc.*, 1987, **109**, 6627–6631.

97. D. Nilsson, T. Kugler, P. Svensson, and M. Berggren, *Sensors Actuators B*, 2002, **86**, 193–197.

98. G. Tarabella, G. Nanda, M. Villani, N. Coppedè, R. Mosca, G. G. Malliaras, C. Santato, S. Iannotta, and F. Cicoira, *Chem. Sci.*, 2012, **3**, 3432.

99. G. Tarabella, A. G. Balducci, N. Coppedè, S. Marasso, P. D'Angelo, S. Barbieri, M. Cocuzza, P. Colombo, F. Sonvico, R. Mosca, and S. Iannotta, *Biochim. Biophys. Acta*, 2013, **1830**, 4374–80.

100. M. Berggren and a. Richter-Dahlfors, *Adv. Mater.*, 2007, **19**, 3201–3213.

101. K. Svennersten, K. C. Larsson, M. Berggren, and A. Richter-Dahlfors, *Biochim. Biophys. Acta*, 2011, **1810**, 276–85.

102. R. M. Owens and G. G. Malliaras, *MRS Bull.*, 2011, **35**, 449–456.

103. S. Y. Yang, B. N. Kim, A. A. Zakhidov, P. G. Taylor, J.-K. Lee, C. K. Ober, M. Lindau, and G. G. Malliaras, *Adv. Mater.*, 2011, **23**, H184–8.

104. D.-J. Kim, N.-E. Lee, J.-S. Park, I.-J. Park, J.-G. Kim, and H. J. Cho, *Biosens. Bioelectron.*, 2010, **25**, 2477–82.

105. P. Lin, X. Luo, I.-M. Hsing, and F. Yan, *Adv. Mater.*, 2011, **23**, 4035–40.

106. S. Tria, L. Jimison, A. Hama, M. Bongo, and R. Owens, *Biosensors*, 2013, **3**, 44–57.

107. L. H. Jimison, S. a Tria, D. Khodagholy, M. Gurfinkel, E. Lanzarini, A. Hama, G. G. Malliaras, and R. M. Owens, *Adv. Mater.*, 2012, **24**, 5919–23.

108. M. Bongo, O. Winther-Jensen, S. Himmelberger, X. Strakosas, M. Ramuz, A. Hama, E. Stavrinidou, G. G. Malliaras, A. Salleo, B. Winther-Jensen, and R. M. Owens, *J. Mater. Chem. B*, 2013, **1**, 3860.

109. P. Lin, F. Yan, J. Yu, H. L. W. Chan, and M. Yang, *Adv. Mater.*, 2010, **22**, 3655–60.

110. D. Khodagholy, T. Doublet, P. Quilichini, M. Gurfinkel, P. Leleux, A. Ghestem, E. Ismailova, T. Hervé, S. Sanaur, C. Bernard, and G. G. Malliaras, *Nat. Commun.*, 2013, **4**, 1575.

111. J. Isaksson, P. Kjäll, D. Nilsson, N. D. Robinson, M. Berggren, and A. Richter-Dahlfors, *Nat. Mater.*, 2007, **6**, 673–9.

112. D. Khodagholy, T. Doublet, M. Gurfinkel, P. Quilichini, E. Ismailova, P. Leleux, T. Herve, S. Sanaur, C. Bernard, and G. G. Malliaras, *Adv. Mater.*, 2011, **23**, H268–72.

113. D. T. Simon, S. Kurup, K. C. Larsson, R. Hori, K. Tybrandt, M. Goiny, E. W. H. Jager, M. Berggren, B. Canlon, and A. Richter-Dahlfors, *Nat. Mater.*, 2009, **8**, 742–6.

114. S. Y. Yang, B. N. Kim, A. A. Zakhidov, P. G. Taylor, J.-K. Lee, C. K. Ober, M. Lindau, and G. G. Malliaras, *Adv. Mater.*, 2011, **23**, H184–8.

115. J. S. Wilson, *Sensor Technology Handbook*, Elsevier, Amsterdam/Boston, 2005.

116. Y. Lei, W. Chen, and A. Mulchandani, *Anal. Chim. Acta*, 2006, **568**, 200–210.

117. M. d’Ischia, A. Napolitano, A. Pezzella, P. Meredith, and T. Sarna, *Angew. Chem. Int. Ed. Engl.*, 2009, **48**, 3914–21.

118. P. Meredith and T. Sarna, *Pigment Cell Res.*, 2006, **19**, 572–94.

119. J. D. Simon, D. Peles, K. Wakamatsu, and S. Ito, *Pigment Cell Melanoma Res.*, 2009, **22**, 563–79.

120. G. Prota, M. d’Ischia, and D. Mascagna, *Melanoma Res.*, 1994, **4**, 351–358.

121. J. D. Simon, L. Hong, and D. N. Peles, *J. Phys. Chem. B*, 2008, **112**, 13201–17.

122. M. Ambrico, P. F. Ambrico, A. Cardone, N. F. Della Vecchia, T. Ligonzo, S. R. Cicco, M. M. Talamo, A. Napolitano, V. Augelli, G. M. Farinola, and M. d’Ischia, *J. Mater. Chem. C*, 2013, **1**, 1018.

123. M. M. Arafat, B. Dinan, S. a Akbar, and a S. M. a Haseeb, *Sensors (Basel).*, 2012, **12**, 7207–7258.

124. G. Blanita and M. D. Lazar, *Micro Nanosyst.*, 2013, **5**, 138–146.

125. Y.-C. Chen, X.-C. Huang, Y.-L. Luo, Y.-C. Chang, Y.-Z. Hsieh, and H.-Y. Hsu, *Sci. Technol. Adv. Mater.*, 2013, **14**, 044407.

126. F. E. Osterloh, *Chem. Soc. Rev.*, 2013, **42**, 2294–2320.

127. M. M. Khin, A. S. Nair, V. J. Babu, R. Murugan, and S. Ramakrishna, *Energy Environ. Sci.*, 2012, **5**, 8075.

128. K. D. Grieger, I. Linkov, S. F. Hansen, and A. Baun, *Nanotoxicology*, 2012, **6**, 196–212.

129. J. R. Peralta-Videa, L. Zhao, M. L. Lopez-Moreno, G. de la Rosa, J. Hong, and J. L. Gardea-Torresdey, *J. Hazard. Mater.*, 2011, **186**, 1–15.

130. A. Amann, M. Corradi, P. Mazzone, and A. Mutti, *Expert Rev. Mol. Diagn.*, 2011, **11**, 207–217.

131. A. R. Murray, E. Kisin, A. Inman, S.-H. Young, M. Muhammed, T. Burks, A. Uheida, A. Tkach, M. Waltz, V. Castranova, B. Fadeel, V. E. Kagan, J. E. Riviere, N. Monteiro-Riviere, and A. A. Shvedova, *Cell Biochem. Biophys.*, 2013, **67**, 461–476.

132. T. Kupka, M. Stachów, E. Chełmecka, K. Pasterny, M. Stobińska, L. Stobiński, and J. Kaminský, *J. Chem. Theory Comput.*, 2013, **9**, 4275–4286.

133. S. Muhammad, H.-L. Xu, R.-L. Zhong, Z.-M. Su, A. G. Al-Sehemi, and A. Irfan, *J. Mater. Chem. C*, 2013, **1**, 5439.

134. V. Mulens, M. D. P. Morales, and D. F. Barber, *ISRN Nanomater.*, 2013, **2013**, 1–14.

135. H.-W. Liang, S. Liu, and S.-H. Yu, *Adv. Mater.*, 2010, **22**, 3925–3937.

136. D. Sundaramurthi, K. S. Vasanthan, P. Kuppan, U. M. Krishnan, and S. Sethuraman, *Biomed. Mater.*, 2012, **7**, 045005.

137. L. Barbosa-Barros, G. Rodríguez, C. Barba, M. Cócera, L. Rubio, J. Estelrich, C. López-Iglesias, A. de la Maza, and O. López, *Small*, 2012, **8**, 807–818.

138. H. Salehizadeh, E. Hekmatian, M. Sadeghi, and K. Kennedy, *J. Nanobiotechnology*, 2012, **10**, 3.

139. V. M. Agranovich, Y. N. Gartstein, and M. Litinskaya, *Chem. Rev.*, 2011, **111**, 5179–5214.

140. R. Ghosh Chaudhuri and S. Paria, *Chem. Rev.*, 2012, **112**, 2373–433.

141. W. T. Al-Jamal and K. Kostarelos, *Acc. Chem. Res.*, 2011, **44**, 1094–1104.

142. K. Miyata, R. J. Christie, and K. Kataoka, *React. Funct. Polym.*, 2011, **71**, 227–234.

143. X.-B. Xiong, A. Falamarzian, S. M. Garg, and A. Lavasanifar, *J. Control. Release*, 2011, **155**, 248–61.

144. H. Wu, R. Yang, B. Song, Q. Han, J. Li, Y. Zhang, Y. Fang, and R. Tenne, *ACS Nano*, 2011, **5**, 1276–1281.

145. L. M. Bronstein and Z. B. Shifrina, *Chem. Rev.*, 2011, **111**, 5301–44.

146. M. Hamidi, A. Azadi, and P. Rafiei, *Adv. Drug Deliv. Rev.*, 2008, **60**, 1638–49.

147. M. Homberger and U. Simon, *Philos. Trans. A. Math. Phys. Eng. Sci.*, 2010, **368**, 1405–53.

148. J. Pardeike, A. Hommoss, and R. H. Müller, *Int. J. Pharm.*, 2009, **366**, 170–184.

149. J. W. Wiechers and N. Musee, *J. Biomed. Nanotechnol.*, 2010, **6**, 408–431.

150. B. R. Cuenya, *Thin Solid Films*, 2010, **518**, 3127–3150.

151. T. V Duncan, *J. Colloid Interface Sci.*, 2011, **363**, 1 – 24.

152. S. K. Sahoo, S. Parveen, and J. J. Panda, *Nanomedicine Nanotechnology, Biol. Med.*, 2007, **3**, 20–31.

153. R. Kessler, *Environ. Health Perspect.*, 2011, **119**.

154. S. Giordano, P. Adamo, V. Spagnuolo, and B. M. Vaglieco, *J. Environ. Sci.*, 2010, **22**, 1357–1363.

155. R. D. Handy, Æ. F. Von Der Kammer, Æ. J. R. Lead, Æ. Richard, and O. Æ. Mark, *Ecotoxicology*, 2008, **17**, 287–314.

156. A. B. G. Lansdown, *J. Wound Care*, 2002, **11**, 125 – 130.

157. M. Yamanaka, K. Hara, and J. Kudo, *Appl. Environ. Microbiol.*, 2005, **71**, 7589–93.

158. E. Pollert, G. Goglio, S. Mornet, and E. Duguet, in *Nanomaterials: A Danger or a Promise?*, eds. R. Brayner, F. Fiévet, and T. Coradin, Springer London, London, 2013, pp. 99–129.

159. C. Corot and D. Warlin, *Wiley Interdiscip. Rev. Nanomed. Nanobiotechnol.*, 2013, **5**, 411–22.

160. V. H. L. Lee, H. Ghandehari, and P. Couvreur, *Adv. Drug Deliv. Rev.*, 2013, **65**, 21–23.

161. G. G. Daaboul, a Yurt, X. Zhang, G. M. Hwang, B. B. Goldberg, and M. S. Ünlü, *Nano Lett.*, 2010, **10**, 4727–31.

162. K. Lindfors, T. Kalkbrenner, P. Stoller, and V. Sandoghdar, *Phys. Rev. Lett.*, 2004, **93**, 037401.

163. S. Nie and S. R. Emory, *Science (80-.).*, 1997, **275**, 1102 – 1106.

164. I. Reimold, D. Domke, J. Bender, C. A. Seyfried, H. Radunz, and G. Fricker, *Eur. J. Pharm. Biopharm.*, 2008, **70**, 627–632.

165. A. Dubes, P. Shahgaldian, A. W. Coleman, and C. B. Lyon, *Eur. J. Pharm. Biopharm.*, 2003, **55**, 279–282.

166. A. Mayer and M. Antonietti, *Colloid Polym. Sci.*, 1998, **276**, 769–779.

167. L. Fumagalli, D. Esteban-Ferrer, A. Cuervo, J. L. Carrascosa, and G. Gomila, *Nat. Mater.*, 2012, **11**, 808–16.

168. C. Latkoczy, R. Kägi, M. Fierz, M. Ritzmann, D. Günther, and M. Boller, *J. Environ. Monit.*, 2010, **12**, 1422–9.

169. M. A. van Dijk, M. Lippitz, D. Stolwijk, and M. Orrit, *Opt. Express*, 2007, **15**, 2273–2287.

170. F. Ignatovich and L. Novotny, *Phys. Rev. Lett.*, 2006, **96**, 013901.

171. F. V. Ignatovich, D. Topham, and L. Novotny, *IEEE J. Sel. Top. Quantum Electron.*, 2006, **12**, 1292–1300.

172. T. Lu, H. Lee, T. Chen, S. Herchak, J.-H. Kim, S. E. Fraser, R. C. Flagan, and K. Vahala, *Proc. Natl. Acad. Sci. U. S. A.*, 2011, **108**, 5976–9.

173. S. Person, B. Deutsch, A. Mitra, and L. Novotny, *Nano Lett.*, 2011, **11**, 257–61.

174. X. Hong, E. M. P. H. van Dijk, S. R. Hall, J. B. Götte, N. F. van Hulst, and H. Gersen, *Nano Lett.*, 2011, **11**, 541–7.

175. A. Chatterjee, M. Santra, N. Won, S. Kim, J. K. Kim, S. Bin Kim, and K. H. Ahn, *J. Am. Chem. Soc.*, 2009, **131**, 2040–1.

176. Y.-H. Lin and W.-L. Tseng, *Chem. Commun. (Camb).*, 2009, 6619–21.

177. Y.-G. Zhou, N. V Rees, and R. G. Compton, *Angew. Chem. Int. Ed. Engl.*, 2011, **50**, 4219–21.

178. P. I. Nikitin, P. M. Vetoshko, and T. I. Ksenevich, *J. Magn. Magn. Mater.*, 2007, **311**, 445–449.

179. J. Zhu, S. K. Ozdemir, Y. Xiao, L. Li, L. He, and L. Yang, *Nat. Photonics*, 2010, **4**, 46 – 49.

180. S. X. Wang and G. Li, *IEEE Trans. Magn.*, 2008, **44**, 1687–1702.

181. P. Eitenne, G. Creuzet, A. Friederich, and J. Chazelas, *Phys. Rev. Lett.*, 1988, **61**.

182. G. Binasch, P. Griinberg, F. Saurenbach, and W. Zinn, *Phys. Rev. B*, 1989, **39**, 4828–4830.

183. J.-L. Fraikin, T. Teesalu, C. M. McKenney, E. Ruoslahti, and A. N. Cleland, *Nat. Nanotechnol.*, 2011, **6**, 308–13.

184. J. W. Costerton, P. S. Stewart, and E. P. Greenberg, *Science*, 1999, **284**, 1318–22.

185. D. de Beer, P. Stoodley, F. Roe, and Z. Lewandowski, *Biotechnol. Bioeng.*, 1994, **43**, 1131–8.

186. C. Beloin, A. Roux, and J.-M. Ghigo, *Curr. Top. Microbiol .Immunol.*, 2008, **322**, 249–299.

187. P. N. Danese, L. A. Pratt, and R. Kolter, *J. Bacteriol.*, 2000, **182**, 3593–3596.

188. H.-C. Flemming and J. Wingender, *Nat. Rev. Microbiol.*, 2010, **8**, 623–33.

189. I. W. Sutherland, *Trends Microbiol.*, 2001, **9**, 222–7.

190. P. N. Danese, L. A. Pratt, S. L. Dove, and R. Kolter, *Mol. Microbiol.*, 2000, **37**, 424–32.

191. R. M. Donlan, *Emerg. Infect. Dis.*, 2002, **8**, 881–890.

192. R. Van Houdt and C. W. Michiels, *Res. Microbiol.*, 2005, **156**, 626–33.

193. A. Reisner, J. a J. Haagensen, M. a Schembri, E. L. Zechner, and S. Molin, *Mol. Microbiol.*, 2003, **48**, 933–46.

194. C. Prigent-Combaret, G. Prensier, T. T. Le Thi, O. Vidal, P. Lejeune, and C. Dorel, *Environ. Microbiol.*, 2000, **2**, 450–64.

195. L. a Pratt and R. Kolter, *Mol. Microbiol.*, 1998, **30**, 285–93.

196. P. Stoodley, K. Sauer, D. G. Davies, and J. W. Costerton, *Annu. Rev. Microbiol.*, 2002, **56**, 187–209.

197. K. Vasilev, J. Cook, and H. J. Griesser, *Expert Rev. Med. Devices*, 2009, **6**, 553–67.

198. N. Cole, E. B. H. Hume, A. K. Vijay, P. Sankaridurg, N. Kumar, and M. D. P. Willcox, *Invest. Ophthalmol. Vis. Sci.*, 2010, **51**, 390–5.

199. D. Pavithra and M. Doble, *Biomed. Mater.*, 2008, **3**, 034003.

200. A. J. Bai and V. R. Rai, *Compr. Rev. Food Sci. Food Saf.*, 2011, **10**, 183–193.

201. J. W. Costerton, K.-J. Cheng, G. G. Geesey, T. I. Ladd, J. C. Nickel, M. Dasgupta, and T. J. Marrie, *Ann. Rev. Microbiol.*, 1987, **41**, 435–464.

202. L. Hall-Stoodley, J. W. Costerton, and P. Stoodley, *Nat. Rev. Microbiol.*, 2004, **2**, 95–108.

203. M. P. Schultz, J. A. Bendick, E. R. Holm, and W. M. Hertel, *Biofouling*, 2011, **27**, 87–98.

204. B. Orgaz, M. M. Lobete, C. H. Puga, and C. S. Jose, *Int. J. Mol. Sci.*, 2011, **12**, 817–28.

205. Y. Lequette, G. Boels, M. Clarisse, and C. Faille, *Biofouling*, 2010, **26**, 421–31.

206. P. S. Stewart and J. W. Costerton, *Lancet*, 2001, **358**, 135–8.

207. T. F. Mah and G. a O'Toole, *Trends Microbiol.*, 2001, **9**, 34–9.

208. N. Høiby, T. Bjarnsholt, M. Givskov, S. Molin, and O. Ciofu, *Int. J. Antimicrob. Agents*, 2010, **35**, 322–32.

209. M. Morikawa, *J. Biosci. Bioeng.*, 2006, **101**, 1–8.

210. R. Singh, D. Paul, and R. K. Jain, *Trends Microbiol.*, 2006, **14**, 389–97.

211. R. Zuo, *Appl. Microbiol. Biotechnol.*, 2007, **76**, 1245–53.

212. D. Di Gioia, L. Sciubba, L. Bertin, C. Barberio, L. Salvadori, S. Frassinetti, and F. Fava, *Water Res.*, 2009, **43**, 2977–2988.

213. I. Banerjee, R. C. Pangule, and R. S. Kane, *Adv. Mater.*, 2011, **23**, 690–718.

214. T. Böcking, K. A. Kilian, K. Gaus, and J. J. Gooding, *Langmuir*, 2006, **22**, 3494–6.

215. S. Yuan, D. Wan, B. Liang, S. O. Pehkonen, Y. P. Ting, K. G. Neoh, and E. T. Kang, *Langmuir*, 2011, 2761–2774.

216. C. S. Gudipati, J. A. Finlay, J. A. Callow, M. E. Callow, and K. L. Wooley, *Langmuir*, 2005, **21**, 3044–53.

217. F. Boulmedais, B. Frisch, O. Etienne, P. Lavalle, C. Picart, J. Ogier, J.-C. Voegel, P. Schaaf, and C. Egles, *Biomaterials*, 2004, **25**, 2003–2011.

218. E. Armstrong, K. G. Boyd, and J. G. Burgess, *Biotechnol. Annu. Rev.*, 2000, **6**, 221–41.

219. L. Cegelski, J. S. Pinkner, N. D. Hammer, C. K. Cusumano, S. Hung, E. Chorell, V. Åberg, J. N. Walker, P. C. Seed, F. Almqvist, M. R. Chapman, and S. J. Hultgren, *Nat. Chem. Biol.*, 2009, **5**, 913–919.

220. D. W. Jackson, K. Suzuki, L. Oakford, J. W. Simecka, M. E. Hart, and T. Romeo, *J. Bacteriol.*, 2002, **184**, 290–301.

221. U. Göransson, M. Sjögren, E. Svangård, P. Claeson, and L. Bohlin, *J. Nat. Prod.*, 2004, **67**, 1287–90.

222. A. Guyomard, E. Dé, T. Jouenne, J.-J. Malandain, G. Muller, and K. Glinel, *Adv. Funct. Mater.*, 2008, **18**, 758–765.

223. J. Chapman, C. Hellio, T. Sullivan, R. Brown, S. Russell, E. Kiterringham, L. Le Nor, and F. Regan, *Int. Biodeterior. Biodegradation*, 2013.

224. D. Dourou, C. S. Beauchamp, Y. Yoon, I. Geornaras, K. E. Belk, G. C. Smith, G.-J. E. Nychas, and J. N. Sofos, *Int. J. Food Microbiol.*, 2011, **149**, 262–268.

225. L. V. Poulsen, *LWT - Food Sci. Technol.*, 1999, **32**, 321–326.

226. G. Melino, *Nature*, 2001, **412**, 23.

227. J. F. R. Kerr, A. H. Wyllie, and A. R. Currie, *Br. J. Cancer*, 1972, **26**, 239–257.

228. G. Kroemer, L. Galluzzi, P. Vandenabeele, J. Abrams, E. Alnemri, E. Baehrecke, M. Blagosklonny, W. El-Deiry, P. Golstein, D. Green, M. Hengartner, R. Knight, S. Kumar, S. Lipton, W. Malorni, G. Nuñez, M. Peter,

J. Tschopp, J. Yuan, M. Piacentini, B. Zhivotovsky, and G. Melino, *Cell Death Differ.*, 2009, **16**, 3–11.

229. I. Herr, *Blood*, 2001, **98**, 2603–2614.

230. T. Sugiyama and Y. Sadzuka, *Clin. Cancer Res.*, 1999, **5**, 413–416.

231. M. . Beers and W. . Berkow, *The Merk Manual*, 17th edn., 1999.

232. S. Fulda, W. Wick, M. Weller, and K.-M. Debatin, *Nat. Med.*, 2002, **8**, 808–15.

233. A. H. Wyllie, J. F. R. Kerr, and A. R. Currie, *Int. Rev. Cytol.*, 1980, **68**, 251–306.

234. D. W. Nicholson, A. Ali, N. A. Thornberry, J. P. Vaillancourt, C. K. Ding, M. Gallant, Y. Gareau, P. R. Griffin, M. Labelle, and Y. A. Lazebnik, *Nature*, 1995, **376**, 37–43.

235. Y. Gavrieli, *J. Cell Biol.*, 1992, **119**, 493–501.

236. H. Lecoeur, *Exp. Cell Res.*, 2002, **277**, 1–14.

237. M. d'Ischia and G. Prota, *Pigment Cell Melanoma Res.*, 1997, **10**, 370–376.

238. L. Zecca, F. a Zucca, H. Wilms, and D. Sulzer, *Trends Neurosci.*, 2003, **26**, 578–80.

239. H. Lee, S. M. Dellatore, W. M. Miller, and P. B. Messersmith, *Science*, 2007, **318**, 426–30.

240. N. F. Della Vecchia, R. Avolio, M. Alfè, M. E. Errico, A. Napolitano, and M. d'Ischia, *Adv. Funct. Mater.*, 2013, **23**, 1331–1340.

241. J. McGinness, P. Corry, and P. Proctor, *Science (80-.).*, 1974, **183**, 853–855.

242. P. Meredith, C. J. Bettinger, M. Irimia-Vladu, a B. Mostert, and P. E. Schwenn, *Rep. Prog. Phys.*, 2013, **76**, 034501.

243. A. B. Mostert, B. J. Powell, F. L. Pratt, G. R. Hanson, T. Sarna, I. R. Gentle, and P. Meredith, *Proc. Natl. Acad. Sci. U. S. A.*, 2012, **109**, 8943–7.

244. S. Gidanian and P. J. Farmer, *J. Inorg. Biochem.*, 2002, **89**, 54–60.

245. K. Svennersten, K. C. Larsson, M. Berggren, and A. Richter-Dahlfors, *Biochim. Biophys. Acta*, 2011, **1810**, 276–85.

246. G. Tarabella, F. Mahvash Mohammadi, N. Coppedè, F. Barbero, S. Iannotta, C. Santato, and F. Cicoira, *Chem. Sci.*, 2013, **4**, 1395.

247. P. N. Bartlett, P. R. Birkin, J. H. Wang, F. Palmisano, and G. De Benedetto, *Anal. Chem.*, 1998, **70**, 3685–94.

248. Z. Zhu, J. T. Mabeck, C. Zhu, N. C. Cady, A. Batt, and G. G. Malliaras, *Chem. Comm.*, 2004, 1556–1557.

249. J. a. DeFranco, B. S. Schmidt, M. Lipson, and G. G. Malliaras, *Org. Electron.*, 2006, **7**, 22–28.

250. J. Ouyang, Q. Xu, C.-W. Chu, Y. Yang, G. Li, and J. Shinar, *Polymer (Guildf).*, 2004, **45**, 8443–8450.

251. X. Crispin, S. Marciniak, W. Osikowicz, G. Zotti, A. W. D. V. A. N. D. E. R. Gon, F. Louwet, M. Fahlman, L. Groenendaal, F. D. E. Schryver, and W. R. Salaneck, 2561–2583.

252. L. Ascione, A. Pezzella, V. Ambrogi, C. Carfagna, and M. D'Ischia, *Photochem. Photobiol.*, 2013, **89**, 314–8.

253. D. a. Bernards, D. J. Macaya, M. Nikolou, J. a. DeFranco, S. Takamatsu, and G. G. Malliaras, *J. Mater. Chem.*, 2008, **18**, 116.

254. H. Tang, P. Lin, H. L. W. Chan, and F. Yan, *Biosens. Bioelectron.*, 2011, **26**, 4559–63.

255. F. Lin and M. C. Lonergan, *Appl. Phys. Lett.*, 2006, **88**, 133507.

256. M. C. Lonergan, C. H. Cheng, B. L. Langsdorf, and X. Zhou, *J. Am. Chem. Soc.*, 2002, **124**, 690–701.

257. R. Edge, M. d'Ischia, E. J. Land, a Napolitano, S. Navaratnam, L. Panzella, a Pezzella, C. a Ramsden, and P. a Riley, *Pigment Cell Res.*, 2006, **19**, 443–50.

258. S. Gidanian and P. J. Farmer, *J. Inorg. Biochem.*, 2002, **89**, 54–60.

259. D. O. N. Ho, X. Sun, and S. Sun, *Acc. Chem. Res.*, 2011, **44**, 875–882.

260. O. V Salata, *J. Nanobiotechnology*, 2004, **6**, 1–6.

261. J. I. N. Xie, G. Liu, H. S. Eden, H. U. A. Ai, and X. Chen, *Acc. Chem. Res.*, 2011, **44**, 883–892.

262. J.-H. Lee, Y.-M. Huh, Y. Jun, J. Seo, J. Jang, H.-T. Song, S. Kim, E.-J. Cho, H.-G. Yoon, J.-S. Suh, and J. Cheon, *Nat. Med.*, 2007, **13**, 95–9.

263. J. Dobson, *Drug Dev. Res.*, 2006, **67**, 55–60.

264. B. Thiesen and A. Jordan, *Int. J. Hyperthermia*, 2008, **24**, 467–74.

265. T. Toccoli, E. Borga, H. Blond, D. Maniglio, L. Minati, C. Fasoli, M. Pola, C. Corradi, and S. Iannotta, *Org. Electron.*, 2012, **13**, 1716–1721.

266. N. Nitin, L. E. W. LaConte, O. Zurkiya, X. Hu, and G. Bao, *J. Biol. Inorg. Chem.*, 2004, **9**, 706–12.

267. R. Massart, *IEEE Trans. Magn.*, 1981, **MAG-17**, 1247 – 1248.

268. P. D. Nellist and S. J. Pennycook, *Adv. IMAGING ELECTRON Phys.*, 2000, **113**, 147 – 203.

269. A. Pranzetti, S. Mieszkin, P. Iqbal, F. J. Rawson, M. E. Callow, J. a Callow, P. Koelsch, J. a Preece, and P. M. Mendes, *Adv. Mater.*, 2013, **25**, 2181–5.

270. J. Y. Wong, R. Langer, and D. E. Ingber, 1994, **91**, 3201–3204.

271. M. H. Bolin, K. Svennersten, D. Nilsson, A. Sawatdee, E. W. H. Jager, A. Richter-Dahlfors, and M. Berggren, *Adv. Mater.*, 2009, **21**, 4379–4382.

272. A. M. D. Wan, D. J. Brooks, A. Gumus, C. Fischbach, and G. G. Malliaras, *Chem. Commun. (Camb).*, 2009, 5278–80.

273. C. Yao, C. Xie, P. Lin, F. Yan, P. Huang, and I. Hsing, *Adv. Funct. Mater.*, 2013, 1–6.

274. R.-X. He, M. Zhang, F. Tan, P. H. M. Leung, X.-Z. Zhao, H. L. W. Chan, M. Yang, and F. Yan, *J. Mater. Chem.*, 2012, **22**, 22072.

275. R.-X. He, M. Zhang, F. Tan, P. H. M. Leung, X.-Z. Zhao, H. L. W. Chan, M. Yang, and F. Yan, *J. Mater. Chem.*, 2012, **22**, 22072.

276. D. J. Throckmorton, T. J. Shepodd, and A. K. Singh, *Anal. Chem.*, 2002, **74**, 784–9.

277. M. Sessolo, D. Khodagholy, J. Rivnay, F. Maddalena, M. Gleyzes, E. Steidl, B. Buisson, and G. G. Malliaras, *Adv. Mater.*, 2013, **25**, 2135–9.

278. S. M. Soto, A. Smithson, J. A. Martinez, J. P. Horcajada, J. Mensa, and J. Vila, *J. Urol.*, 2007, **177**, 365–8.

279. C. A. Schneider, W. S. Rasband, and K. W. Eliceiri, *Nat. Methods*, 2012, **9**, 671–675.

280. P. G. Taylor, J.-K. Lee, A. A. Zakhidov, M. Chatzichristidi, H. H. Fong, J. A. DeFranco, G. G. Malliaras, and C. K. Ober, *Adv. Mater.*, 2009, **21**, 2314–2317.

281. A. A. Zakhidov, J.-K. Lee, J. A. DeFranco, H. H. Fong, P. G. Taylor, M. Chatzichristidi, C. K. Ober, and G. G. Malliaras, *Chem. Sci.*, 2011, **2**, 1178.

282. M. Camps, J.-F. Briand, L. Guentas-Dombrowsky, G. Culioli, A. Bazire, and Y. Blache, *Mar. Pollut. Bull.*, 2011, **62**, 1032–40.

283. X. Zhang, Y. Zhang, J. Liu, and H. Liu, *Biotechnol. Lett.*, 2013, **35**, 1099–106.

284. M. E. Bayer, E. Carlemalm, and E. Kellenberger, *J. Bacteriol.*, 1985, **162**, 985–991.

285. M. E. Bayer and H. Thurow, *J. Bacteriol.*, 1977, **130**, 911–36.

286. J. F. Wilkinson, *Bacteriol. Rev.*, 1958, **22**, 46–73.

287. X. Zhang, C. Li, and Y. Luo, *Langmuir*, 2011, **27**, 1915–23.

288. L. A. A. Pettersson, S. Ghosh, and O. Ingan, *Org. Electron.*, 2002, **3**, 143–148.

289. D. Wakizaka, T. Fushimi, H. Ohkita, and S. Ito, *Polymer (Guildf).*, 2004, **45**, 8561–8565.

290. X. Chen and O. Inganäs, *J. Phys. Chem.*, 1996, **100**, 15202–15206.

291. A. Baba, J. Lubben, K. Tamada, and W. Knoll, *Langmuir*, 2003, **19**, 9058–9064.

292. H. Xu, A. E. Murdaugh, W. Chen, K. E. Aidala, M. A. Ferguson, E. M. Spain, and M. E. Núñez, *Langmuir*, 2013, **29**, 3000–11.

293. J. Chapman, C. Hellio, T. Sullivan, R. Brown, S. Russell, E. Kiterringham, L. Le Nor, and F. Regan, *Int. Biodeterior. Biodegradation*, 2013.

294. M. Marzocchi, E. Scavetta, A. Bonfiglio, I. Zironi, G. Castellani, G. G. Malliaras, R. M. Owens, and B. Fraboni, 2013, p. 6.

295. A. M. D. Wan, R. M. Schur, C. K. Ober, C. Fischbach, D. Gourdon, and G. G. Malliaras, *Adv. Mater.*, 2012, **24**, 2501–5.

296. Z. Zhu, J. T. Mabeck, C. Zhu, N. C. Cady, A. Batt, and G. G. Malliaras, *Chem. Comm.*, 2004, 1556–1557.

297. J. Isaksson, P. Kjäll, D. Nilsson, N. D. Robinson, M. Berggren, and A. Richter-Dahlfors, *Nat. Mater.*, 2007, **6**, 673–9.

298. A. M. D. Wan, D. J. Brooks, A. Gumus, C. Fischbach, and G. G. Malliaras, *Chem. Commun. (Camb).*, 2009, 5278–80.

299. A. Gumus, J. P. Califano, A. M. D. Wan, J. Huynh, C. a. Reinhart-King, and G. G. Malliaras, *Soft Matter*, 2010, **6**, 5138.

300. L. H. Jimison, S. a Tria, D. Khodagholy, M. Gurfinkel, E. Lanzarini, A. Hama, G. G. Malliaras, and R. M. Owens, *Adv. Mater.*, 2012, **24**, 5919–23.

301. J. Wegener, D. Abrams, W. Willenbrink, H.-J. Galla, and A. Janshoff, *Biotechniques*, 2004, **4**, 590–596.

302. A. Cavazzoni, R. R. Alfieri, C. Carmi, V. Zuliani, M. Galetti, C. Fumarola, R. Frazzi, M. Bonelli, F. Bordi, A. Lodola, M. Mor, and P. G. Petronini, *Mol. Cancer Ther.*, 2008, **7**, 361–70.

303. Y. Filyak, O. Filyak, S. Souchelnytskyi, and R. Stoika, *Eur. J. Pharmacol.*, 2008, **590**, 67–73.

304. A. Litwiniec, A. Grzanka, A. Helmin-Basa, L. Gackowska, and D. Grzanka, *J. Cancer Res. Clin. Oncol.*, 2010, **136**, 717–36.

305. R. G. Larson, *The structure and rheology of complex fluids*, Oxford University Press, New York, 1999.

Scientific contributions

In the following, there is a summary of the scientific contributions I have produced during my PhD, in the form of: publications in peer-reviews journals, contribution at national and international conferences with posters or oral presentations, and the PhD-schools I have attended.

Pubblications:

- A. Romeo, G. Tarabella, P. D'Angelo, C. Caffarra, D. Cretella, P.G. Petronini and S. Iannotta, *Detection of cell death induced by doxorubicin with Organic Electrochemical Transistors*, Advanced Healthcare Materials, IN SUBMISSION
- A. Romeo, G. Tarabella, N. Coppedè, M. Calicchio, F. Rossi, R. Mosca and S. Innotta, *Detecting Functionalised Nanoparticles by Organic Electrochemical Transistors: toward a new class of sensing devices*, Chemical Sciences, IN SUBMISSION
- A. Romeo, A. Hama, M. Ferro, J. Rivnay, S. Iannotta, G.G. Malliaras, and R. Owens, *Conducting polymers: a route to control biofouling*, Advanced Materials, IN SUBMISSION
- G. Tarabella, A. Pezzella, A. Romeo, P. D'Angelo, N. Coppedè, M. Calicchio, M. d'Ischia, R. Mosca and S. Iannotta, *Irreversible evolution of eumelanin redox states detected by an organic electrochemical transistor: en route to bioelectronics and biosensing*, J. Mater. Chem. B, 2013, 1, 3843

Schools and Conferences attended:

- ✓ MRS Fall Meeting 2013
  location ....Hynes Convention Center, Boston, MA.......,
  from ..01/12/2013.........to .... 06/12/2013...........
- ✓ OLIMPIA Summer School – Organic Electronics at the interface with biology
  location.... Centre Microéléctronique de Provence - Ecole des Mines de Saint Etienne – Gardanne, France....................
  from .. 17/09/2013.........to ...... 19/09/2013..............
- ✓ 3rd French-American workshop on bioelectronics.
  location .... Porquerolles island, France..............

from ..10/06/2013.........to .... 14/06/2013............

- ✓ 9th International Conference on Nanosciences and Nanotechnologies (NN12).
  location.... Ioannis Vellidis Congress Center, Thessalonikki, Greece.......
  from .. 03/07/2012.........to ...... 06/07/2012..............

- ✓ *ISSON12 - VI International Summer School on Nanosciences&Nanotechnology, Organic Electronics and Nanomedicine*
  location.... Ioannis Vellidis Congress Center, Thessalonikki, Greece........
  from .. 30/06/2012.........to ...... 07/07/2012..............

- ✓ Summer school “Cell Model Systems”
  location ....Univeristà Tor-Vergata, Rome, Italy....................
  from .. 10/06/2012.........to ...... 15/06/2012..............

- ✓ X National Conference on Nanophase Materials
  location ....Dep. of Physics A. Righi – Università di Bologna........
  from .....06/09/2011......to ..... 08/09/2011...............

Oral contributions and posters:

- ➢ Oral contribution: “Conducting polymers: a route to control biofouling” durante il MRS Fall Meeting 2013.
  Authors: A. Romeo, A. Hama, M. Ferro, J. Rivnay, S. Iannotta, G.G. Malliaras, R. Owens
  location ....Hynes Convention Center, Boston, MA......., from ..01/12/2013.........to .... 06/12/2013...........

- ➢ Poster: “Conducting polymers: a route to control biofouling” at OLIMPIA Summer School. Authors: A. Romeo, A. Hama, M. Ferro, J. Rivnay, S. Iannotta, G.G. Malliaras, R. Owens
  location.... Centre Microéléctronique de Provence - Ecole des Mines de Saint Etienne – Gardanne, France............
  from .. 17/09/2013.........to ...... 19/09/2013..............

- ➢ Oral contribution: “Conducting polymers: a route to control biofouling” durante il **3rd** French-American workshop on bioelectronics. Authors: A. Romeo, A. Hama, M. Ferro, J. Rivnay, S. Iannotta, G.G. Malliaras, R. Owens
  location .... Porquerolles island, France.............. from ..10/06/2013.........to .... 14/06/2013............

- ➢ Poster: “Monitoring drug-induced cellular stress by Oganic Electrochemical Transistors” at 9th International Conference on Nanosciences and Nanotechnologies (NN12). Authors: A.Romeo, G.Tarabella, N.Coppedè, R.Mosca, R. Alfieri, P.G. Petronini, S.Iannotta
  location.... Ioannis Vellidis Congress Center, Thessalonikki, Greece....... from .. 03/07/2012.........to 06/07/2012..............

- Oral contribution: “Organic Electrochemical Transistors for monitoring functionalized magnetic nanoparticles” durante il X Convegno Nazionale Materiali Nanofasici. Authors: A. Romeo, G. Tarabella, N. Coppedè, R. Mosca and S. Iannotta
  location ....Dep. of Phyics A. Righi – Università di Bologna........ from .....06/09/2011......to ..... 08/09/2011................

Stages abroad

International interniship (9 months)
location ..... Departement de Bioéléctronique - Centre Microéléctronique de Provence - Ecole des Mines de Saint Etienne – Gardanne, France.................
from ..11/01/2013 ....to...... 30/09/2013..............

Acknowledgments

The work described in this Thesis has been partially carried out in each of the following institutions: the Institute of Materials for Electronics and Magnetism (IMEM), Parma, Italy, which has represented my scientific “home” during these three years of PhD; the Department of Clinical and Experimental Medicine - Unit of Experimental Oncology, Parma, Italy (results included in Chapter 5); and the Department of BioElectronics – Centre Microelectronics of Provence, Gardanne, France (results included in Chapter 4). As such, this Thesis is the visible top of a huge and submerged work to whom many people have contributed.

I would like to start by expressing my gratefulness to my Supervisor, Dr. Salvatore Iannotta from IMEM, who offered me the opportunity to become involved in the world of Organic Bioelectronics. He taught me a lot about research and how to pursue goals sometimes seemingly unattainable. Thanks a lot for your support, advice and fatherly affection.

Much of this work would not have been possible without the help and the efforts made by many other people in IMEM. First, and of course, a huge thanks goes to my colleague Dr. Giuseppe Tarabella, who has shared with me ideas, doubts, perspectives and long hours of experiments. His experience in Organic Electronics, Physics and Engineering has provided to me a great source of inspiration and the model for much of what I am now in scientific research. I also have to thank Dr. Roberto Mosca for his advice on signal understanding and device fabrication, as well as Dr. Marco Calicchio, Dr. Francesca Rossi, Dr. Nicola Coppedé and Dr. Pasquale d’Angelo, who, in different extent and modalities, have contributed decisively to my PhD.

I would like to express my gratitude also to Prof. Pier Giorgio Petronini and Prof. Roberta Alfieri, chiefs of the Unit of Experimental Oncology in Parma, and to all the people who work there. They hosted me for quite long time and have always made me A particular thanks goes to Cristina Caffarra and Daniele Cretella, young and enthusiast PhD students, who every day embrace the research work with dedication and commitment. In this Department I have learnt all I know about biology, cell cultivation, toxicology, and oncology. Thanks to all of you for showing me the beauty of living systems and the fascination of their intrinsic complexity.

The experience at BEl, a group made of brilliant graduate students and researchers, has been incomparably reach from the professional and human point of view. My gratitude goes *in primis* to Prof. George Malliaras and Prof. Roisin Owens, who carefully supervised me with their bright and smart vision of science. Thanks to Dr. Miriam Huerta and Adel Hama for their essential contribution in bacterial manipulation, and to Marc Ferro and Xenofon Strakosas for great help on device fabrication. Thanks to Pierre Leleux, friend before than office-mate, for enlightening conversations on career development and self-motivation, and thanks also to Dr. Marc Ramuz and Thomas Doublet, extremely valid colleagues as well as amazing partners in our sessions of table-football. A heartfelt thanks goes also to Dr. Jonathan Rivnay, Dr. Esma Ismailova, Dr. Michele Sessolo, Manuelle Bongo, Liza Klots, Eleni Stavrinidou, Sherrine Tria, Cassandre, Vauvillaume, and Prof. Sebastien Sanaur for their precious advice and suggestions, as well as for every single smile, cake, joke and dinner we shared all together. My thought also goes to other people that contributed to make pleasant my experience at the Centre Microelectronics of Provence: thanks to Thierry Camilloni for support with clean-room facilities and for stress-washing beach-volley at lunch-time, and thanks to Eloïse Bihar, Henda Basti and Malika Bella for their friendship and the amount of laughs we had together.

Of course, the successful outcome of a scientific work passes also through the contribution of people that are not strictly connected to the scientific activity itself. I will be eternally grateful to my father, my mother, and my sisters for the support they have provided to me, despite the distance. In every moment I felt your pride for what, with hard work and sacrifice, I have become in these years of study, and this has driven me to get higher and higher. Thank you all from the bottom of my heart.

I would like also to thank my girlfriend, Yvy, for her patience and comprehension over these long years: you made me smile and relax, representing my force and helping me to believe into myself also in the hard times.

Sincerely,

Agostino

Parma, 29 January 2014